

Deep imaging survey of young, nearby austral stars VLT/NACO Near-Infrared Lyot-Coronagraphic Observations

G. Chauvin¹, A.-M. Lagrange¹, M. Bonavita^{2,3}, B. Zuckerman⁴, C. Dumas⁵, M. S. Bessell⁶, J.-L. Beuzit¹, M. Bonnefoy¹, S. Desidera², J. Farihi⁷, P. Lowrance⁸, D. Mouillet¹, and I. Song⁹

¹ Laboratoire d'Astrophysique, Observatoire de Grenoble, UJF, CNRS: 414, Rue de la piscine, 38400 Saint-Martin d'Hères, France

² INAF - Osservatorio Astronomico di Padova, Vicolo dell' Osservatorio 5, 35122 Padova, Italy

³ Università di Padova, Dipartimento di Astronomia, Vicolo dell'Osservatorio 2, 35122 Padova, Italy

⁴ Department of Physics & Astronomy and Center for Astrobiology, University of California: Los Angeles, Box 951562, CA 90095, USA

⁵ European Southern Observatory: Casilla 19001, Santiago 19, Chile

⁶ Research School of Astronomy and Astrophysics Institute of Advance Studies, Australian National University: Cotter Road, Weston Creek, Canberra, ACT 2611, Australia

⁷ Department of Physics & Astronomy, University of Leicester, Leicester LE1 7RH, United Kingdom

⁸ Spitzer Science Center, IPAC/Caltech: MS 220-6, Pasadena, CA 91125, USA

⁹ Department of Physics & Astronomy, University of Georgia, Athens, GA 30602-2451, USA

Received September, 2008

ABSTRACT

Context. High contrast and high angular resolution imaging is the optimal technique to search for substellar companions to nearby stars at physical separations larger than typically 10 AU. Two distinct populations of substellar companions, brown dwarfs and planets, can be probed and characterized. Fossil traces of their different formation processes should be revealed by their respective physical and orbital properties and should then allow testing basic aspects of their respective formation and evolution mechanisms.

Aims. Since November 2002, we have conducted the largest deep imaging survey of the young, nearby associations of the southern hemisphere. Our goal is detection and characterization of substellar companions at intermediate (10 – 500 AU) physical separations. We have observed a sample of 88 stars, mostly G to M dwarfs, that we essentially identify as younger than 100 Myr and closer to Earth than 100 pc.

Methods. The VLT/NACO adaptive optics instrument of the ESO Paranal Observatory was used to explore the faint circumstellar environment between typically 0.1 and 10". Diffraction-limited observations in *H* and *K_s*-band combined with Lyot-coronagraphy enabled us to reach contrast performances as small as 10⁻⁶. The existence of planetary mass companions could therefore be probed. We used a standardized observing sequence to precisely measure the position and flux of all detected sources relative to their visual primary star. Repeated observations at several epochs enabled us to discriminate comoving companions from contaminants.

Results. We report the discovery of 17 new close (0.1 – 5.0 ") multiple systems. HIP 108195 AB and C (F1 III-M6), HIP 84642 AB (*a* ~ 14 AU, K0-M5) and TWA22 AB (*a* ~ 1.8 AU; M6-M6) are confirmed comoving systems. TWA22 AB is likely to be a rare astrometric calibrator that can be used to test evolutionary model predictions. Among our complete sample, a total of 65 targets were observed with deep coronagraphic imaging. About 240 faint companion candidates were detected around 36 stars. Follow-up observations with VLT or HST for 83% of these stars enabled us to identify a large fraction of contaminants. The latest results about the substellar companions to GSC 08047-00232, AB Pic and 2M1207, confirmed during this survey and published earlier, are reviewed. Finally, the statistical analysis of our complete set of coronagraphic detection limits enables us to place constraints on the physical and orbital properties of giant planets between typically 20 and 150 AU.

Conclusions.

Key words. Instrumentation: adaptive optics, high angular resolution – Methods: observational, data analysis, statistical – Techniques: photometric, astrometric – Stars: low-mass, brown dwarfs, planetary systems

1. Introduction

The search for substellar objects, isolated, multiple or companion to nearby stars, has been an important driver for observers in the two last decades. Their detection and characterization contribute to developing our understanding of the formation and evolution of stars, brown dwarfs and planets. Since the discovery of the first unambiguous brown dwarf Gl229 B (Nakajima et al. 1995), the development of new instruments and observing techniques has diversified. Large surveys (2MASS, Skrutskie et al. 1997; DENIS, Epchtein et al. 1997; SLOAN, York et al. 2000) are the best method for the study of isolated substellar objects.

Hundreds of brown dwarfs have been discovered in the field motivating the introduction of the new L and T spectral classes (Delfosse et al. 1997; Kirkpatrick et al 1999; Burgasser et al. 1999). Dedicated spectroscopic observations offer the opportunity to study the physical and chemical processes of these very cool atmospheres, such as grain and molecule formation, vertical mixing and cloud coverage. In the field, in young open clusters or in star forming regions, the study of the initial-mass function and of stellar and substellar multiplicity shows an apparent continuous sequence supporting the idea that stellar mechanisms (collapse, fragmentation, ejection, photo-evaporation of accre-

tion envelopes) form objects over a wide range of masses, down to planetary masses predicted by theoretical models (Bonnell et al. 2007; Burgasser et al. 2007; Zuckerman & Song 2009). Despite limited spatial resolution, a dozen substellar companions to nearby stars have been discovered at wide (≥ 100 AU) orbits (Goldman et al. 1999, Kirkpatrick et al. 2000, Wilson et al. 2001).

To access the near (≤ 5 AU) environment of stars, other observing techniques (radial velocity, transit, micro-lensing, pulsar-timing), are so far best suited. The radial velocity (RV) and transit techniques are nowadays the most successful methods for detecting and characterizing the properties of exoplanetary systems. The RV surveys have focused on main sequence solar-type stars, with numerous narrow optical lines and low activity, to ensure high RV precision. Recently, planet-search programs have been extended to lower and higher mass stars (Endl et al. 2006, Lagrange et al. 2009) and younger and more evolved systems (Joergens et al. 2006, Johnson et al. 2007). Since the discovery of 51 Peg b (Mayor & Queloz 1995), more than 300 exo-planets have been identified featuring a broad range of physical (mass) and orbital (P, e) characteristics (Udry & Santos 2007; Butler et al. 2006). This technique also revealed the existence of the so-called brown dwarf desert at small (≤ 5 AU) separations (Grether & Lineweaver 2006). The bimodal aspect of the secondary mass distribution indicates different formation mechanisms for two populations of substellar companions, brown dwarfs and planets. The transit technique coupled with RV enables determination of the radius and density of giant planets and thus a probe of their internal structure. Moreover, spectral elements of a planetary atmosphere can be revealed during primary or secondary eclipse (Swain et al. 2008, Grillmair et al. 2008).

To extend such systematic characterization at larger scales (≥ 10 AU), the deep imaging technique is particularly well suited to probe the existence of planets and brown dwarf companions and complete our view of planetary formation and evolution. To access small angular separations, the space telescope (HST) or the combination of Adaptive Optics (AO) system with very large ground-based telescopes (Palomar, CFHT, Keck, Gemini, Subaru, VLT) have become mandatory. Moreover, deep imaging surveys take advantage of exhaustive work on identification of young (≤ 100 Myr), nearby (≤ 100 pc) stellar associations. Due to their youth and proximity, such stars offer an ideal niche for detection of warm planetary mass companions that are still moderately bright at near-infrared wavelengths. Since the recognition of the TW Hydrae association (TWA; Kastner et al. 1997; Webb et al. 1999), more than 200 young, nearby stars have been identified. Many such stars reside in several coeval moving groups (e.g., TWA, β Pictoris, Tucana-Horologium, η Cha, AB Dor, Columba and Carinae), sharing common kinematics, photometric and spectroscopic properties (see Zuckerman & Song 2004, hereafter ZS04; Torres et al. 2008, T08). A few young brown dwarf companions have been detected from space, HR 7329 B and TWA5 B (Lowrance et al. 2000, 1999), and from the ground, GSC 08047-00232 B (Chauvin et al. 2005a). Companions down to the planetary mass regime were discovered around the star AB Pic (Chauvin et al. 2005c) and the young brown dwarf 2M1207 (Chauvin et al. 2004, 2005b). Various deep imaging surveys of young, nearby stars have recently been completed using different high contrast imaging techniques such as coronagraphy, differential imaging or L -band imaging (see Table 1). A significant number have reported a null-detection result of substellar companions. Kasper et al. (2007), Lafrenière et al. (2007) and Nielsen et al. (2008) have initiated a statistical analysis to

Table 1. Deep imaging surveys of young (< 100 Myr), nearby (< 100 pc) stars dedicated to the search for planetary mass companions and published in the literature. The telescope and the instrument (Tel/Instr.), the imaging mode (CI: coronagraphic imaging; Sat-DI; saturated direct imaging; DI direct imaging; SDI: simultaneous differential imaging; ADI: angular differential imaging) and filters, the field of view (FoV) and the number of stars observed (#) are given. The typical survey sensitivity in terms of mass is also reported with the survey reference.

Tel/Instr.	Mode & Filter	FoV (arcsec)	#	Mass (M_{Jup})	Ref.
3.6m/ADONIS	CI, $H - K$	13×13	29	5	(1)
NTT/Sharp	Sat-DI, K	11×11	23	5	(2)
NTT/Sofi	Sat-DI, H	13×13	10	5	(2)
HST/NICMOS	DI, H	19×19	45	1	(3)
VLT/NaCo	Sat-DI, $H - K$	14×14	28	5	(4)
VLT/NaCo	SDI, H	5×5	45	1	(5)
VLT/NaCo	DI, L'	28×28	22	1	(6)
Gemini/NIRI	ADI, H	22×22	85*	1	(7)

- REFERENCES: (1) Chauvin et al. 2003, (2) Neuhäuser et al. 2003, (3) Lowrance et al. 2005, (4) Masciadri et al. 2005, (5) Biller et al. 2007, (6) Kasper et al. 2007, (7) Lafrenière et al. 2007

- (*): half have age estimates younger than 200 Myr (see Fig. 1, Lafrenière et al. 2007)

constrain the physical and orbital properties (mass, period, eccentricity distributions) of a giant planet population. Despite the model-dependency on the mass predictions, the approach is attractive for exploiting the complete set of detection performances of the survey and characterizing the outer portions of exo-planetary systems.

Deep imaging surveys were performed on other classes of targets: distant young associations (Taurus, Chamaeleon, Lupus, Upper Sco), nearby intermediate-age (0.1 – 1.0 Gyr) stars, very nearby stars and old stars with planets detected by RV. Additional substellar companions were detected with masses at the edge or inside the planetary mass regime around the star, DH Tau (Itoh et al. 2005), GQ Lup (Neuhäuser et al. 2005), CHXR 73 (Luhman et al. 2006), HD230030 (Metchev et al. 2006) and more recently IRXS J160929.1-210524 (Lafrenière et al. 2008) and CT Cha (Schmidt et al. 2008). The uncertain fraction of brown dwarf secondaries led various teams (McCarthy & Zuckerman 2004; Carson et al. 2005, 2006; Metchev et al. 2008) to test the extension of the brown desert to intermediate separations. Another purpose was to probe the existence and the impact of wide massive substellar companions to exoplanetary systems detected by RV (Patience et al. 2002; Luhman & Jayawardhana 2002; Chauvin et al. 2006; Mugrauer et al. 2007; Eggenberger et al. 2007). Only very recently, an important breakthrough has been achieved with the imaging detection of planetary mass companions HR 8799 bcd (Marois et al. 2008b), Fomalhaut b (Kalas et al. 2008) and the candidate β Pic b (Lagrange et al. 2009). Such discoveries offer new attractive perspectives for current on-going surveys until the arrival of the second generation of deep imaging instruments like Gemini Planet Imager (GPI; Macintosh et al. 2006) and VLT/SPHERE (Dohlen et al. 2006).

In this paper we report results of a deep coronagraphic imaging survey of several young, nearby austral stars, aimed at discovering substellar companions. In regards to previous works (see Table 1), it represents one of the largest and deepest surveys obtained so far on this class of targets. This survey, initi-

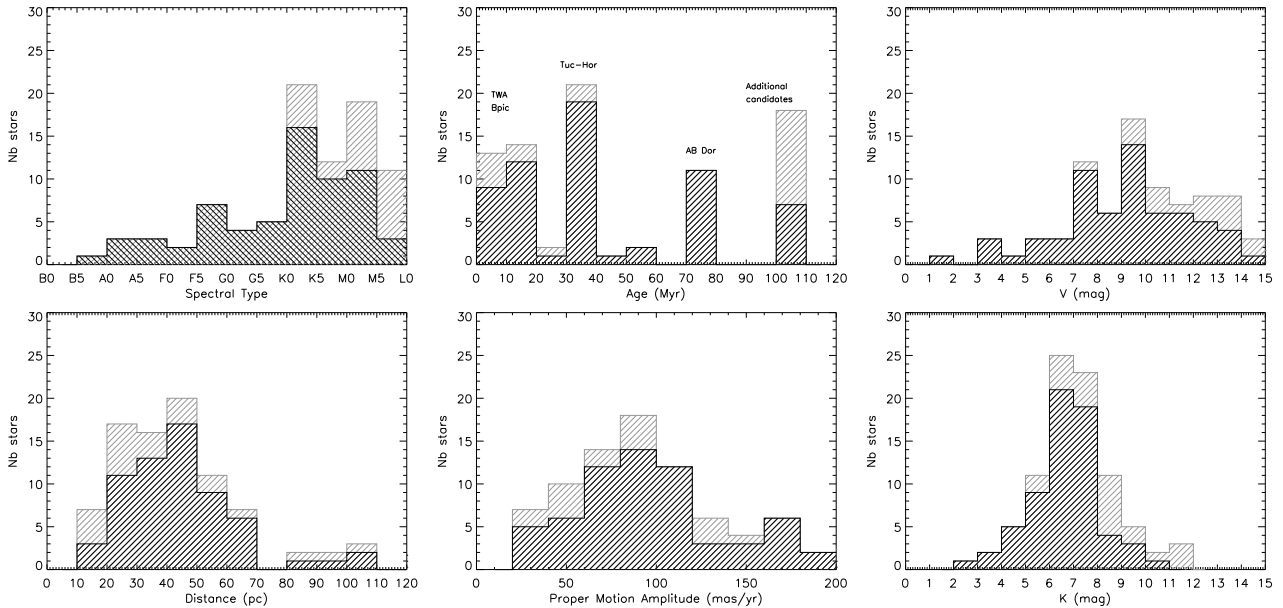


Fig. 1. Histograms summarizing the main properties of the sample of young, nearby stars observed with NACO at VLT. *Top-Left:* Histogram of spectral types for the stars observed in coronagraphic imaging (*crossed lines*) and in direct imaging (*simple lines*). *Top-Middle:* Histogram of ages for members of known young, nearby associations (TWA, β Pic, Tuc-Hor, AB Dor) and additional young candidates. *Top-Right:* Histogram of V-band fluxes. The performances of the AO correction with the NACO visible-WFS decreases between $12 \leq V \leq 16$. *Bottom-Right:* Histogram of K-band fluxes. The coronagraphic mode is not efficient anymore for stars fainter than $K \geq 9 - 10$.

ated in November 2000 with the ADONIS/SHARPII instrument on a 3.6 m telescope (Chauvin et al. 2003), was then extended with the VLT/NACO instrument between November 2002 and October 2007. In Section 2, the sample definition and properties are presented. In Section 3, we describe the characteristics of the VLT/NACO instrument and the different observing set-up and modes that we used. The different observing campaigns, the atmospheric conditions and the observing strategy are detailed in Section 4. The dedicated data reduction and analysis to clean the science images, to calibrate our measurements, to derive the relative position and photometry of the detected sources in the NACO field of view and to estimate the detection performances are reported in Section 5. We then present the main results of our survey in Section 6, including the discovery of new close binary systems and the identification of background contaminants and comoving companions. In Section 7, we finally consider the detection sensitivity of our complete survey to statistically constrain the physical and orbital properties of the population of giant planets with 20 – 150 AU physical separations.

2. Sample Selection

The building up of our target sample relied on a synergy between the exhaustive work of young, nearby stars identification and selection criteria (age, distance, binarity and observability) to optimize the detection of close-in planetary mass companions with NACO at VLT. Youth indicators generally rely on the use of photometry and pre-main sequence isochrones, spectroscopic line (Lithium and H_{α}) analysis and study of X-ray activity and IR excess (see ZS04). Association membership is inferred from coordinates, proper motion, radial velocity and distance estimation. Since the beginning of the present survey, the number of known young, nearby stars more than doubled and newly identified members were regularly included in our target sample. Previously known binaries (see Tables 2 and 3) with $1.0 - 12.0''$

separation were excluded to avoid degrading the NACO AO and/or coronagraphic detection performances. Our initial complete sample was composed of 88 stars; 51 are members of young, nearby comoving groups, 32 are young, nearby stars currently not identified as members of any currently known association and 5 have been reclassified by us as older (>100 Myr) systems.

For stars not in a known moving group (Table 3), based on existing data we employed as many of the techniques for age dating as possible (see, e.g., Section 3 in ZS04). The principal diagnostics were Lithium abundance, Galactic space motion UVW, and fractional X-ray luminosity (Figs. 3, 6 and 4, respectively in ZS04). With the possible exception of a few of the FS stars (see following paragraph), all Table 3 stars with ages 100 Myr or less have UVW in or near the “good UVW box” in Fig. 6 of ZS04. With the exception of the A-type stars (unknown Lithium abundances), all Table 3 stars have Lithium abundances (we have measured) consistent with the ages we list and their spectral type (as per Fig. 3 in ZS04). With the exception of the A-type stars, X-ray fluxes are consistent with Fig. 4 in ZS04 for the indicated ages. Age uncertainties for non-FS stars in Table 3 are typically 50% of the tabulated age (i.e., 30 ± 15 Myr, 100 ± 50 Myr). The ages of the two A-type stars are based on UVW and location on a young star HR diagram.

When their radial velocity is known (based on our echelle spectra) then the FS stars usually have a “good UVW”. In all cases they are strong X-ray emitters and also have H alpha in emission, usually strongly. Lithium is usually not detected in the FS stars, or occasionally weakly. Because the data sets for these stars are sometimes incomplete (e.g., radial velocity not measured) and because fractional X-ray luminosity and UVW are imprecise measures of age, we have assigned an age of 100 Myr to all observed FS stars. Perhaps a few FS stars have ages older than 100 Myr (FS 588 being the most likely of these). But, similarly, some are likely younger than 100 Myr. By assuming an

Table 2. Sample of southern young, nearby stars observed during our VLT/NACO deep imaging survey. In addition to name, coordinates, galactic latitude (b), spectral type, distance and V and K photometry, the observing filter is given. All sources were observed in direct imaging, we have therefore indicated the 65 stars observed in addition in coronagraphy (CI). Finally, the multiplicity status of the primary and the presence of companion candidates (CCs) are also reported. For the multiplicity status we have flagged the following information: binary (B), triple (T) and quadruple (Q); new (N) or known/cataloged (K) multiple system; identified visual (VIS), Hipparcos astrometric (HIP) and spectroscopic (SB) binary system; and a final flag in case of a confirmed physical (Ph) or comoving (Co) system, but nothing if only an optical binary. FS stars are from a paper by Fuhrmeister & Schmitt (2003).

Name	α [J2000]	δ [J2000]	b (deg)	SpT	d (pc)	Age (Myr)	V (mag)	K (mag)	Mode & Filter	Stellar Multiplicity	Note
TWA											
TWA22 AB	10 17 26.9	-53 54 28	2	M5	18	8	13.2	7.69	CI, Ks	B (N/VIS/Ph)	CCs
SSSPMJ1102	11 02 09.83	-34 30 35	23	M8	65	8		11.88	Ks		
TWA3 AB	11 10 28.8	-37 32 04	21	M3	42	8	12.1	6.77	CI, H	B (K/VIS/Co)	
Twa14	11 13 26.3	-45 23 43	14	M0	63	8	13.8	8.50	CI, Ks		CCs
Twa12	11 21 05.6	-38 45 16	21	M2	32	8	13.6	8.05	CI, Ks		CCs
2M1139	11 39 51.1	-31 59 21	28	M8	49	8		11.50	Ks		
HIP57524	11 47 24.6	-49 53 03	11	G5	104	8	9.1	7.51	CI, H		CCs
Twa23	12 07 27.4	-32 47 0	30	M1	37	8	12.7	7.75	CI, H		
2M1207	12 07 33.4	-39 32 54	23	M8	52	8		11.95	Ks	B (N/VIS/Co)	
Twa25	12 15 30.7	-39 48 42	22	M5	44	8	11.4	7.31	CI, Ks		
HR4796 A	12 36 01.0	-39 52 10	23	A0	67	8	5.8	5.77	CI, H	B (K/VIS/Co)	
Twa17	13 20 45.4	-46 11 38	17	K5	133	8	12.6	9.01	CI, H		CCs
β Pictoris											
HIP27321	05 47 17.0	-51 03 59	-31	A5	20	12	3.9	3.53	CI, Ks		
V343Nor B	15 38 56.9	-57 42 18	-2	M4	40.0	12	14.8	9.19	CI, H	T (K/VIS+SB2/Co+Ph)	
HD155555 AB	17 17 25.5	-66 57 03	-16	K1	31.4	12	6.9	4.70	CI, H	T (K/SB2+VIS/Ph+Co)	CCs
TYC-8742-2065 AB	17 48 33.7	-53 06 43	-13	K0	42	12	9.0	6.78	H	B (K/SB2 and VIS/Ph)	
HIP88399 A	18 03 03.4	-51 38 56	-14	F5	46.9	12	7.0	5.91	CI, Ks	B (K/VIS/Co)	CCs
HIP92024	18 45 26.9	-64 52 16	-24	A7V	29.2	12	4.8	4.25	CI, Ks		CCs
CD-641208 AB	18 45 37.0	-64 51 46	-24	K7	29.2	12	9.5	6.10	CI, H	B (N/VIS)	
OES1847	18 50 44.5	-31 47 47	-14	K5	50	12	10.9	7.46	CI, H		CCs
HIP92680	18 53 05.8	-50 10 49	-21	K0V	49.6	12	8.4	6.37	CI, Ks		CCs
HIP95270	19 22 58.9	-54 32 16	-26	F5	50.6	12	7.0	5.91	CI, H		CCs
Tucana-Horologium											
HIP1113	00 13 53.01	-74 41 17	-42	G6V	43.7	30	8.7	6.96	CI, Ks		
HIP1481	00 18 26.1	-63 28 38	-59	F9V	41.0	30	8.0	6.15	CI, Ks		CCs
CD-7824	00 42 20.2	-77 47 40	-40	K5	69	30	10.4	7.53	CI, H		
HIP3556	00 45 28.1	-51 37 33	-58	M1	38.5	30	11.9	7.62	CI, Ks		CCs
HIP6485	01 23 21.2	-57 28 50	-59	G6	49.3	30	8.5	6.85	CI, Ks		CCs
HIP6856	01 28 08.6	-52 38 19	-64	K1	37.1	30	9.1	6.83	CI, Ks		CCs
HD13246 AB	02 07 26.1	-59 40 45	-55	F8V	45.0	30	7.5	6.20	CI, Ks	B (K/SB and VIS/Ph)	
GSC08056-00482	02 36 51.5	-52 03 04	-58	M3	25	30	12.1	7.50	CI, Ks		
HIP21632 B	04 38 45.6	-27 02 02	-40	M3V	54.7	30	7.5	10.41	CI, Ks*		CCs
HIP30034	06 19 12.9	-58 03 15	-30	K2	45.5	30	9.1	6.98	CI, H		CCs
HIP100751 AB	20 25 38.9	-56 44 06	-35	B7	56	30	1.9	2.48	CI, Ks	B (K/SB/Ph)	
HIP105404 ABC	21 20 59.8	-52 28 40	-44	K0V	46.0	30	8.9	6.57	CI, Ks	T (K/SB3/Ph)	CC
HIP107947	21 52 09.7	-62 03 09	-44	F6	45	30	7.2	6.03	CI, Ks		CCs
HIP108195 ABC	21 55 11.4	-61 53 12	-45	F3	47	30	5.9	4.91	CI, Ks	T (K+N/VIS/Ph+Co)	CCs
AB Dor											
HIP5191 A	01 06 26.1	-14 17 47	-76	K1	50	70	9.5	7.34	CI, H	B (K/VIS/Co)	
HIP25283	05 24 30.2	-38 58 11	-33	K7	18	70	9.2	5.92	CI, H	B (K/VIS/Co)	
ABDor BaBb	05 28 44.3	-65 26 46	-33	M3	15	70	13.0	7.34	CI, H	Q (K/VIS/Ph)	
HIP26369	05 36 55.1	-47 57 48	-32	K7	24	70	9.8	6.61	CI, H	B (K/VIS/Co)	
HIP26373	05 36 56.8	-47 57 53	-32	K0	24	70	7.9	5.81	CI, H	B (K/VIS/Co)	
HIP30314	06 22 30.9	-60 13 07	-27	G0V	23.5	70	6.5	5.04	CI, Ks	B (K/VIS?)	CCs
GSC08894-00426	06 25 55.4	-60 03 29	-27	M2	22	70	12.7	7.21	CI, Ks		CCs
HIP31878	06 39 50.0	-61 28 42	-25	K7	21.9	70	9.7	6.50	CI, Ks		
HIP76768 AB	15 40 28.4	-18 41 45	28	K7	43	70	10.2	6.95	CI, Ks	B (K/VIS/Co)	CCs
HIP113579	23 00 19.2	-26 09 13	-65	G1	32	70	7.5	5.94	CI, Ks		CCs
HIP118008	23 56 10.7	-39 03 08	-77	K3	22.1	70	8.2	5.91	CI, H		
η Cha, Near Cha, Columba and Carina											
M0838	08 38 51.1	-79 16 13	-22	M5	97	6	16.5	10.43	Ks		
HIP58285(TCha)	11 57 13.7	-79 21 32	-16	F5	66.4	10	11.4	6.95	CI, Ks		CCs
GSC08047-00232 A	01 52 14.6	-52 19 33	-62	K3	85	30	10.9	8.41	CI, Ks	B (K/VIS/Co)	
TYC-9390-0322 AB	05 53 29.1	-81 56 53	-29	K0	54	30	9.1	6.94	H	B (N/VIS)	

- (*): S13 camera used in that case

Table 3. Sample of southern young, nearby stars observed

Name	α [J2000]	δ [J2000]	b (deg)	SpT	d (pc)	Age (Myr)	V (mag)	K (mag)	Mode & Filter	Stellar Multiplicity	Note
Additional young candidates											
BTR99 AB	01 23 17.0	-79 41 32	-37	K0	103	10	10.1	7.07	CI, H	B (N/VIS)	
CD-53386 AB	02 01 53.7	-52 34 53	-61	K3	120	30	11.0	8.60	H	B (N/VIS)	
FS75	02 04 53.2	-53 46 16	-60	M4	30	100	15.0	9.6	Ks		
FS84	02 22 44.2	-60 22 47	-53	M4	20	100	13.7	8.2	Ks		
GSC08862-00019	02 58 04.6	-62 41 15	-49	K4	138	20	11.7	8.91	CI, Ks		CCs
TYC6461-1120 A	04 00 03.7	-29 02 16	-48	K0	62	40	9.6	7.15	CI, Ks	B (N/VIS/Co)	CCs
HIP28474 AB	06 00 41.3	-44 53 50	-27	G8	53.7	100	9.1	7.32	CI, H	B (N/VIS)	
FS388 ABC	06 43 45.3	-64 24 39	-25	M4	22	100	14.0	8.4	Ks	T (N/VIS)	
FS465 AB	08 17 39.4	-82 43 30	-24	M4	10	100	12.6	6.6	Ks	B (N/VIS)	
HIP41307	08 25 39.6	-03 54 23	18	A0	38	100	3.9	4.08	CI, Ks		
FS485	08 47 22.6	-49 59 57	-4	M2	33	100	12.0	7.71	Ks		
FS488 AB	08 54 02.4	-30 51 36	9	M5	15	100	13.4	8.10	Ks	B (N/VIS)	
HIP51386	10 29 42.2	+01 29 28	47	F5	31.5	50	6.9	5.52	CI, Ks		CCs
FS588	11 20 06.1	-10 29 47	46	M3	20	100	12.1	7.0	Ks		
HIP59315	12 10 06.4	-49 10 50	13	G5	37.8	100	8.2	6.50	CI, H		CCs
CD-497027	12 21 55.6	-49 46 12	13	K0	89	20	10.1	8.01	Ks		
HIP61468	12 35 45.5	-41 01 19	21	A7	34.6	100	5.1	4.57	CI, H		
TYC-8992-0605	12 36 38.9	-63 44 43	0	K3	50	10	9.9	7.37	CI, H		CCs
TYC-09012-1005	13 44 42.6	-63 47 49	-1	K5	95	10	11.0	7.74	CI, H		CCs
TYC-7818-0504 AB	14 30 13.5	-43 50 09	16	K5	100	10	10.4	7.64	H	B (N/VIS)	
HIP74405	15 12 23.4	-75 15 15	-15	K0	50.2	100	9.4	7.38	CI, H		
TYC-7846-1538	15 53 27.3	-42 16 02	9	G1	48	30	7.9	6.34	CI, H		CCs
HIP80448 ABC	16 25 17.5	-49 08 52	0	K1	45.5	100	7.1	5.70	H	T (K/SB+VIS/Ph+Co)	
HIP84642 AB	17 18 14.7	-60 27 27	-13	K0	54.6	40	9.5	7.53	CI, Ks	B (N/VIS)	CCs
FS903	17 37 46.5	-13 14 47	9	K7	45	100	10.2	6.835	CI, Ks		CCs
FS979 AB	18 35 20.8	-31 23 24	-11	M5	18	100	13.1	7.8	Ks	B (N/VIS)	CCs
FS1017	19 19 20.2	-01 33 54	-6	M5	25	100	16.6	9.667	Ks		CCs
FS1035	19 42 12.8	-20 45 48	-20	M5	20	100	14.4	8.756	Ks		CCs
HIP98495	20 00 35.5	-72 54 37	-31	A0	33.3	50	3.9	3.80	CI, H		
HIP102626	20 47 45.0	-36 35 40	-38	K0	44.4	30	9.4	6.79	CI, H	B (K/HIP?)	
FS1136 AB	21 49 06.2	-64 12 55	-43	M5	25	100	15.5	9.5	CI, Ks	B (N/VIS)	
FS1174	22 44 08.0	-54 13 20	-54	M4	30	100	13.4	8.5	Ks		CCs
Reclassified as older systems											
HIP7805	01 40 24.1	-60 59 57	-55	F2	67	≥ 100	7.7	6.63	CI, H		
HIP69562 ABC	14 14 21.3	-15 21 21	42	K5V	26.5	≥ 100	10.5	6.60	Ks	T (N/VIS)	
HIP76107	15 32 36.7	-52 21 21	3	M0	30.6	≥ 100	11.0	7.60	CI, Ks	B (K/HIP?)	CCs
HIP96334	19 35 09.7	-69 58 32	-29	G1V	35.4	≥ 100	7.9	6.30	CI, Ks		CCs
HIP107705 AB	21 49 05.8	-72 06 09	-39	M0	16.1	200	9.8	5.65	Ks	B (N/VIS)	

overall uniform age of 100 Myr for the sample of FS stars, we are probably somewhat overestimating their mean age. The age determination of the ensemble of FS stars is likely to be accurate to within about a factor 2 in general, although the age of some FS stars could well lie outside of this range.

The sample properties are summarized in Tables 2 and 3 and illustrated in Fig. 1. 93% of the selected stars are younger than about 100 Myr and 94% closer than 100 pc. The spectral types cover the sequence from B to M spectral types with 19% BAF stars, 48% GK stars and 33% M dwarfs.

3. Observations

3.1. Telescope and instrument

NACO¹ is the first Adaptive Optics instrument that was mounted at the ESO Paranal Observatory near the end of 2001 (Rousset et al. 2002). NACO provides diffraction limited images in the near infrared (nIR). The observing camera CONICA (Lenzen et al. 2002) is equipped with a 1024 × 1024 pixel Aladdin InSb

array. NACO offers a Shack-Hartmann visible wavefront sensor and a nIR wavefront sensor for red cool (M5 or later spectral type) sources. nIR wavefront sensing was only used on 8% of our sample. Note that in May 2004, the CONICA detector was changed and the latter detector was more efficient thanks to an improved dynamic, a lower readout noise and cleaner arrays. Among NACO's numerous observing modes, only the direct and coronagraphic imaging modes were used. The two occulting masks offered for Lyot-coronagraphy have a diameter of $\varnothing = 0.7''$. and $\varnothing = 1.4''$. According to the atmospheric conditions, we used the broad band filters H and K_s , the narrow band filters, NB1.64, NB1.75 and Br γ ² and a neutral density filter (providing a transmissivity factor of 0.014). In order to correctly sample the NACO PSF (better than Nyquist), the S13 and S27 objectives were used, offering mean plate scales of 13.25 and 27.01 mas per pixel and fields of view of 14'' × 14'' and 28'' × 28'' respectively.

Our deep imaging survey was initiated during guaranteed time observations shared between different scientific programs and scheduled between November 2002 and September 2003.

¹ <http://www.eso.org/instruments/naos/>

² see filters description: <http://www.eso.org/instruments/naco/inst/filters.html>

Table 4. Summary of the different observing campaigns of our survey. For each campaign, we report the ESO programme numbers, the observation type, Guaranteed Time (GTO) or Open Time (OT), if obtained in visitor (Vis) or service (Ser) modes, the starting nights of observation, the number of nights allocated and the time loss. Finally, the number of visits, corresponding to the number of observing sequences executed on new and follow-up targets, is given.

ESO Program	Mode	Start. Night (UT-date)	Night (Nb)	Loss (%)	Visits (Nb)
070.C-0565(A)	GTO-Vis	26-11-2002	1		6
070.D-0271(B)	GTO-Vis	16-03-2003	1.5		8
071.C-0507(A)	GTO-Vis	07-06-2003	0.5	50	2
071.C-0462(A)	GTO-Vis	07-09-2003	0.5	50	2
072.C-0644(A)	OT-Vis	05-03-2004	1	100	0
072.C-0644(B)	OT-Vis	05-03-2004	1	0	9
073.C-0469(A)	OT-Vis	27-04-2004	1	0	16
073.C-0469(B)	OT-Vis	25-09-2004	1	0	12
075.C-0521(A)	OT-Vis	06-05-2005	1	0	15
075.C-0521(B)	OT-Vis	19-08-2005	0.5	0	10
076.C-0554(A)	OT-Vis	08-01-2006	1	0	13
076.C-0554(B)	OT-Vis	26-02-2006	1	30	8
078.C-0494(A)	OT-Ser	2006/2007	0.7	30	7
079.C-0908(A)	OT-Ser	2007	1	0	10
Total	-	-	11.7		127

The survey was extended using open time observations between March 2004 and June 2007. The open time observations were shared between classical visitor mode and remote service mode as offered by ESO at the Paranal Observatory. The observing programs, observing modes, the number of nights allocated, the time loss due to technical or weather reasons and the number of targets observed per run are reported in Table 4.

3.2. Image quality

For ground-based telescopes, atmospheric conditions have always been critical to ensure astronomical observations of good quality. Although AO instruments aim at compensating the distortion induced by atmospheric turbulence, the correction quality (generally measured by the *strehl ratio* and *Full Width Half Maximum (FWHM)* parameters) is still related to the turbulence speed and strength. For bright targets, the NACO AO system can correct for turbulence with a coherent time (τ_0) longer than 2 ms. For faster ($\tau_0 \leq 2$ ms) turbulence, the system is always late and the image quality and the precision of astrometric and photometric measurements are consequently degraded. During our NACO observing runs, the averaged τ_0 was about 5 ms and larger than 2 ms 80% of the time. The average seeing conditions over all runs was equal to 0.8'' (which happens to be the median seeing value measured in Paranal over the last decade³). Fig. 2 shows the (*strehl ratio*) performances of the NACO AO system with the visible wavefront sensor as a function of the correlation time of the atmosphere τ_0 , the seeing and the primary visible magnitude. As expected, the degradation of the performances is seen with a decrease of τ_0 , the coherent length (r_0), inversely proportional to the seeing) and the primary flux. Still, the results clearly demonstrate the good NACO performances and capabilities over a wide range of observing conditions.

³ <http://www.eso.org/gen-fac/pubs/astclim/paranal/seeing/adaptive-optics/statfwhm.html>

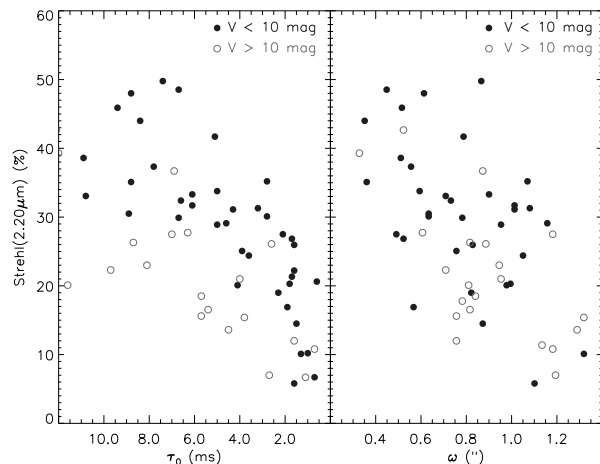


Fig. 2. VLT/NACO adaptive optics system performances. Strehl ratio at 2.20 μm as a function of the correlation time τ_0 and the seeing ω of the atmospheric turbulence for two regimes of V -band magnitude of the primary star (AO reference target). Only the targets observed with the visible WFS are plotted. Close binaries have also been rejected. The results demonstrate the good behavior of NACO over a wide range of stellar magnitudes and under different turbulent conditions. A clear degradation of the performances is seen for decreasing τ_0 , increasing ω and fainter visible ($V \geq 10$) targets. A clear drop is seen for τ_0 faster than 2 ms, the limit of the NACO wavefront sensor sampling frequency.

3.3. Observing strategy

The VLT/NACO survey was conducted as a continuation of our earlier coronagraphic survey with the ADONIS/SHARPII instrument at the ESO 3.6 m telescope at La Silla Observatory (Chauvin et al. 2003). A similar observing strategy was adopted to optimize the detection of faint close substellar companions. Most of our stars are relatively bright ($K_s \leq 10$) in nIR. To improve our detection performances, we have opted for the use of Lyot coronagraphy. High contrast imaging techniques, such as Lyot and phase mask coronagraphy, L -band saturated imaging and simultaneous differential imaging, enable achievement of contrasts of 10^{-5} to 10^{-6} . Their main differences are inherent in the nature of the substellar companions searched and the domain of separations explored. Broad-band nIR Lyot coronagraphy and thermal (L' -band or 4 μm) saturated imaging are among the most sensitive techniques at typical separations between 1.0 to 10.0''. The contrast performances are currently mandatory to access the planetary mass regime when searching for faint close companions.

To measure precisely the positions of the faint sources detected in the coronagraphic field relative to the primary star, a dedicated observing block was executed. This block was composed of three successive observing sequences and lasted in total ~ 45 min (including pointing). After the centering of the star behind the coronagraphic mask, a deep coronagraphic observing sequence on source was started. Several exposures of less than one minute each were accumulated to monitor the star centering and the AO correction stability. An effective exposure time of 300 sec was generally spent on target. During the second sequence, a neutral density or a narrow band filter was inserted and the occulting mask and Lyot stop removed. The goal was to precisely measure the star position behind the coronagraphic mask

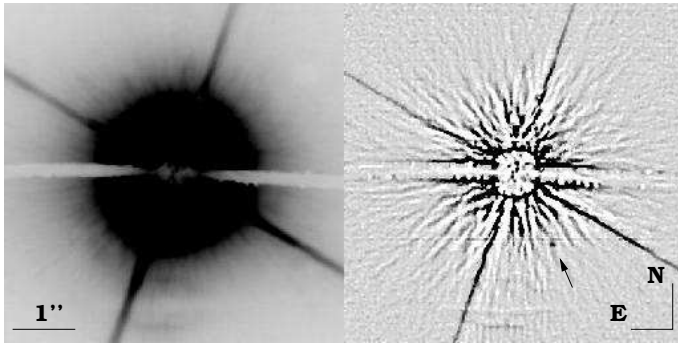


Fig. 3. *Left:* VLT/NACO coronagraphic image of HIP 95270 obtained in H -band with the S13 camera. The small ($\varnothing = 0.7''$) coronagraphic mask was used. *Right:* Coronagraphic image after high-pass filtering. A kernel of $3 \times FWHM$ is used to remove the low spatial frequencies of the coronagraphic PSF wings. A fake $\Delta H = 12$ companion has been inserted at $1.2''$ from the star to test the detection performances. Minimum and maximum thresholds of the filtered image were divided by a factor 15 to show the fake companion and the PSF residuals.

(once corrected for filter shifts). An effective exposure time of 60 sec was spent on source. Counts were adjusted to stay within the 1% linearity range of the detector. The image is also used to estimate the quality of the AO correction. Finally, the last sequence was the coronagraphic sky. This measure was obtained $\sim 45''$ from the star using a jittering pattern of several offset positions to avoid any contaminants in the final median sky. In case of positive detections, whenever possible, the companion candidates (CCs) were re-observed to check whether a faint object shared common proper motion with the primary star. Depending on each object's proper motion (see Fig. 1), the timespan between successive epochs was about 1-2 years. When comoving companions were identified, images were recorded with additional nIR filters to directly compare the spectral energy distribution with that predicted by (sub)stellar evolutionary models.

4. Data reduction and analysis

4.1. Cosmetic and image processing

Classical cosmetic reduction including bad pixels removal, flat-fielding, sky subtraction and shift-and-add, was made with the *Eclipse*⁴ reduction software developed by Devillar (1997) for both direct and coronagraphic imaging observations. Median filtering by a kernel of 3×3 pixels was applied to correct for remaining hot pixels. To remove the central part of the PSF in our reduced coronagraphic images, two methods were applied. The first method considered different angular sectors uncontaminated by the diffraction spikes and by the coronagraphic mask support. For each sector, the PSF azimuthal average is calculated, circularised and subtracted from the coronagraphic image. The alternative method was to apply directly a high-pass filter with a kernel of $3 \times FWHM$ (assuming the theoretical $FWHM$ at each observing set-up). As a result, low spatial frequencies, including the coronagraphic PSF wings, were removed from the reduced image. Finally, each resulting image was inspected by eye for the CCs identification. Fig. 3 is an illustration of the data processing applied to the coronagraphic images of HIP 95270, in the case of the second method.

Table 5. Mean plate scale and true north orientation for each observing run. The astrometric field Θ_1 Ori C field and the astrometric binary IDS21506S5133 (van Dessel & Sinachopoulos 1993) were the calibrators.

ESO Program	UT Date	Obj.	Platescale (mas)	True north (deg)
070.C-0565	21-11-2002	S13	13.24 ± 0.05	-0.05 ± 0.10
	21-11-2002	S27	27.01 ± 0.05	0.08 ± 0.18
070.D-0271	16-03-2003	S13	13.21 ± 0.11	-0.05 ± 0.10
071.C-0507	29-05-2003	S13	13.24 ± 0.05	-0.10 ± 0.10
	03-06-2003	S27	27.01 ± 0.05	0.01 ± 0.19
071.C-0507	07-09-2003	S13	13.24 ± 0.05	0.05 ± 0.10
072.C-0644	05-03-2004	S13	13.24 ± 0.05	0.04 ± 0.10
	05-03-2004	S27	27.01 ± 0.05	-0.18 ± 0.20
073.C-0469	27-04-2004	S27	27.01 ± 0.05	0.08 ± 0.20
073.C-0469	22-09-2004	S13	13.25 ± 0.05	0.20 ± 0.10
	22-09-2004	S27	27.01 ± 0.05	0.0 ± 0.19
075.C-0521	19-08-2005	S13	13.25 ± 0.06	-0.02 ± 0.10
	19-08-2005	S27	27.01 ± 0.06	-0.07 ± 0.11
076.C-0654	08-01-2006	S13	13.25 ± 0.06	0.18 ± 0.10
	08-01-2006	S27	27.02 ± 0.06	0.12 ± 0.13
076.C-0654	28-02-2006	S13	13.25 ± 0.06	0.19 ± 0.10
	28-02-2006	S27	27.02 ± 0.05	0.13 ± 0.14
078.C-0494	24-10-2006	S13	13.26 ± 0.07	-0.19 ± 0.23
	23-12-2006	S13	13.26 ± 0.08	-0.23 ± 0.15
	22-10-2006	S27	27.01 ± 0.03	-0.30 ± 0.16
	25-12-2006	S27	27.01 ± 0.04	-0.20 ± 0.18
079.C-0908	18-07-2007	S27	27.01 ± 0.05	-0.06 ± 0.15

4.2. Astrometric calibration

The astrometric calibration of high angular resolution images as provided by NACO is not a simple task. As NACO is not a multi-conjugated AO system, the diffraction limited images have a small FoV limited by the anisoplanatism angle. Therefore, classical high-precision astrometric techniques over crowded fields of thousands of stars cannot be transposed. In addition, ESO does not currently provide any detector distortion map. For this reason, astrometric calibrators were observed within a week for each observing run (in visitor and service mode) to determine a mean platescale and the true north orientation. Our primary astrometric calibrator was the Θ_1 Ori C field observed with HST by McCaughrean & Stauffer (1994). The same set of stars (TCC058, 057, 054, 034 and 026) were observed with the same observing set-up (K_s with S27 and H with S13) to avoid introduction of systematic errors. When not observable, we used as secondary calibrator the astrometric binary IDS21506S5133 (van Dessel & Sinachopoulos 1993), yearly recalibrated with the Θ_1 Ori C field. The mean orientation of true north and the mean platescale of the S13 and S27 cameras are reported in Table 5.

4.3. Companion candidate characterization

For direct imaging, the relative photometry and astrometry of visual binaries were obtained using the classical deconvolution algorithm of Véran & Rigaut (1998). This algorithm is particularly adapted for stellar field analysis. Several PSF references were used to measure the influence of the AO correction. They were selected to optimize a set of observing criteria relative to the target observation (observing time, airmass, spectral type and V or K -band flux according to the wavefront sensor).

In coronagraphy, the relative astrometry of the CCs was obtained using a 2D-gaussian PSF fitting. The deconvolution algorithm of Véran & Rigaut (1998) and the maximization of

⁴ <http://www.eso.org/projects/aot/eclipse/>

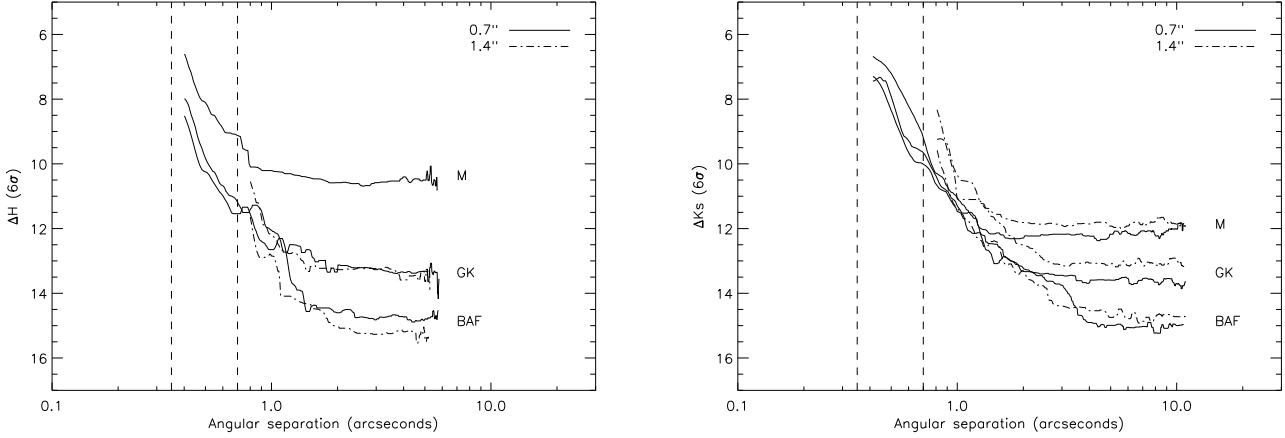


Fig. 4. *Left:* VLT/NACO coronagraphic detection limits in H-band (combined with the S13 camera). The median detection limits are given for different target spectral types (BAF, GK and M stars) and for the 0.7'' (solid line) and 1.4'' (dash dotted line) coronagraphic masks. *Right:* VLT/NACO coronagraphic detection limits in K_s -band (combined with the S27 camera). The median detection limits are also given for different target spectral types and coronagraphic masks.

the cross-correlation function were applied using the primary star (directly imaged) as PSF reference. The shifts (≤ 1 pixel) induced between direct and coronagraphic images taken with different filters, including neutral density, have been accounted for. For the relative photometry, classical aperture ($R_{ap} = 2 \times FWHM$) photometry with residual sky-subtraction and classical deconvolution were used. For faint sources detected at less than $\sim 10 \sigma$, the background subtraction become more critical and is responsible for larger uncertainties in the deconvolution analysis. Our analysis was then limited to a 2D-gaussian fitting coupled to aperture photometry to derive the relative astrometry and photometry.

For observations obtained at several epochs, the proper motion and parallactic motion of the primary star were taken into account to investigate the nature of detected faint CCs. The relative positions recorded at different epochs can be compared to the expected evolution of the position measured at the first epoch under the assumption that the CC is either a stationary background object or a comoving companion (see below). For the range of semi-major axes explored, any orbital motion can be considered of lower order compared with the primary proper and parallactic motions.

4.4. Detection limits

The coronagraphic detection limits were obtained using combined direct and coronagraphic images. On the final coronagraphic image, the pixel-to-pixel noise was estimated within a box of 5×5 pixels sliding from the star to the limit of the NACO field of view. Angular directions free of any spike or coronagraphic support contamination were selected. Additionally, the noise estimation was calculated within rings of increasing radii, a method which is more pessimistic at close angular separation due to the presence of coronagraphic PSF non-axisymmetric residuals. Final detection limits at 6σ were obtained after division by the primary star maximum flux and multiplication by a factor taking into account the ratio between the direct imaging and coronagraphic integration times and the difference of filter transmissions and bandwidths. Spectral type correction due to the use of different filters has been simulated and is smaller than 0.04 mag. The variation of the image quality (*strehl ratio*) over

the observation remains within 10% and should not impact our contrast estimation from more than 0.1 mag. The median detection limits, using the sliding box method, are reported in Fig. 4. They are given for observations obtained in H- and K_s -bands, with the $\phi = 0.7''$ and $\phi = 1.4''$ coronagraphic masks and for different target spectral types (BAF, GK and M stars) and will be used for the following statistical analysis of the survey.

At large separations ($\geq 1.0 - 2.0''$) from the star when limited by detector read-out noise or background noise, the contrast variation with the primary spectral type is actually related to the primary nIR brightness. This is shown in Fig. 5 in the case of K_s -band detection limits at $5.0''$ as a function of the primary K_s apparent magnitude. The contrast varies linearly due to the flux normalization. At shorter separations, the situation is more complex as AO deep images are actually limited by the speckle noise. Our detection limits remain constant over a wide range of primary K_s apparent magnitudes.

All published deep imaging surveys dedicated to planet search (Masciadri et al. 2005; Kasper et al. 2007; Lafrenière et al. 2007; Biller et al. 2007), including this one, derived detection threshold assuming that the residual noise in the final processed image follows a Gaussian intensity distribution. A typical detection threshold at 5 or 6σ is then usually assumed over the complete angular range. Whereas the approximation of a Gaussian distribution for the residual noise is valid within the detector read-out noise or background noise regime, careful analysis by Marois et al. (2008a) shows that this is not adequate at small separations when speckle noise limited (typically $\leq 1.0 - 2.0''$ in our survey; see Fig. 4). In this regime, AO deep images are actually not limited by random, short-lived atmospheric speckles, but by instrumental quasi-static speckles. A non-gaussian distribution of the residual noise must be taken into account to specify a detection threshold at a given confidence level. Therefore, our current 6σ detection threshold at small separations is probably too optimistic. However, the systematic error induced in our sensitivity limits is probably of lower significance than uncertainties in planet age and use of uncalibrated planet evolutionary models as described below.

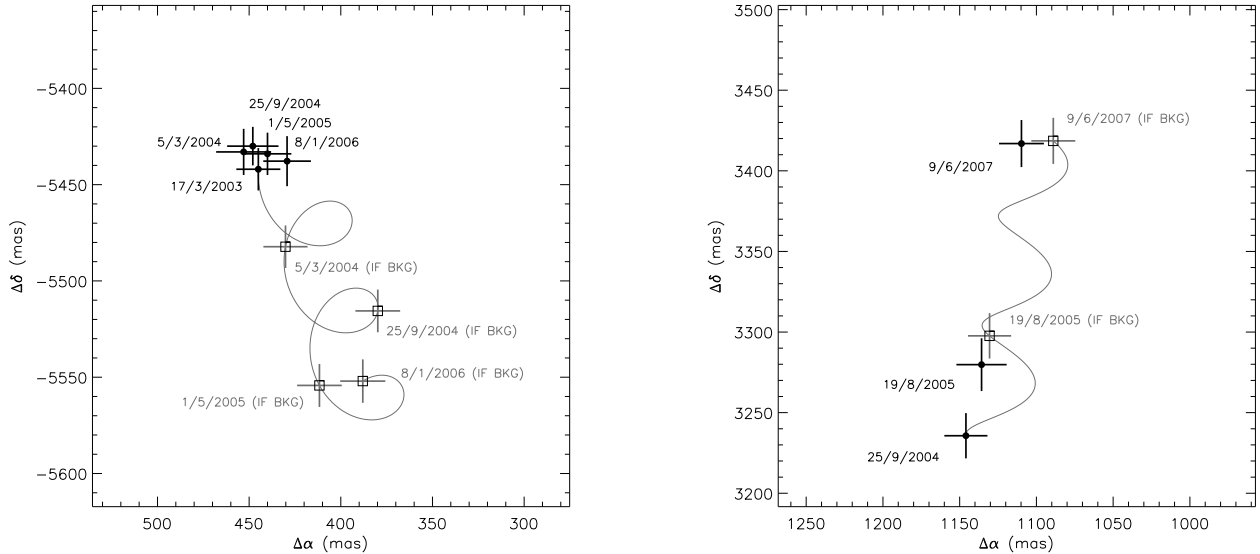


Fig. 6. VLT/NACO Measurements (*full circles* with uncertainties) of the offset positions of the comoving companion AB Pic b to A (*left*) and of the CC relative to 0ES1847 (*right*). For each diagram, the expected variation of offset positions, if the candidate is a background object, is shown (*solid line*). The variation is estimated based on the parallactic and proper motions of the primary star, as well as the initial offset position of the CC from A. The *empty boxes* give the corresponding expected offset positions of a background object for the different epochs of observations (with uncertainties). In the case of AB Pic b, the relative positions do not change with time confirming that AB Pic b is comoving. On the contrary, the relative position of the CC to 0ES1847 varies in time as predicted for a background stationary contaminant. For our sample, astrometric follow-up over 1-2 years enabled a rapid identification.

5. Results

The main purpose of our survey was the detection of close brown dwarf and planetary mass companions using the deep imaging technique on an optimized sample of nearby stars. Compared to other works, our strategy has been successful with the confirmation of the brown dwarf companion to GSC 08047-00232 (Chauvin et al. 2003; 2005a) and the discoveries of one planetary mass companion, around the young brown dwarf 2MASSW J1207334-393254 (hereafter 2M1207; Chauvin et al. 2004; 2005c) and one companion at the planet/brown dwarf boundary to the young star AB Pic (Chauvin et al. 2005b).

In this section, we detail the three main results of this survey:

1. the identification of a large fraction of contaminants in the close angular environment of our sample of young, nearby stars. This identification step is necessary for the statistical analysis of our complete set of detection limits (see below). Contaminants identification serves in addition to the preparation of future deep imaging search of exoplanets that will re-observe most of these stars.
2. the discovery of several new close stellar multiple systems, despite our binary rejection process. Three systems are actually confirmed to be comoving. One is a possible low-mass calibrator for the predictions of evolutionary models.
3. Finally, we review the status of the three substellar companions, confirmed with NACO, in regards of the latest results in the literature and from our survey.

5.1. Contaminant identification

Among the complete sample composed of 88 stars, a total of 65 were observed with coronagraphic imaging. The remaining 23 targets were observed in direct or saturated imaging because the system was resolved as a $1.0 - 12''$ visual binary inappropriate for deep coronagraphic imaging, because the atmospheric conditions were unstable or because the system was simply too faint to warrant efficient use of the coronagraphic mode.

Among the 65 stars observed with both direct imaging and coronagraphy, nothing was found around 29 (45%) stars and at least one CC was detected around the 36 (55%) others. A total of ~ 236 CCs were detected. To identify their nature, 14 (39%) systems were observed at two epochs (at least) with VLT and 16 (44%) have combined VLT and HST observations at more than a one year interval (Song et al. 2009, in prep). Finally, 6 (17%) were observed at only one epoch and require further follow-up observations. The position and photometry of each detected CC relative to its primary star, at each epoch, are given in Tables 7-13. For multi-epoch observations, to statistically test the probability that the CCs are background objects or comoving companions, a χ^2 probability test of $2 \times N_{epochs}$ degrees of freedom (corresponding to the measurements: separations in the $\Delta\alpha$ and $\Delta\delta$ directions for the number N_{epochs} of epochs) was applied. This test takes into account the uncertainties in the relative positions measured at each epoch and the uncertainty in the primary proper motion and parallax (or distance). Fig. 6 gives an illustration of a ($\Delta\alpha$, $\Delta\delta$) diagram that was used to identify a stationary background contaminant near 0ES1847. A status of each CC has been assigned as confirmed companion (C; $P_{\chi^2} < 0.1\%$), background contaminant (B; $P_{\chi^2} > 99\%$), probably background (PB;

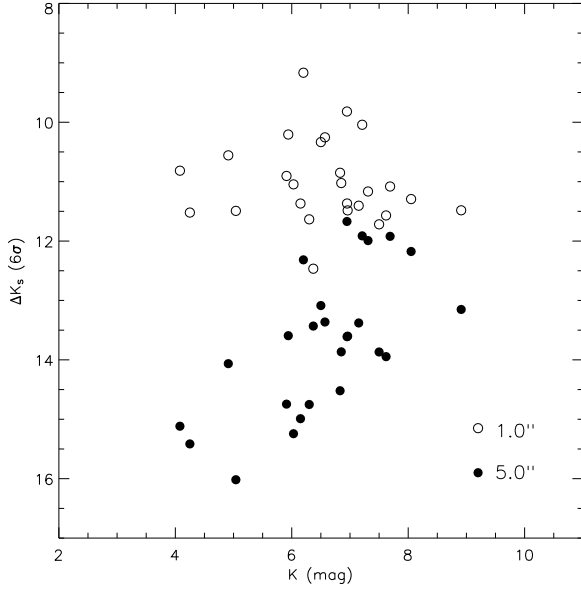


Fig. 5. VLT/NACO coronagraphic detection limits in K_s -band as a function of the primary star brightness for two angular separations (1.0'' and 5.0''). Two regimes can be seen; one at large separations (shown here at 5.0'') when the detection is limited by detector read-out noise or background noise. The contrast varies then linearly with the primary K_s apparent magnitude due to the flux normalization; a second regime at shorter separations (shown here at 1.0'') when the detection is speckle noise limited. Instrumental quasi-static speckles are expected to dominate random, short-lived atmospheric speckles and the contrast remains relatively constant over a wide range of primary K_s apparent magnitudes.

$P_{\chi^2} > 99\%$, but combining data from two different instruments) and undefined (U). Over the complete coronagraphic sample, 1% of the CCs detected have been confirmed as comoving companions, 43% have been identified as probable background contaminants and about 56% need further follow-up observations. The remaining CCs come mostly from the presence of background crowded fields in the field of view of the 6 stars observed at one epoch.

Among the 23 stars and brown dwarfs observed only in direct or saturated imaging, several have been resolved as tight multiple systems (see below). 4 stars (FS1174, FS979, FS1017 and FS1035) have at least one substellar CC (see Tables 12, 13 and 14). FS1035 was observed at two successive epochs and the faint object detected at $\sim 5.6''$ has been identified as a contaminant.

5.2. Close stellar multiple systems

5.2.1. New visual binaries

Our survey was not aimed at detecting new stellar binaries. Known bright equal-mass binaries of 1.0 – 12.0'' separation were rejected from our sample as they degrade the coronagraphic detection performances by limiting dynamical range. A few tight binaries were kept when both components could be placed behind the coronagraphic masks. Despite our binary rejection process, 17 new close visual multiple systems were re-

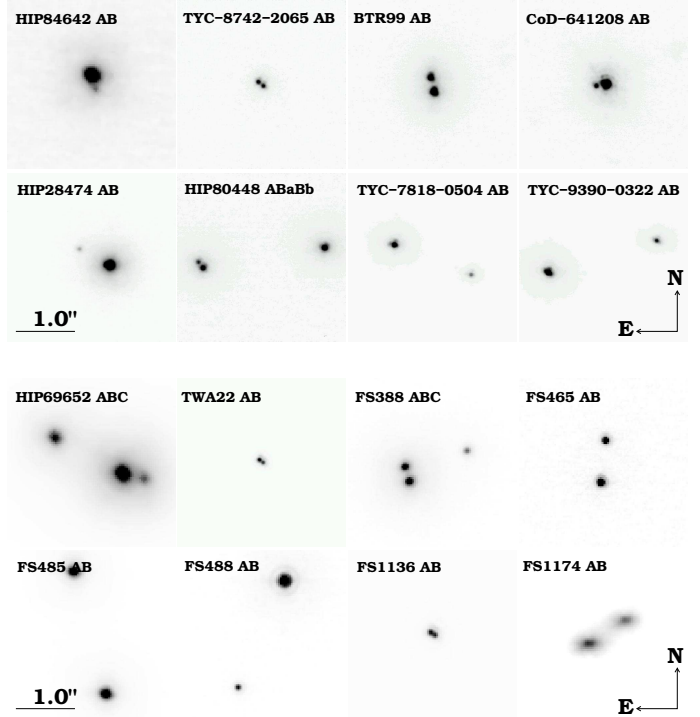


Fig. 7. New visual binaries resolved with NACO at VLT. HIP 108195 AB, HIP 84642 AB and TWA22 AB were in addition confirmed as comoving multiple systems. TWA22 AB was monitored for 4 years to constrain the binary orbit and determine its total dynamical mass (see Bonnefoy et al. 2009, accepted)

solved (see Fig. 7 and 8). They include 13 tight resolved binaries and 4 triple systems. Their relative flux and position are reported in Table 6. Their separations range between 0.1 – 5.0'' and their H and K_s contrasts between 0.0 – 4.8 mag. Among them, HIP 108195 ABC, HIP 84642 AB and TWA22 AB were observed at different epochs and are confirmed as comoving systems.

5.2.2. The comoving multiple systems HIP 108195 ABC and HIP 84642 AB

Close to the Hipparcos double star HIP 108195 AB (F3, 46.5 pc), member of Tuc-Hor, we resolved a faint source at $4.96''$ ($\Delta_{proj} = 230$ AU; i.e. $a \sim 290$ AU). In addition to a confirmation that HIP 108195 AB is a comoving pair, we found that the fainter source is a third component of this comoving multiple system (Fig. 8). Combined distance, age and apparent photometry are compatible with an M5-M7 dwarf according to PMS model predictions (Siess et al. 2000) and places the companion at the stellar/brown dwarf boundary.

HIP 84642 (K0, 58.9 pc) is not reported as a double star in the Hipparcos Visual Double Stars catalog (Dommanget et al. 2000), possibly due to the small angular separation and the flux ratio with the visual companion. Based on combined VLT/NACO images from our programme and from the SACY survey (Huélamo et al. 2009, in prep), we confirm that the companion shares common proper motion with HIP 84642. This object is likely to be an M4-M6 young dwarf comparing its photometry to predictions of PMS models. Based on the statistical relation between projected separation and semi-major

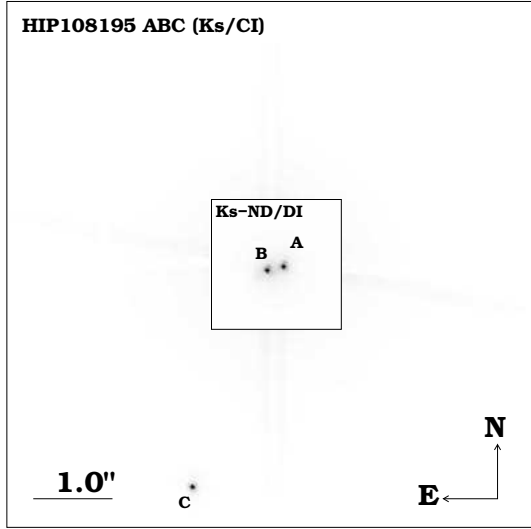


Fig. 8. Composite VLT/NACO K_s -band image of the triple comoving system HIP108195 ABC. The inner part shows the direct image (DI) of HIP108195 AB (attenuated by a factor ~ 100) using the K_s -band with a neutral density filter to avoid saturation. Both components of the astrometric binary cataloged by Hipparcos are resolved. The outer part shows the deeper coronagraphic image obtained in K_s -band with the C component about 100 times fainter than A or B.

Table 6. Relative positions and K_s and H -band contrast of the new binaries resolved by NACO at VLT. Contrast uncertainty is about 0.1 mag.

Name	UT Date	Δ (mas)	P.A. (deg)	ΔK_s (mag)
HIP108195 AB	19-08-2005	339 ± 5	102.7 ± 0.2	0.0
AC	19-08-2005	4964 ± 9	158.4 ± 0.2	4.8
HIP84642 AB	05-06-2007	220 ± 14	191.3 ± 0.8	2.5
TYC-8742-2065 AB	27-04-2004	114 ± 2	232.5 ± 0.4	0.2
BTR99 AB	25-09-2004	264 ± 3	12.8 ± 0.3	0.5
CoD-641208 AB	25-09-2004	178 ± 3	95.3 ± 0.4	2.3
HIP80448 BaBb	27-04-2004	134 ± 2	37.5 ± 0.7	1.1
HIP69652 AB	26-02-2006	319 ± 6	256.8 ± 0.5	1.3
AC	26-02-2006	1123 ± 6	61.8 ± 0.4	0.8
TWA22 AB	05-03-2004	100 ± 5	80.2 ± 0.2	0.4
FS388 AB	08-01-2006	224 ± 5	16.4 ± 0.6	0.3
AC	08-01-2006	963 ± 6	297.7 ± 0.2	1.6
FS465 AB	08-01-2006	619 ± 6	353.4 ± 0.3	0.7
FS488 AB	08-01-2006	1710 ± 7	156.6 ± 0.1	2.8
FS485 AB	26-02-2006	1862 ± 7	14.7 ± 0.1	0.2
FS1136 AB	19-08-2005	74 ± 5	122.0 ± 0.8	0.2
FS1174 AB	19-08-2005	626 ± 6	302.7 ± 0.5	0.4

Name	UT Date	Δ (mas)	P.A. (o)	ΔH (mag)
HIP28474 AB	27-04-2004	613 ± 3	61.7 ± 0.2	3.8
TYC-7818-0504 AB	17-03-2003	1463 ± 6	111.3 ± 0.2	1.7
TYC-9390-0322 AB	17-03-2003	2005 ± 7	286.3 ± 0.1	1.6

axis of Couteau (1960), HIP84642 AB is likely to be a tight ($\Delta_{proj} = 14$ AU; $a \sim 18$ AU; K0-M5) binary with a period of several tens of years.

5.2.3. The young, tight astrometric binary TWA22 AB

The tight (~ 100 mas; $a \sim 1.8$ AU) binary TWA22 AB was observed at several epochs. We aimed at monitoring the system orbit to determine the total dynamical mass of this system using an accurate distance determination (17.53 ± 0.21 pc, Teixeira et al. 2009, submitted). The physical properties (luminosity, effective temperature and surface gravity) of each component were obtained based on near-infrared photometric and spectroscopic observations. By comparing these parameters with evolutionary model predictions, we consider the age and the association membership of the binary. A possible under-estimation of the mass predicted by evolutionary model for young stars close to the sub-stellar boundary is presented in two dedicated papers (Bonnetfoy et al. 2009, accepted; Teixeira et al. 2009, accepted).

5.3. Substellar companions

We review below the latest results about the three substellar companions GSC 08047-00232 B, AB Pic b and 2M1207 b since their initial companionship confirmation. Recent age, distance, astrometric and spectroscopic measurements enable us to refine their predicted physical properties and their origin in regards to other confirmed substellar companions in young, nearby associations.

5.3.1. GSC 08047-00232 B

Based on the ADONIS/SHARPII observations of two dozen probable association members of Tuc-Hor, Chauvin et al. (2003) identified a $20 \pm 5 M_{Jup}$ candidate to GSC 08047-00232 (CoD-52381). This candidate was independently detected by Neuhäuser et al. (2003) with the SHARP instrument at the ESO *New Technology Telescope* (NTT). Neuhäuser & Guenther (2004) acquired H - and K -band spectra and derived a spectral type $M8 \pm 2$, corroborated by Chauvin et al. (2005a). Finally, in the course of our VLT/NACO observations, we confirmed that GSC 08047-00232 B was comoving with A (Chauvin et al. 2005a). Mass, effective temperature and luminosity were determined by comparing its JHK photometry with evolutionary model predictions and the Tuc-Hor age and photometric distance for the system. The results are reported in Table 7 and compared to the complete list of confirmed substellar companions discovered among the young, nearby associations. Membership in Tuc-Hor and the assigned age of GSC 08047-00232 AB have been debated for a time. Further studies of loose young associations sharing common kinematical and physical properties recently led Torres et al. (2008) to identify GSC 08047-00232 AB as a high-probability (80%) member of the Columba association of age 30 Myr, confirming the young age and the brown dwarf status of GSC 08047-00232 B.

5.3.2. AB Pic b

During our survey, a $13 \pm 2 M_{Jup}$ companion was discovered near the young star AB Pic (Chauvin et al. 2005b). Initially identified by Song et al. (2003) as a member of Tuc-Hor, the membership of AB Pic has been recently discussed by Torres et al. (2008) who attached this star to the young (~ 30 Myr) Columba association. Additional astrometric measurements of the relative position of AB Pic b to A firmly confirm the companionship reported by Chauvin et al. (2005b; see Fig. 6, *left panel*). Based on age, distance and nIR photometry, Chauvin et al. (2005b) derived the physical properties of AB Pic b based on evolutionary

models (see Table 7). As per the three young substellar companions to TWA5A, HR7329 and GSC 08047-00232, AB Pic b is located at a projected physical separation larger than 80 AU. Formation by core accretion of planetesimals seems unlikely because of inappropriate timescales to form planetesimals at such large distances. Gravitational instabilities within a protoplanetary disk (Papaloizou & Terquem 2001; Rafikov 2005; Boley 2009) or Jeans-mass fragmentation proposed for brown dwarf and stellar formation appear to be more probable pathways to explain the origin of the Table 7 secondaries.

5.3.3. 2M1207 b

Among the young candidates of our sample, a small number of very low mass stars and brown dwarfs were selected to take advantage of the unique capability offered by NACO at VLT to sense the wavefront in the IR. Most were observed in direct and saturated imaging. This strategy proved to be successful with the discovery of a planetary mass companion in orbit around the young brown dwarf 2M1207 (Chauvin et al. 2004; 2005c). HST/NICMOS observations independently confirmed this result (Song et al. 2006). A low signal-to-noise spectrum in H-band enabled Chauvin et al. (2004) to suggest a mid to late-L dwarf spectral type, supported by its very red nIR colors. Additional low signal-to-noise spectroscopic observations compared with synthetic atmosphere spectra led Mohanty et al. (2007) to suggest an effective spectroscopic temperature of 1600 ± 100 K and a higher mass of $8 \pm 2 M_{\text{Jup}}$. To explain the companion under-luminosity, Mohanty et al. (2007) have suggested the existence of a circum-secondary edge-on disk responsible for a gray extinction of ~ 2.5 mag between 0.9 and $3.8 \mu\text{m}$. However, synthetic atmosphere models clearly encounter difficulties in describing faithfully the late-L to mid-T dwarfs transition (~ 1400 K for field L/T dwarfs), corresponding to the process of cloud clearing. Similar difficulties have been encountered by Marois et al. (2008b) to reproduce all photometric data of the three planetary mass companions to HR 8799 that fall also at the edge or inside the transition of cloudy to cloud-free atmospheres. In the case of 2M1207 b, future spectroscopic or polarimetric observations should help to distinguish between the two scenarios (obscured or non-obscured by a circumstellar disk). Recent precise parallax determinations (Gizis et al. 2007; Ducourant et al. 2008) allowed a reevaluation of the distance and the physical properties of the companion (see Table 7).

6. Statistical analysis

6.1. Context

Over the past years, a significant number of deep imaging surveys have been reported in the literature, dedicated to the search for exoplanets around young, nearby stars (Chauvin et al. 2003; Neuhäuser et al. 2003; Lowrance et al. 2005; Masciadri et al. 2005; Biller et al. 2007; Kasper et al. 2007; Lafrenière et al. 2007). Various instruments and telescopes were used with different imaging techniques (coronagraphy, angular or spectral differential imaging, L' -band imaging) and observing strategies. None of those published surveys have reported the detection of planetary mass companions that could have formed by a core-accretion model (as expected for a large fraction of planet candidates reported by RV measurements). Several potential planetary mass companions were discovered, but generally at relatively large physical separations or with a small mass-ratio with their primaries, suggesting a formation mechanisms sim-

ilar to (sub)stellar binaries and stars. Only very recently, planet candidates perhaps formed by core-accretion have been imaged around the stars Fomalhaut (Kalas et al. 2008), HR 8799 (Marois et al. 2008b) and β Pictoris (Lagrange et al. 2009), initiating the study of giant exo-planets at the (mass, distance) scale of our solar system.

Confronted with a null-detection of planets formed by core-accretion, several groups (Kasper et al. 2007; Lafrenière et al. 2007; Nielsen et al. 2008) have developed statistical analysis tools to exploit the complete deep imaging performances of their surveys. A first approach is to test the consistency of various sets of (mass, eccentricity, semi-major axes) parametric distributions of a planet population in the specific case of a null detection. A reasonable assumption is to extrapolate and normalize planet mass, period and eccentricity distributions using statistical results of RV studies at short periods. Given the detection performances of a survey, the rate of detected simulated planets (over the complete sample) enables derivation of the probability of non-detection of a given planet population associated with a normalized distribution set. Then comparison with a survey null-detection sample tests directly the statistical significance of each distribution and provides a simple approach for constraining the outer portions of exoplanetary systems.

A second more general approach aims at actually constraining the exoplanet fraction f within the physical separation and mass probed by the survey, in the case of null or positive detections. Contrary to what was assumed before, f becomes an output of the simulation, that actually depends on the assumed (mass, period, eccentricity) distributions of the giant planet population. This statistical analysis aims at determining f within a confidence interval as a function of mass and semi-major axis, given a set of individual detection probabilities p_j directly linked to the detection limits of each star observed during the survey and the considered giant planet distributions. One can refer to the work of Lafrenière et al. (2007) and Carson et al. (2006), for a general description of the statistical formalism applied for this analysis.

For our survey, we will consider the specific case of a null detection of planet formation by core-accretion within a Poisson statistical formalism that leads to a simple analytical solution for the exoplanet fraction upper limit (f_{max}). In the following, we will consider both approaches to exploit the full survey detection potential.

6.2. Simulation description

The simulation process is similar to the one adopted by Kasper et al. (2007), Lafrenière et al. (2007) and Nielsen et al. (2008). Due to the important spectral type dispersion of our sample, we have included in addition a planet mass dependency on primary mass. The different steps of the simulation process are described below:

1. Our simulation star sample is composed of 65 stars observed in coronagraphic imaging mode (see Table 2 and 3). Binaries that could impact the presence of a planet within a range of semi-major axis of $a = [5 - 150]$ AU were removed. Apparent magnitude, distance, age and mass are the prime simulation parameters.
2. The detection limits were converted to predicted masses using COND03 and DUSTY evolutionary models of Chabrier et al. (2000) and Baraffe et al. (2003). COND03 models are adapted to predict properties of cool (≤ 1700 K) substellar objects, whereas DUSTY model predictions were considered

Table 7. Properties of the confirmed comoving substellar companions discovered in the young, nearby associations: TW Hydrae (Twa), β Pictoris (β Pic), Columba (Col) and Carina (Car). Tentative spectral type have been determined from nIR spectroscopic observations, whereas masses and effective temperatures are predicted by evolutionary models based on the nIR photometry, the age and the distance of the system. (*), for 2M1207 b, Mohanty et al. (2007) suggests a higher mass of $8 \pm 2 M_{\text{Jup}}$ and the existence of a circum-secondary edge-on disk to explain their measured effective spectroscopic temperature of 1600 ± 100 K.

Name	Grp	Age (Myr)	d (pc)	SpT _A	SpT _B	M_B (M_{Jup})	T_{eff}^B (K)	$q_{B/A}$	Δ_{proj} (AU)
TWA5	TWA	8	(45-50)	M1.5	M8.5	25 ± 5	2500 ± 150	0.055	93 ± 10
HR7329	β Pic	12	$48.2^{+1.8}_{-1.6}$	A0V	M8	25 ± 5	2550 ± 150	0.010	199 ± 10
GSC-08047-00232	Tuc-Hor/Col	30	(85-95)	K3V	$M9^{+1}_{-3}$	20 ± 5	2100 ± 200	0.025	295 ± 30
AB Pic	Tuc-Hor/Car	30	$46.0^{+1.6}_{-1.5}$	K2V	$L1^{+2}_{-1}$	13 ± 2	1700 ± 200	0.015	250 ± 10
2M1207	TWA	8	$52.4^{+1.7}_{-1.1}$	M8	late-L	$4 \pm 1^*$	$1150 \pm 150^*$	0.16^*	40 ± 2

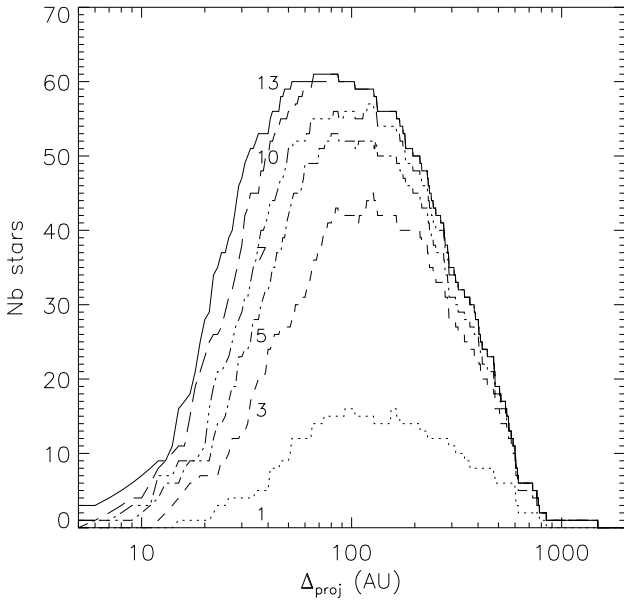


Fig. 9. Histogram of projected physical separations explored, for various planetary masses (1, 3, 5, 7, 10 and 13) M_{Jup} , in the close vicinity of the 65 young, nearby stars observed with NACO at VLT in coronagraphy. Contrast performances have been converted into masses based on the nIR photometry, age and distance of the primary stars.

for hotter temperatures. Based on our (6σ) individual detection limits and target (distance, age, H or K_s -band magnitude) properties, we derived the space of predicted masses and projected physical separation explored around each star of the sample (see histogram in Fig. 9).

- For the giant planet population, we have considered input distributions based on parametric laws for mass and period extrapolated from RV studies. The eccentricity distribution was chosen to follow the empirical planet distributions of RV planets. For mass and period, we consider power laws $dN/dM_p \sin i \propto (M_p \sin i)^\alpha$ and $dN/dP \propto P^\beta$ respectively. In addition, the influence of a planetary mass distribution scaled as a function of the stellar mass ($M_p \propto M_*^\gamma$) was tested.
- Monte Carlo simulations were run to take into account the the exoplanet distributions and orbital phase. For each run, 10,000 values of $M_p \sin i$ and P are randomly generated, following the adopted exoplanet distributions, together with all

the other orbital elements, which are supposed to be uniformly distributed. The real characteristics of each target star (mass, distance) are taken into account to evaluate the semi-major axis and projected physical separation of the planets.

- The final step is a comparison with the survey null-detection results and detection performances: either for a derivation of a non-detection probability and thus constraining the statistical significance of various sets of input distributions or for a derivation of the planet fraction upper limit (f_{max}) for a given set of exoplanet distributions. Dead zones of our coronagraphic images due to the presence of the mask support or the diffraction spikes have been considered in our detection performances and simulations.

6.3. Statistical results

6.3.1. Extrapolating radial velocity distributions

As a starting point, we used the mass and period distributions derived by Cumming et al. (2008) with $\alpha = -1.31$ and $\beta = -0.74$. We considered a giant planet frequency of 8.5% in the range 0.3 – 15 M_{Jup} for periods less than 1986 days (≤ 3 AU for a 1 M_\odot host star). The resulting value is consistent with RV studies of Marcy et al. (2005). Running several sets of simulations, we explored independently the influence of period, planet mass and primary mass distributions on the non-detection probability determined as a function of the period cut-off. The period cut-off was chosen to correspond to a semi-major axis cut-off between 20 and 150 AU. The results are reported in Fig. 10, to study the impact of the planet mass power law index α with $\beta = -0.74$ and $\gamma = 0.0$ (Top), of β the period power law index with $\alpha = -1.31$ and $\gamma = 0.0$ (Middle), and the evolution implied by a planet mass dependency with the primary mass when γ varies and $\alpha = -1.31$ and $\beta = -0.74$ (Bottom). As reference, Cumming et al. (2008) extrapolated distributions are reported in *thick solid* lines in all panels of Fig. 10. As a result, the non-detection probability of our survey as a function of the period cut-off is more sensitive to the variation of β , the period power law index. A reasonable set of values can significantly be excluded for large semi-major axis cut-off. In comparison, the influence of α and γ remains limited under the current assumptions.

6.3.2. Exoplanet fraction upper limit

The probability of planet detection for a survey of N stars is described by a binomial distribution, given a success probability $f p_j$ with f the fraction of stars with planets and p_j the individual detection probabilities of detecting a planet if present around the

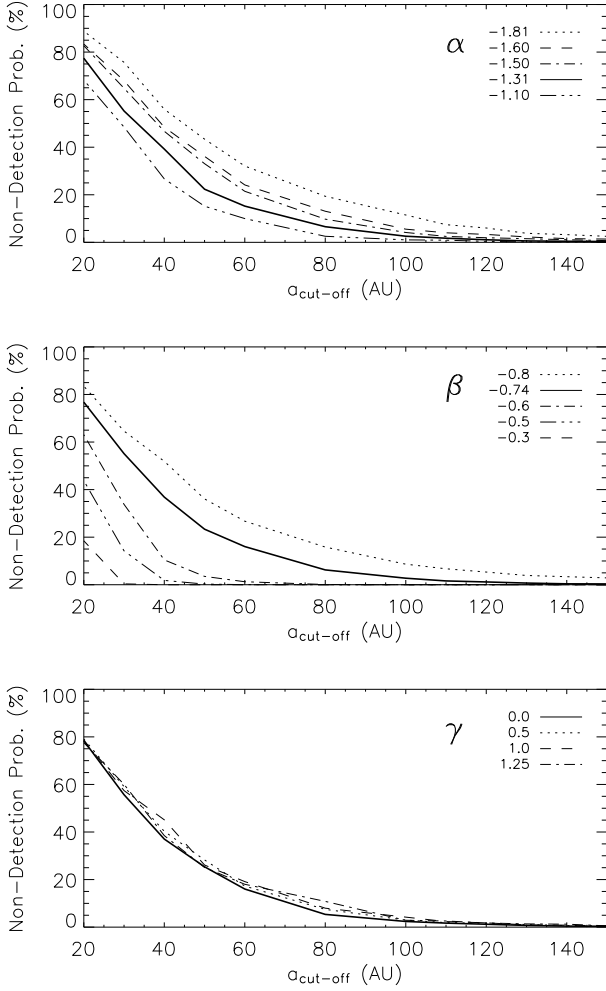


Fig. 10. Non-detection probability for our survey, based on various sets of period and mass distributions as a function of the semi-major axis cut-off of the period distribution. Mass and period distributions are extrapolated and normalized from RV studies. *Top:* Variation of the non-detection probability with α and fixing $\beta = -0.74$ and $\gamma = 0.0$. *Middle:* Variation of the non-detection probability with β and fixing $\alpha = -1.31$ and $\gamma = 0.0$. *Bottom:* Variation with γ a planet mass scaling with the primary mass and fixing $\alpha = -1.31$ and $\beta = -0.74$.

star j . In our case, we can consider a null detection result and replace each individual p_j by $\langle p_j \rangle$ the mean survey detection probability of detecting a planet if present. Finally, assuming that the number of expected detected planets is small compared to the number of stars observed ($f \langle p_j \rangle \ll 1$), the binomial distribution can be approximated by a Poisson distribution to derive a simple analytical solution for the exoplanet fraction upper limit f_{\max} for a given level of credibility CL.

$$f_{\max} = \frac{-\ln(1 - \text{CL})}{N \langle p_j \rangle} \quad (1)$$

We consider the period and mass power law indexes from Cumming et al. (2008) $\alpha = -1.31$, $\beta = -0.74$ and $\gamma = 1.25$ for the period and mass distribution of giant planet. For the set of detection limits of our survey, we can then determine $\langle p_j \rangle$, the survey mean probability of detecting a planet if present around each star of our sample. Then, given a confidence level $\text{CL} = 0.95$,

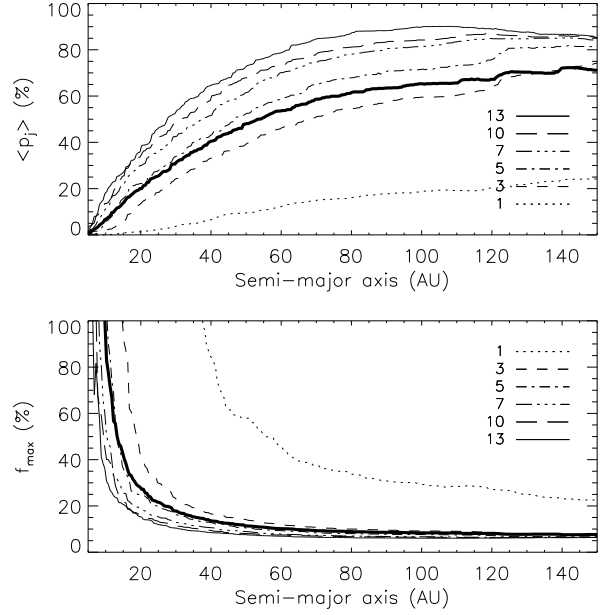


Fig. 11. *Top:* Survey mean detection probability derived as a function of semi-major axis assuming parametric mass and period distributions derived by Cumming et al. (2008), i.e with $\alpha = -1.31$, $\beta = -0.74$ and $\gamma = 1.25$. The results are reported for individual masses: 1, 3, 5, 7, 10 and 13 M_{Jup} . The integrated probability for the planetary mass regime is shown with the *thick solid line*. *Bottom:* Planet fraction upper limit derived as a function of semi-major axis, given the same mass and period distributions.

we obtain f_{\max} as a function of planet mass and semi-major axis. The survey mean detection probability and f_{\max} are reported in Fig. 11. It is important to note that both results depend on the assumed (mass, period, eccentricity) distributions of the giant planet population. Similar to other deep imaging surveys, our study begins to constrain the fraction of stars with giant planets to less than 10% for semi-major axes larger than typically 40 AU for this specific set of period, mass and eccentricity distributions. We also see that we barely constrain the fraction of 1 M_{Jup} planets potentially detectable for 24% of our targets (67% for the 3 M_{Jup} planets). Increasing the sample size will enable refinement of the statistical constraints on the upper limits of the fraction of stars with giant planets as a function of their mass and semi-major axis. However, a number of intrinsic limitations (detection threshold, age determination and model calibration) remain that will have to be overcome to draw more robust conclusions. Future work gathering detection performances from multiple surveys should help refine our knowledge of the occurrence of giant planets at wide orbits (> 10 AU) and thus complement RV survey results.

6.4. Limitations

Added to the detection threshold determination (detailed previously), the age determination of the young, nearby stars and the use of uncalibrated evolutionary models are the three main limitations that directly impact the estimation of the explored planetary masses from observed luminosities. Added to the current assumption made on the extrapolation of close-in exoplanet distributions at wide orbits, they limit the current relevancy of all

statistical analysis of deep imaging surveys aimed at constraining the population of giant planets.

6.4.1. Age determination

Ages of young stars near the Sun are deduced based on photometric, spectroscopic and kinematics studies; various diagnostics are commonly used, depending on the spectral type and age of a given star. Details may be found in ZS04 and T08. In general, the most reliable ages are obtained for stars that can be placed reliably into a moving group or association.

Our sample is composed of 88 stars, including 51 members of known young, nearby associations (TWA, β Pic, Tuc-Hor and AB Dor). Ages for the TWA and β Pic associations have been reasonably well constrained by various and independent (stellar properties characterization and dynamical trace-back) studies to: 8_{-3}^{+4} Myr (TWA; de la Reza et al. 2006; Barrado y Navasúes 2006; Scholz et al. 2007) and 12_{-4}^{+8} Myr (β Pic, Zuckerman et al. 2001b, Ortega et al. 2004) respectively. Isochrones, lithium depletion and X-ray luminosities indicate an age for Tuc-Hor of 30 Myr (Zuckerman et al. 2001a). The age of the AB Dor association is in some dispute (see Zuckerman et al. 2004, Luhman et al. 2005, Luhman & Potter 2006, Lopez-Santiago et al. 2006, Janson et al. 2007, Ortega et al. 2007, Close et al. 2007, Boccaletti et al. 2008, Torres et al. 2008). In our simulations, we have assumed an age of 70 Myr for AB Dor stars.

In our statistical analysis of 65 stars observed in coronagraphic imaging mode, 45 are confirmed members of known associations while 17 are young candidates, currently not identified as members of any kinematic group which makes an age estimate particularly difficult. An excellent example of a young star not known to be a member of the above listed moving groups is HR 8799, identified by Marois et al (2008b) as orbited by 3 giant planets but with an age uncertainly between 30 and 160 Myr. In our analysis, age is directly used to convert the detection limits to mass using evolutionary models. Therefore, age determination remains a main limitation in this work and others to constrain reliably the properties of a putative population of giant planets around young, nearby stars.

6.4.2. Evolutionary models

Evolutionary model predictions are commonly used to infer substellar masses from observed luminosities, as we did to convert our survey detection performances into planetary mass limits. For stars and brown dwarfs formed by gravitational collapse and fragmentation, models consider the idealized description of non-accreting systems contracting at large initial radii. Remaining circumstellar material, accretion and uncertainties related to choice of initial conditions imply that comparison between observations and models are quite uncertain at young ≤ 100 Myr ages (Baraffe et al. 2002). This could be even worse for young giant planets; the implementation of the core-accretion mechanism as initial conditions for evolutionary calculation could substantially change the model predictions (Marley et al. 2007). Then massive giant planets could be significantly fainter than equal-mass objects formed in isolation via gravitational collapse. However, a critical issue is treatment of the accretion shock through which most of the giant planet mass is processed and which remains highly uncertain. In previous analyses of survey detection performances, only predictions from Chabrier et al. (2000) and Baraffe et al. (2003) models were used. Use of Burrows et al. (2003), assuming the same initial

conditions, does not change significantly the results (Nielsen et al. 2008).

7. Conclusions

We have conducted a deep adaptive optics imaging survey with NACO at the VLT of 88 nearby stars of the southern hemisphere. Our selection criteria favored youth (≤ 100 Myr) and proximity to Earth (≤ 100 pc) to optimize the detection of close planetary mass companions. Known visual binaries were excluded to avoid degrading the NACO AO and/or coronagraphic detection performances. Among our sample, 51 stars are members of young, nearby comoving groups. 32 are young, nearby stars currently not identified as members of any currently known association and 5 have been reclassified as older (≥ 100 Myr) systems. The spectral types cover the sequence from B to M spectral types with 19% BAF stars, 48% GK stars and 33% M dwarfs. The separation investigated typically ranges between 0.1'' to 10'', i.e. between typically 10 to 500 AU. A sample of 65 stars was observed in deep coronagraphic imaging to enhance our contrast performances to 10^{-6} and to be sensitive to planetary mass companions down to 1 M_{Jup} (at 24% of our sample) and 3 M_{Jup} (at 67%). We used a standard observing sequence to precisely measure the position and the flux of all detected sources relative to their visual primary star. Repeated observations at several epochs enabled us to discriminate comoving companions from background objects. The main results are that:

- we discovered of 17 new close (0.1 – 5.0'') multiple systems. HIP 108195 AB and C (F1III-M6), HIP 84642 AB ($a \sim 14$ AU, K0-M5) and TWA22 AB ($a \sim 1.8$ AU; M6-M6) are confirmed as comoving systems. TWA22 AB, with 80% of its orbit already resolved, is likely to be a rare astrometric calibrator for testing evolutionary model predictions.
- about 236 faint CCs were detected around 36 stars observed in coronagraphy. Follow-up observations with VLT or HST for 30 stars enabled us to identify their status. 1% of the CCs detected have been confirmed as comoving companions, 43% have been identified as probable background contaminants and about 56% need further follow-up observations. The remaining CCs come mostly from the presence of crowded fields in the background of the 6 stars observed at one epoch.
- we confirmed previously discovered substellar companions around GSC 08047-00232, AB Pic and 2M1207 and placed them in the perspective of confirmed substellar companions among young, nearby associations.
- finally, the statistical analysis of our complete set of detection limits enables us to constrain at large semi-major axes, 20 to a few 100 AU, various mass, period and eccentricity distributions of giant planets extrapolated and normalized from RV surveys. It enables us to derive limits on the occurrence of giant planets for a given set of physical and orbital distributions. The survey starts constraining significantly the population of giant planet for masses $\geq 3 M_{\text{Jup}}$.

In the first few years following the discovery of the companion to 2M1207 (Chauvin et al. 2004), all planetary mass companions were discovered at relatively wide separations or with small mass ratio with their primaries. However, the recent discoveries of planetary mass objects around the star Fomalhaut (Kalas et al. 2008), HR 8799 (Marois et al. 2008b) and β Pictoris (Lagrange et al. 2009), now open a new era for the deep imaging study of giant planets that probably formed like those of our solar system.

In the perspective of on-going and future deep imaging instruments either from the ground (Gemini/NICI, Subaru/HiCIAO, SPHERE, GPI, EPICS) or from space (JWST, TPF/Darwin), this work represents a pioneer successful study, providing, with other surveys, precise information (stellar and substellar multiplicity, non-detections and background contaminants) to better characterize the overall environment of young, nearby stars, that will be prime targets for future exoplanets search.

Acknowledgements. We thank the ESO Paranal staff for performing the service mode observations. We also acknowledge partial financial support from the PNPS and Agence National de la Recherche, in France, from INAF through PRIN 2006 “From disk to planetary systems: understanding the origin and demographics of solar and extrasolar planetary systems” and from NASA in the USA. We also would like to thank France Allard and Isabelle Baraffe for their inputs on evolutionary models and synthetic spectral libraries. Finally, our anonymous referee for her/his detailed and very constructive report.

References

- Baraffe I., Chabrier G., Allard F. & Hauschildt P.H. 2002, *A&A* 382, 563
 Baraffe, I., Chabrier, G., Barman, T. S., Allard, F., & Hauschildt, P. H. 2003, *A&A*, 402, 701
 Barrado Y Navascués D. 2006, *A&A*, 459, 511
 Biller B.A., Close L.M., Masciadri E. et al. 2007, *ApJS*, 173, 143
 Boccaletti A., Chauvin G., Baudoz P. & Beuzit J.-L. 2008, *A&A*, 482, 939
 Boley A.C. 2009, *ApJ*, 695, L53
 Bonnell I. A., Larson R. B. & Zinnecker H. 2007, *Protostars and Planets V*, 951, 149-164
 Burgasser A. J., Kirkpatrick J. D., Brown M. E. et al. 1999, *ApJ*, 522, 65
 Burgasser A. J., Reid I.N., Siegler N. et al. 2007, *Protostars and Planets V*, 951, 427-441
 Burrows A., Sudarsky D. & Lunine J.I. 2003, *ApJ*, 596, 587
 Butler R. P., Wright J.T., Marcy G.W. et al. 2006, *ApJ*, 646, 505
 Carson J. C., Eikenberry S. S., Brandl B. R., Wilson, J. C. & Hayward T. L. 2005, *AJ*, 130, 1212
 Carson J. C., Eikenberry S. S., Smith J. J. & Cordes, J. M. 2006, *AJ*, 132, 1146
 Chabrier, G., Baraffe, I., Allard, F., & Hauschildt, P. H. 2000, *ApJ*, 542, 464
 Chauvin G., Thomson M., Dumas C. et al. 2003, *A&A*, 404, 157
 Chauvin G., Lagrange A.-M., Dumas C. et al. 2004, *A&A*, 425, L25
 Chauvin G., Lagrange A.-M., Lacombe F. et al. 2005a, *A&A*, 430, 1027
 Chauvin G., Lagrange A.-M., Dumas C. et al., 2005b, *A&A*, 438, L25
 Chauvin G., Lagrange A.-M., Zuckerman B. et al. 2005c, *A&A*, 438, L29
 Chauvin G., Lagrange A.-M., Udry S. et al. 2006, *A&A*, 456, 1165
 Close, Laird M.; Thatte, Niranjan; Nielsen, Eric L. et al. 2007, *ApJ*, 665, 736
 Couteau, P. 1960, *J. Obs.*, 43, 13
 Cumming A., Butler R. P., Marcy G. W. et al. 2008, *PASP*, 120, 531
 de la Reza R., Jilinski E. & Ortega V.G. 2006, *AJ*, 131, 2609
 Delfosse X., Tinney C. G., Forveille, T. et al. 1997, *A&A*, 327, 25
 Devillar N. 1997, *The messenger*, 87
 Dohlen K., Beuzit J.-L., Feldt M. et al. 2006, *SPIE*, 6269, 24
 Dommanget, J. & Nys, O. 2000, *A&A*, 363, 991
 Ducourant C., Teixeira R., Chauvin G. et al. 2008, *A&A*, 477, L1
 Eggenberger A., Udry S., Chauvin G. et al. 2007, *A&A*, 474, 273
 Endl M., Cochran W.D., Krster M. et al. 2006, *ApJ*, 649, 436
 Epchtein N., de Batz B., Capoani L., Chevallier L. et al. 1997, *Msngr*, 87, 27
 Fuhrmeister & Schmitt 2003, *A&A* 403, 247
 Gizis, J., Jao, W., Subsavage, J.P., Henry, T.J., 2007, *ApJ*, 669, L45-L48
 Goldman B., Delfosse X., Forveille T. et al. 1999, *A&A*, 351, L5
 Grether & Lineweaver 2006, *ApJ*, 640, 1051
 Grillmair C.J., Burrows A., Charbonneau D. et al. 2008, *Nature*, 456, 767
 Itoh Y., Hayashi M., Tamura M. et al. 2005, *ApJ*, 620, 984
 Janson M., Brandner W., Lenzen R. et al. 2007, *A&A*, 462, 615
 Joergens V. 2006, *A&A*, 446, 1165
 Johnson J.A., Fischer D.A., Marcy G.W. et al. 2007, *ApJ*, 665, 785
 Kalas P., Graham J. R., Chiang E. et al. 2008, *Science*, 322, 1345
 Kastner, J.H., Zuckerman, B., Weintraub, D.A. & Forveille T. 1997, *Science* 277, 67
 Kasper M., Apai D., Janson M. & Brandner W. 2007, *A&A*, 472, 321
 Kirkpatrick J. D., Reid I. N., Liebert J. et al. 1999, *ApJ* 519, 802
 Kirkpatrick J. D., Reid I. N., Liebert J. et al. 2000, *ApJ* 120, 447
 Lafrenière, David; Doyon, René; Marois, Christian et al. 2007, *ApJ*, 670, 1367
 Lafrenière D., Jayawardhana R., van Kerkwijk M.H. et al. 2008, *ApJ*, 689, 153
 Lagrange A.-M., Gratadour D., Chauvin G. et al. 2009, *A&A*, 493, L21
 Lagrange A.-M., Desort M., Galland F., Udry S. & Mayor M. 2009, *A&A*, 495, 335
 Lenzen, R., Hofmann, R., Bizenberger, P. & Tusche, A., 1998, *SPIE*, Vol. 3354
 López-Santiago J., Montes D., Crespo-Chacón I., & Fernández-Figueroa M.J. 2006, *ApJ*, 643, 1160
 Lowrance, P. J., McCarthy, C., Becklin, E. E. et al. 1999, *ApJ*, 512, L69
 Lowrance, P. J., Schneider, G., Kirkpatrick, J. et al. 2000, *ApJ*, 541, L390
 Lowrance P.J., Becklin E.E., Schneider G. et al. 2005, *AJ*, 130, 1845
 Luhman, K. & Jayawardhana, R. 2002, *ApJ*, 566, 1132
 Luhman K.L., Stauffer J.R. & Mamajek E.E. 2005, 628, L69
 Luhman K.L. & Potter D. 2006, *ApJ*, 638, 887
 Luhman K.L., Wilson J.C., Brandner W. et al. 2006, *ApJ*, 649, 894
 Marcy G., Butler R. P., Fischer D. et al. 2005, *PTHP*, 158, 24
 Marley M.S., Fortney J.J., Hubickyj O., Bodenheimer P. & Lissauer J.J. 2007, *ApJ*, 655, 541
 Marois C., Lafrenière D., Macintosh B. & Doyon R. 2008a, *ApJ*, 673, 647
 Marois C., Macintosh B., Barman, T. et al. 2008b, *Science* 322, 1348
 Masciadri, E., Mundt, R., Henning, Th. & Alvarez, C. 2005, *ApJ*, 625, 1004
 Mayor, M. & Queloz, D. 1995, *Nature* 378, 355
 McCarthy, C. & Zuckerman, B. 2004, *AJ*, 127, 2871
 McCaughrean M.J. & Stauffer J.R. 1994, *AJ*, 108, 1382
 Macintosh B., Troy M. Doyon R. et al. 2006, *SPIE*, 6272, 20
 Masciadri E., Mundt R., Henning Th., Alvarez C. & Barrado y Navascués D. 2005, *ApJ*, 625, 1004
 Metchev S. & Hillenbrand L. 2006, *ApJ*, 651, 1166
 Metchev S. & Hillenbrand L. 2008, *ApJ*, 676, 1281
 Mohanty S., Jayawardhana R., Huéramo N. & Mamajek E. 2007, *ApJ*, 657, 1064
 Mugrauer M., Seifahrt A. & Neuhäuser R. 2007, *MNRAS*, 378, 1328
 Nakajima T., Oppenheimer B.R., Kulkarni S.R. et al. 1995, *Nature* 378, 463
 Neuhäuser, R., Guenther, E.W., Alves, J. et al. 2003, *AN*, 324, 535
 Neuhäuser, R. & Guenther, E.W. 2004, *A&A*, 420, 647
 Neuhäuser R., Guenther E.W., Wuchterl G. et al. 2005, *A&A*, 435, 13
 Nielsen E.L., Close L.M., Biller B.A., Masciadri E. & Lenzen R. 2008, *ApJ*, 674, 466
 Ortega V. G., de la Reza R., Jilinski E. & Bazzanella B. 2004, *ApJ*, 609, 243
 Ortega, V. G.; Jilinski, E.; de La Reza, R.; Bazzanella, B. 2007, *MNRAS*, 377, 441
 Papaloizou, J. C. B., Terquem, C. 2001, *MNRAS*, 325, 221
 Patience J., White R.J., Ghez, A. M. et al. 2002, *ApJ*, 581, 654
 Rafikov R.R. 2005, *ApJ*, 621, L69
 Rousset G., Lacombe F., Puget P. et al., 2002, *SPIE*, Vol. 4007
 Schmidt T.O.B., Neuhäuser R., Seifahrt A. et al. 2008, arXiv0809.2812S
 Scholz A., Coffey J., Brandeker A. & Jayawardhana R. 2007, *ApJ*, 662, 1254
 Siess L., Dufour, E. & Forestini M. 2000, *A&A*, 358, 593
 Skrutskie M. F., Schneider S. E., Stiening R., Strom S. E. et al. 1997, *ASSL*, 210, 25
 Song I., Zuckerman B. & Bessell M.S. 2003, *ApJ*, 599, 342
 Song I., Schneider G., Zuckerman B. et al. 2006, *ApJ*, 26, 282
 Swain M.R., Vasisht G. & Tinetti G. 2008, *Nature*, 452, 329
 Torres C.A.O., Quast G.R., Melo C.H.F. & Sterzik M.F. 2008, *Handbook of Star Forming Regions, Volume II: The Southern Sky*, ASP Monograph Publications, Vol. 5, p.757
 Udry S. & Santos N. C. 2007, *ARA&A*, 45, 397
 van Dessel E. & Sinachopoulos D. 1993, *A&AS*, 100, 517
 Véran, J.P. & Rigaut, F. 1998, *SPIE*, 3353, 426
 Webb R. A., Zuckerman B., Platais I. et al. 1999, *ApJ* 512, L63
 Wilson J.C., Kirkpatrick J.D., Gizis J.E. et al. 2001, *AJ*, 122, 1989
 York D. G., Adelman J., Anderson J. E. Jr et al. 2000, *AJ*, 120, 1579
 Zuckerman B., Song I. & Webb R.A. 2001a, *ApJ*, 559, 388
 Zuckerman B., Song I., Bessell M.S. & Webb R.A. 2001b, *ApJ*, 562, 87
 Zuckerman B., Song I. & Bessell M.S. 2004, *ApJ*, 613, L65
 Zuckerman, B. & Song, I. 2004, *ARAA*, 42, 685
 Zuckerman & Song 2009, *A&A*, 493, 1149

Table 8. Characterization and identification (for multi-epochs observations) of all faint sources detected during the VLT/NACO survey. Target name, observing date and set-up are given, as well as the different sources identified with their relative position, relative flux and their status identification based on follow-up observations. Sources referred as undefined (U) are objects detected at only one epoch, (B) objects identified as stationary background contaminants and (C) confirmed comoving companion. When VLT observations are combined to other instrumentation (HST, USNO, 2MASS), a flag or a reference is reported in the last column.

Name	Candidate	UT Date	Filter	Separation (arcsec)	P.A. ($^{\circ}$)	Δm (mag)	Status	Note
GSC08047-00232	cc-1	23/11/2002	K_s	3.274 ± 0.012	358.85 ± 0.23	6.3 ± 0.1	C	
		07/09/2003	K_s	3.266 ± 0.011	358.89 ± 0.23			
		05/03/2004	K_s	3.260 ± 0.012	358.82 ± 0.22			
HIP30034 (AB Pic)	cc-1	17/03/2003	H	5.460 ± 0.014	175.33 ± 0.18	7.6 ± 0.1	C	
		05/03/2004	H	5.450 ± 0.016	175.13 ± 0.21			
		26/09/2004	H	5.453 ± 0.014	175.10 ± 0.20			
		01/05/2005	H	5.452 ± 0.015	175.37 ± 0.20			
		08/01/2006	H	5.455 ± 0.014	175.49 ± 0.21			
HIP6856	cc-1	26/11/2002	K_s	4.585 ± 0.014	105.70 ± 0.30	10.6 ± 0.2	B	
		08/06/2003	K_s	4.547 ± 0.014	105.80 ± 0.30			
	cc-2	07/09/2003	K_s	4.503 ± 0.013	105.40 ± 0.30	12.8 ± 0.2	B	
		26/11/2002	K_s	2.830 ± 0.013	85.40 ± 0.30			
		08/06/2002	K_s	2.791 ± 0.015	85.30 ± 0.30			
TWA19 A	cc-1	07/06/2003	H	3.574 ± 0.019	303.66 ± 0.35	10.3 ± 0.2	B	
		08/01/2006	H	3.507 ± 0.012	305.78 ± 0.20			
HIP95270	cc-1	25/09/2004	H	4.826 ± 0.019	250.45 ± 0.23	11.9 ± 0.2	B	
		19/08/2005	H	4.825 ± 0.027	251.29 ± 0.19			
	cc-2	25/09/2004	H	5.806 ± 0.023	274.00 ± 0.13			
		19/08/2005	H	5.839 ± 0.035	274.52 ± 0.11			
HIP59315	cc-1	27/04/2004	H	5.412 ± 0.020	97.71 ± 0.22	9.3 ± 0.3	B	
		06/05/2005	H	5.526 ± 0.021	96.89 ± 0.21			
HIP84586	cc-1	27/04/2004	H	7.960 ± 0.026	120.23 ± 0.19	11.3 ± 0.2	B	
		27/04/2004	K_s	7.860 ± 25	119.55 ± 0.23			
GSC-08894-00426	cc-1	05/03/2004	H	9.904 ± 0.028	246.13 ± 0.21	15.1 ± 0.2	B	
		26/02/2006	K_s	9.917 ± 0.024	245.36 ± 0.15			
HIP108195 AB	cc-1	26/02/2006	K_s	4.966 ± 0.010	158.22 ± 0.14	5.4 ± 0.2	C	stellar
		18/06/2007	K_s	4.962 ± 0.012	158.22 ± 0.20			
	cc-2	26/02/2006	K_s	13.041 ± 0.025	190.71 ± 0.14			
		18/06/2007	K_s	12.920 ± 0.026	191.44 ± 0.20			
TYC-09012-1005-1	cc-1	27/04/2004	H	3.709 ± 0.015	21.20 ± 0.24	6.1 ± 0.1	B	
		08/05/2007	K_s	3.790 ± 0.014	22.68 ± 0.22			
	cc-2	27/04/2004	H	6.725 ± 0.025	50.64 ± 0.28			
		08/05/2007	K_s	6.826 ± 0.025	50.87 ± 0.27			
	cc-3	27/04/2004	H	3.010 ± 0.013	141.40 ± 0.31			
		08/05/2007	K_s	3.029 ± 0.011	139.80 ± 0.27			
	cc-4	27/04/2004	H	4.771 ± 0.019	188.03 ± 0.22			
		08/05/2007	K_s	4.695 ± 0.018	186.84 ± 0.20			
	cc-5	27/04/2004	H	3.686 ± 0.015	245.09 ± 0.25			
		08/05/2007	K_s	3.565 ± 0.013	245.14 ± 0.23			
	cc-6	27/04/2004	H	2.814 ± 0.012	302.49 ± 0.29			
		08/05/2007	K_s	2.753 ± 0.010	304.57 ± 0.25			
	cc-7	27/04/2004	H	5.591 ± 0.021	307.61 ± 0.28			
		08/05/2007	K_s	5.528 ± 0.020	308.73 ± 0.27			
	cc-8	27/04/2004	H	4.800 ± 0.019	324.79 ± 0.27			
08/05/2007		K_s	4.765 ± 0.017	326.40 ± 0.25				
cc-9	27/04/2004	H	5.264 ± 0.021	339.50 ± 0.23				
	08/05/2007	K_s	5.262 ± 0.020	340.93 ± 0.22				
cc-10	27/04/2004	H	2.691 ± 0.012	121.77 ± 0.29				
	08/05/2007	K_s	2.751 ± 0.010	119.75 ± 0.24				
cc-11	27/04/2004	H	4.324 ± 0.017	146.38 ± 0.27				
	08/05/2007	K_s	4.332 ± 0.016	144.88 ± 0.25				
cc-12	27/04/2004	H	5.996 ± 0.024	180.21 ± 0.21				
	08/05/2007	K_s	5.930 ± 0.023	179.20 ± 0.2				
cc-13	08/05/2007	K_s	1.566 ± 0.009	28.17 ± 0.36	U			
cc-14	08/05/2007	K_s	3.809 ± 0.015	59.80 ± 0.27	U			
cc-15	08/05/2007	K_s	5.608 ± 0.021	52.01 ± 0.28	U			

Table 9. Table 7 - cont

Name	Candidate	UT Date	Filter	Separation (arcsec)	P.A. ($^{\circ}$)	Δm (mag)	Status	Note
	cc-16	08/05/2007	K _s	5.083 ± 0.020	81.32 ± 0.22	11.3 ± 0.2	U	
	cc-17	08/05/2007	K _s	7.208 ± 0.027	53.12 ± 0.27	10.5 ± 0.2	U	
	cc-1	08/05/2007	K _s	8.158 ± 0.030	51.12 ± 0.27	11.1 ± 0.2	U	
	cc-19	08/05/2007	K _s	7.650 ± 0.029	61.15 ± 0.24	10.5 ± 0.2	U	
	cc-20	08/05/2007	K _s	6.792 ± 0.026	80.03 ± 0.21	11.1 ± 0.2	U	
	cc-21	08/05/2007	K _s	7.705 ± 0.030	75.99 ± 0.21	9.2 ± 0.2	U	
	cc-22	08/05/2007	K _s	6.870 ± 0.027	103.87 ± 0.22	11.4 ± 0.2	U	
	cc-23	08/05/2007	K _s	7.838 ± 0.030	110.93 ± 0.22	10.9 ± 0.2	U	
	cc-24	08/05/2007	K _s	7.538 ± 0.028	132.55 ± 0.29	11.3 ± 0.2	U	
	cc-25	08/05/2007	K _s	4.932 ± 0.019	134.47 ± 0.31	11.5 ± 0.2	U	
	cc-26	08/05/2007	K _s	6.124 ± 0.023	144.73 ± 0.27	11.3 ± 0.2	U	
	cc-27	08/05/2007	K _s	8.245 ± 0.031	153.07 ± 0.24	10.2 ± 0.2	U	
	cc-28	08/05/2007	K _s	2.783 ± 0.012	130.62 ± 0.33	10.8 ± 0.2	U	
	cc-29	08/05/2007	K _s	3.180 ± 0.013	151.96 ± 0.27	10.4 ± 0.2	U	
	cc-30	08/05/2007	K _s	6.175 ± 0.024	162.80 ± 0.22	10.3 ± 0.2	U	
	cc-31	08/05/2007	K _s	1.475 ± 0.009	174.39 ± 0.33	10.1 ± 0.2	U	
	cc-32	08/05/2007	K _s	4.265 ± 0.017	211.89 ± 0.27	10.3 ± 0.2	U	
	cc-33	08/05/2007	K _s	3.552 ± 0.015	218.25 ± 0.30	10.8 ± 0.2	U	
	cc-34	08/05/2007	K _s	2.453 ± 0.011	218.09 ± 0.33	10.1 ± 0.2	U	
	cc-35	08/05/2007	K _s	5.548 ± 0.021	234.93 ± 0.27	10.5 ± 0.2	U	
	cc-36	08/05/2007	K _s	4.715 ± 0.019	248.43 ± 0.24	11.1 ± 0.2	U	
	cc-37	08/05/2007	K _s	4.672 ± 0.019	253.54 ± 0.23	9.9 ± 0.2	U	
	cc-38	08/05/2007	K _s	2.808 ± 0.012	258.37 ± 0.25	10.8 ± 0.2	U	
	cc-39	08/05/2007	K _s	1.933 ± 0.010	296.55 ± 0.32	10.7 ± 0.2	U	
	cc-40	08/05/2007	K _s	2.948 ± 0.013	299.78 ± 0.28	10.5 ± 0.2	U	
	cc-41	08/05/2007	K _s	2.387 ± 0.011	307.50 ± 0.33	11. ± 0.2	U	
	cc-42	08/05/2007	K _s	3.077 ± 0.013	273.18 ± 0.24	11.8 ± 0.2	U	
GSC00862-0019-1	cc-1	22/11/2002	K _s	7.780 ± 0.020	3.58 ± 0.22	3.5 ± 0.2	B	USNO
TWA22 AB	cc-1	27/04/2004	H	5.096 ± 0.018	340.78 ± 0.25			
		26/02/2006	K _s	5.070 ± 0.017	343.91 ± 0.21	9.7 ± 0.2	B	
	cc-2	27/04/2004	H	4.786 ± 0.016	5.90 ± 0.26			
		26/02/2006	K _s	4.867 ± 0.016	8.85 ± 0.21	7.5 ± 0.2	B	
	cc-3	27/04/2004	H	7.103 ± 0.020	14.89 ± 0.23			
		26/02/2006	K _s	7.217 ± 0.020	16.82 ± 0.18	6.1 ± 0.2	B	
	cc-4	27/04/2004	H	11.298 ± 0.029	20.84 ± 0.21			
		26/02/2006	K _s	11.428 ± 0.027	22.04 ± 0.16	10.2 ± 0.2	B	
	cc-5	27/04/2004	H	9.984 ± 0.030	31.87 ± 0.22			
		26/02/2006	K _s	10.151 ± 0.025	32.97 ± 0.18	10.8 ± 0.2	B	
	cc-6	27/04/2004	H	12.557 ± 0.037	36.83 ± 0.22			
		26/02/2006	K _s	12.798 ± 0.031	38.28 ± 0.18	10.9 ± 0.2	B	
	cc-7	27/04/2004	H	11.191 ± 0.032	121.56 ± 0.21			
		26/02/2006	K _s	11.348 ± 0.027	120.74 ± 0.17	9.7 ± 0.2	B	
	cc-8	27/04/2004	H	8.755 ± 0.028	130.40 ± 0.24			
		26/02/2006	K _s	8.889 ± 0.023	129.15 ± 0.20	9.6 ± 0.2	B	
	cc-9	27/04/2004	H	4.395 ± 0.017	160.47 ± 0.27			
		26/02/2006	K _s	4.409 ± 0.016	157.12 ± 0.24	11.5 ± 0.2	B	
	cc-10	27/04/2004	H	7.045 ± 0.020	163.39 ± 0.23			
		26/02/2006	K _s	7.036 ± 0.019	161.34 ± 0.18	10.7 ± 0.2	B	
	cc-11	27/04/2004	H	12.575 ± 0.037	142.06 ± 0.22			
		26/02/2006	K _s	12.650 ± 0.030	141.10 ± 0.18	10.6 ± 0.2	B	
	cc-12	27/04/2004	H	12.965 ± 0.039	138.25 ± 0.23			
		26/02/2006	K _s	13.061 ± 0.031	137.36 ± 0.19	11.0 ± 0.2	B	
	cc-13	27/04/2004	H	14.471 ± 0.039	152.71 ± 0.21			
		26/02/2006	K _s	14.485 ± 0.033	151.74 ± 0.16	11.2 ± 0.2	B	
	cc-14	27/04/2004	H	13.474 ± 0.028	179.70 ± 0.21			
		26/02/2006	K _s	13.383 ± 0.028	178.69 ± 0.15	8.6 ± 0.2	B	
	cc-15	27/04/2004	H	10.628 ± 0.027	195.67 ± 0.21			
		26/02/2006	K _s	10.487 ± 0.024	194.57 ± 0.16	11.0 ± 0.2	B	

Table 10. Contaminants and companion identified

Name	Candidate	UT Date	Filter	Separation (arcsec)	P.A. ($^{\circ}$)	Δm (mag)	Status	Note
	cc-16	27/04/2004	H	6.266 ± 0.019	193.90 ± 0.24			
		26/02/2006	K_s	6.133 ± 0.018	191.73 ± 0.19	10.4 ± 0.2	B	
	cc-17	27/04/2004	H	3.466 ± 0.017	227.25 ± 0.37	10.8 ± 0.2	PB	HST
	cc-18	27/04/2004	H	13.912 ± 0.037	205.66 ± 0.21			
		26/02/2006	K_s	13.701 ± 0.031	204.91 ± 0.16	10.2 ± 0.2	B	
	cc-19	27/04/2004	H	14.827 ± 0.040	207.38 ± 0.20			
		26/02/2006	K_s	14.611 ± 0.033	206.70 ± 0.16	9.7 ± 0.2	B	
	cc-20	27/04/2004	H	9.794 ± 0.028	241.51 ± 0.22			
		26/02/2006	K_s	9.516 ± 0.024	241.37 ± 0.17	7.0 ± 0.2	B	
	cc-21	27/04/2004	H	14.004 ± 0.040	235.61 ± 0.21	8.9 ± 0.2	U	
	cc-22	27/04/2004	H	13.297 ± 0.037	239.78 ± 0.21	10.6 ± 0.2	U	
	cc-23	27/04/2004	H	13.353 ± 0.033	251.30 ± 0.21	10.1 ± 0.2	U	
	cc-24	27/04/2004	H	6.902 ± 0.019	264.46 ± 0.23	10.5 ± 0.2	U	
	cc-25	27/04/2004	H	10.633 ± 0.032	310.28 ± 0.23			
		26/02/2006	K_s	10.454 ± 0.026	311.58 ± 0.19	11.1 ± 0.2	B	
	cc-26	27/04/2004	H	10.342 ± 0.032	318.06 ± 0.24			
		26/02/2006	K_s	10.204 ± 0.026	319.54 ± 0.19	9.5 ± 0.2	B	
	cc-27	27/04/2004	H	16.843 ± 0.049	317.34 ± 0.23	9.7 ± 0.2	U	
	cc-28	26/02/2006	K_s	4.552 ± 0.016	207.87 ± 0.24	11.3 ± 0.2	PB	HST
0ES1847	cc-1	25/09/2004	H	3.433 ± 0.014	19.50 ± 0.18			
		09/06/2007	H	3.593 ± 0.014	17.99 ± 0.17	11.1 ± 0.2	B	
	cc-2	25/09/2004	H	1.946 ± 0.010	74.66 ± 0.24			
		09/06/2007	H	1.946 ± 0.009	69.29 ± 0.25	11.3 ± 0.2	B	
	cc-3	25/09/2004	H	5.033 ± 0.018	68.11 ± 0.17			
		09/06/2007	H	5.053 ± 0.018	66.21 ± 0.18	10.7 ± 0.2	B	
	cc-4	25/09/2004	H	5.196 ± 0.020	80.45 ± 0.13			
		09/06/2007	H	5.688 ± 0.022	81.30 ± 0.13	13.5 ± 0.2	B	
	cc-5	25/09/2004	H	3.913 ± 0.015	155.61 ± 0.19			
		09/06/2007	H	3.724 ± 0.014	155.30 ± 0.19	11.5 ± 0.2	B	
	cc-6	25/09/2004	H	3.756 ± 0.016	173.50 ± 0.15			
		09/06/2007	H	3.559 ± 0.015	174.35 ± 0.15	11.0 ± 0.2	B	
	cc-7	25/09/2004	H	7.100 ± 0.027	175.19 ± 0.12			
		09/06/2007	H	6.907 ± 0.027	175.71 ± 0.12	11.0 ± 0.2	B	
	cc-8	25/09/2004	H	4.684 ± 0.019	185.48 ± 0.13			
		09/06/2007	H	4.379 ± 0.018	186.28 ± 0.14	12.6 ± 0.2	B	
	cc-9	25/09/2004	H	5.777 ± 0.021	198.20 ± 0.15			
		09/06/2007	H	5.628 ± 0.021	199.45 ± 0.16	12.6 ± 0.2	B	
TYC-7846-1538-1	cc-1	27/04/2004	H	4.658 ± 0.017	59.39 ± 0.21		B	
		06/05/2005	K_s	4.755 ± 0.019	59.35 ± 0.26	10.8 ± 0.3	B	
	cc-2	27/04/2004	H	7.703 ± 0.025	54.64 ± 0.21	12.6 ± 0.3	U	
	cc-3	27/04/2004	H	9.121 ± 0.029	127.94 ± 0.22		U	
	cc-4	27/04/2004	H	5.287 ± 0.020	196.43 ± 0.15		B	
		06/05/2005	K_s	5.185 ± 0.021	195.89 ± 0.22	9.9 ± 0.3	B	
	cc-5	06/05/2005	K_s	5.874 ± 0.023	247.71 ± 0.24	12.6 ± 0.3	U	
TCha	cc-1	05/03/2004	K_s	3.762 ± 0.068	227.75 ± 1.37	11.4 ± 0.1	U	
	cc-2	05/03/2004	K_s	9.326 ± 0.026	327.22 ± 0.21	11.8 ± 0.2	U	
	cc-3	05/03/2004	K_s	12.045 ± 0.026	14.47 ± 0.20	11.7 ± 0.3	U	
TWA17	cc-1	17/03/2003	H	2.637 ± 0.011	109.39 ± 0.21	10.4 ± 0.2	U	
	cc-2	17/03/2003	H	1.833 ± 0.009	335.39 ± 0.28	9.3 ± 0.2	U	
	cc-3	17/03/2003	H	3.977 ± 0.016	181.71 ± 0.14	7.7 ± 0.2	U	
	cc-4	17/03/2003	H	6.026 ± 0.019	317.01 ± 0.25	9.9 ± 0.2	U	
TWA25	cc-1	16/03/2003	K_s	8.922 ± 0.025	341.62 ± 0.22	11.2 ± 0.3	PB	HST
TWA12	cc-1	17/03/2003	K_s	5.695 ± 0.020	296.32 ± 0.26	10.9 ± 0.3	PB	HST
	cc-2	17/03/2003	K_s	6.344 ± 0.021	245.90 ± 0.24	8.4 ± 0.3	PB	MZ04, HST
	cc-3	17/03/2003	K_s	6.769 ± 0.019	5.38 ± 0.23	11.5 ± 0.3	PB	HST
TYC-8992-0605-1	cc-1	17/03/2003	H	4.567 ± 0.018	356.39 ± 0.13			
		27/04/2004	H	4.581 ± 0.019	356.98 ± 0.22	10.4 ± 0.2	B	
	cc-2	17/03/2003	H	2.462 ± 0.010	63.53 ± 0.24			
		27/04/2004	H	2.530 ± 0.011	63.52 ± 0.28	8.9 ± 0.2	B	
	cc-3	17/03/2003	H	6.509 ± 0.020	50.64 ± 0.23			
		27/04/2004	H	6.574 ± 0.025	50.54 ± 0.28	9.1 ± 0.2	B	

Table 11. Contaminants and companion identified

Name	Candidate	UT Date	Filter	Separation (arcsec)	P.A. ($^{\circ}$)	Δm (mag)	Status	Note
	cc-4	17/03/2003	H	4.691 ± 0.017	66.56 ± 0.18			
		27/04/2004	H	4.763 ± 0.019	66.30 ± 0.24	10.3 ± 0.2	B	
	cc-5	17/03/2003	H	6.891 ± 0.025	70.95 ± 0.15			
		27/04/2004	H	6.971 ± 0.027	70.51 ± 0.22	11.2 ± 0.2	B	
	cc-6	17/03/2003	H	3.166 ± 0.014	97.83 ± 0.16			
		27/04/2004	H	3.229 ± 0.014	96.97 ± 0.23	9.3 ± 0.2	B	
	cc-7	17/03/2003	H	2.554 ± 0.011	111.75 ± 0.22			
		27/04/2004	H	2.606 ± 0.012	110.53 ± 0.27	8.5 ± 0.2	B	
	cc-8	17/03/2003	H	6.360 ± 0.023	112.51 ± 0.16			
		27/04/2004	H	6.411 ± 0.025	111.87 ± 0.23	10.1 ± 0.2	B	
	cc-9	17/03/2003	H	2.322 ± 0.010	145.80 ± 0.28			
		27/04/2004	H	2.351 ± 0.011	144.03 ± 0.32	10.5 ± 0.2	B	
	cc-10	17/03/2003	H	5.411 ± 0.017	134.01 ± 0.25			
		27/04/2004	H	5.456 ± 0.021	133.00 ± 0.30	10.7 ± 0.2	B	
	cc-11	17/03/2003	H	6.066 ± 0.019	134.44 ± 0.25			
		27/04/2004	H	6.105 ± 0.023	133.49 ± 0.30	11.1 ± 0.2	B	
	cc-12	17/03/2003	H	6.642 ± 0.026	179.24 ± 0.12			
		27/04/2004	H	6.626 ± 0.026	178.39 ± 0.21	8.5 ± 0.2	B	
	cc-13	17/03/2003	H	2.534 ± 0.010	226.43 ± 0.31			
		27/04/2004	H	2.474 ± 0.011	225.66 ± 0.36	10.7 ± 0.2	B	
	cc-14	17/03/2003	H	7.632 ± 0.025	210.15 ± 0.19			
		27/04/2004	H	7.583 ± 0.029	209.49 ± 0.24	9.0 ± 0.2	B	
	cc-15	17/03/2003	H	7.159 ± 0.022	228.54 ± 0.23			
		27/04/2004	H	7.085 ± 0.027	227.98 ± 0.29	11.1 ± 0.2	B	
V343Nor B	cc-1	05/03/2004	H	2.303 ± 0.009	42.41 ± 0.32	6.7 ± 0.2	PB	HST
	cc-2	05/03/2004	H	5.656 ± 0.020	63.36 ± 0.18	8.7 ± 0.2	PB	HST
	cc-3	05/03/2004	H	6.121 ± 0.023	78.82 ± 0.13	7.2 ± 0.2	PB	HST
	cc-4	05/03/2004	H	3.313 ± 0.014	103.55 ± 0.17	7.5 ± 0.2	PB	HST
	cc-5	05/03/2004	H	5.232 ± 0.017	135.05 ± 0.26	4.7 ± 0.2	U	
	cc-6	05/03/2004	H	7.940 ± 0.024	136.49 ± 0.24	4.5 ± 0.2	U	
	cc-7	05/03/2004	H	7.551 ± 0.027	161.27 ± 0.15	7.7 ± 0.2	U	
	cc-8	05/03/2004	H	5.234 ± 0.019	157.88 ± 0.17	8.1 ± 0.2	U	
	cc-9	05/03/2004	H	6.503 ± 0.025	169.91 ± 0.13	7.2 ± 0.2	U	
	cc-10	05/03/2004	H	4.444 ± 0.018	185.95 ± 0.14	7.4 ± 0.2	PB	HST
	cc-11	05/03/2004	H	5.215 ± 0.020	188.31 ± 0.13	5.2 ± 0.2	U	
	cc-12	05/03/2004	H	1.421 ± 0.008	205.46 ± 0.34	7.3 ± 0.2	PB	HST
	cc-13	05/03/2004	H	2.724 ± 0.010	221.71 ± 0.29	7.4 ± 0.2	PB	HST
	cc-14	05/03/2004	H	6.000 ± 0.019	225.61 ± 0.25	5.8 ± 0.2	U	
	cc-15	05/03/2004	H	7.233 ± 0.022	226.59 ± 0.24	7.4 ± 0.2	U	
	cc-16	05/03/2004	H	2.438 ± 0.011	248.22 ± 0.22	9.1 ± 0.2	PB	HST
	cc-17	05/03/2004	H	5.924 ± 0.021	295.92 ± 0.18	5.1 ± 0.2	PB	HST
	cc-18	05/03/2004	H	6.807 ± 0.021	313.78 ± 0.25	7.7 ± 0.2	PB	HST
TYC-6461-1120-1 AB	cc-1	08/01/2006	K _s	7.212 ± 0.013	33.68 ± 0.13	11.7 ± 0.2	PB	HST
	cc-2	08/01/2006	K _s	11.665 ± 0.022	137.29 ± 0.13	10.9 ± 0.2	U	
HIP76768 AB	cc-1	18/08/2005	K _s	8.903 ± 0.023	103.47 ± 0.22	10.7 ± 0.3	U	
	cc-2	18/08/2005	K _s	11.571 ± 0.035	224.06 ± 0.24	10.9 ± 0.3	U	
HIP6485	cc-1	08/01/2006	K _s	10.790 ± 0.029	322.12 ± 0.19	18.7 ± 0.2	PB	HST
TWA14	cc-1	08/01/2006	K _s	16.798 ± 0.038	45.40 ± 0.18	7.6 ± 0.3	U	
	cc-2	08/01/2006	K _s	14.653 ± 0.033	143.98 ± 0.17	8.2 ± 0.3	U	
	cc-3	08/01/2006	K _s	10.233 ± 0.026	223.30 ± 0.20	9.0 ± 0.3	U	
	cc-4	08/01/2006	K _s	2.451 ± 0.015	240.97 ± 0.39	12.0 ± 0.3	PB	HST
HIP84642 AB	cc-1	05/06/2007	K _s	14.663 ± 0.043	51.36 ± 0.22	10.9 ± 0.2	U	
	cc-2	05/06/2007	K _s	7.316 ± 0.022	67.68 ± 0.23	10.0 ± 0.2	U	
	cc-3	05/06/2007	K _s	5.871 ± 0.018	103.39 ± 0.24	10.8 ± 0.2	U	
	cc-4	05/06/2007	K _s	11.579 ± 0.030	70.64 ± 0.21	12.8 ± 0.2	U	
	cc-5	05/06/2007	K _s	12.915 ± 0.033	201.71 ± 0.21	8.2 ± 0.2	B	Hu08
	cc-6	05/06/2007	K _s	10.810 ± 0.027	194.72 ± 0.21	12.1 ± 0.2	U	
	cc-7	05/06/2007	K _s	12.023 ± 0.033	206.74 ± 0.21	12.8 ± 0.2	U	
	cc-8	05/06/2007	K _s	3.926 ± 0.017	315.16 ± 0.36	11.8 ± 0.2	U	
HIP107947	cc-1	19/08/2005	K _s	11.094 ± 0.025	33.18 ± 0.15	14.5 ± 0.2	U	
HIP51386	cc-1	26/02/2006	K _s	5.242 ± 0.0100	187.08 ± 0.14	10.9 ± 0.1	PB	HST
	cc-2	26/02/2006	K _s	12.191 ± 0.023	176.01 ± 0.15	12.8 ± 0.2	U	

Table 12. Contaminants and companion identified

Name	Candidate	UT Date	Filter	Separation (arcsec)	P.A. ($^{\circ}$)	Δm (mag)	Status	Note
HIP88399	cc-1	24/09/2004	K_s	11.242 ± 0.028	17.93 ± 0.21	13.3 ± 0.2	PB	HST
	cc-2	24/09/2004	K_s	13.045 ± 0.038	36.55 ± 0.22	$15. \pm 0.2$	U	
	cc-3	24/09/2004	K_s	11.155 ± 0.034	46.37 ± 0.24	14.6 ± 0.2	U	
	cc-4	24/09/2004	K_s	14.598 ± 0.043	138.5 ± 0.23	$12. \pm 0.2$	U	
	cc-5	24/09/2004	K_s	14.774 ± 0.043	138.87 ± 0.22	11.6 ± 0.2	U	
	cc-6	24/09/2004	K_s	9.735 ± 0.023	178.36 ± 0.22	13.9 ± 0.2	U	
	cc-7	24/09/2004	K_s	7.354 ± 0.021	198.90 ± 0.23	13.3 ± 0.2	U	
	cc-8	24/09/2004	K_s	10.144 ± 0.031	322.37 ± 0.23	14.5 ± 0.2	PB	HST
HIP76107	cc-1	06/05/2005	K_s	4.635 ± 0.017	56.81 ± 0.25	5.3 ± 0.1	U	
	cc-2	06/05/2005	K_s	2.191 ± 0.010	31.99 ± 0.32	9.4 ± 0.2	U	
	cc-3	06/05/2005	K_s	2.549 ± 0.011	57.18 ± 0.30	8.1 ± 0.2	U	
	cc-4	06/05/2005	K_s	2.671 ± 0.012	57.54 ± 0.30	9.3 ± 0.2	U	
	cc-5	06/05/2005	K_s	5.338 ± 0.021	112.95 ± 0.23	9.4 ± 0.2	U	
	cc-6	06/05/2005	K_s	6.038 ± 0.023	114.83 ± 0.24	9.0 ± 0.2	U	
	cc-7	06/05/2005	K_s	6.077 ± 0.023	131.39 ± 0.29	10.5 ± 0.2	U	
	cc-8	06/05/2005	K_s	4.219 ± 0.017	140.92 ± 0.29	10.2 ± 0.2	U	
	cc-9	06/05/2005	K_s	2.729 ± 0.012	153.00 ± 0.28	9.2 ± 0.2	U	
	cc-10	06/05/2005	K_s	2.908 ± 0.013	167.35 ± 0.25	8.2 ± 0.2	U	
	cc-11	06/05/2005	K_s	3.200 ± 0.014	167.50 ± 0.24	9.2 ± 0.2	U	
	cc-12	06/05/2005	K_s	6.578 ± 0.025	158.18 ± 0.23	10.1 ± 0.2	U	
	cc-13	06/05/2005	K_s	6.729 ± 0.026	170.23 ± 0.21	8.5 ± 0.2	U	
	cc-14	06/05/2005	K_s	6.387 ± 0.025	193.80 ± 0.22	10.3 ± 0.2	U	
	cc-15	06/05/2005	K_s	8.177 ± 0.031	216.20 ± 0.26	8.9 ± 0.2	U	
	cc-16	06/05/2005	K_s	7.925 ± 0.030	215.24 ± 0.26	10.3 ± 0.2	U	
	cc-17	06/05/2005	K_s	6.519 ± 0.025	289.28 ± 0.22	9.2 ± 0.2	U	
	cc-18	06/05/2005	K_s	1.759 ± 0.009	287.32 ± 0.31	9.8 ± 0.2	U	
	cc-19	06/05/2005	K_s	4.703 ± 0.022	294.11 ± 0.29	10.7 ± 0.2	U	
	cc-20	06/05/2005	K_s	1.726 ± 0.015	294.01 ± 0.53	10.2 ± 0.2	U	
	cc-21	06/05/2005	K_s	5.171 ± 0.023	130.22 ± 0.33	10.6 ± 0.2	U	
	cc-22	06/05/2005	K_s	4.701 ± 0.022	176.12 ± 0.26	10.6 ± 0.2	U	
	cc-23	06/05/2005	K_s	6.606 ± 0.028	208.78 ± 0.27	10.4 ± 0.2	U	
HIP21632 B	cc-1	22/10/2006	K_s	7.415 ± 0.037	239.87 ± 0.31	4.8 ± 0.2	PB	HST
HIP30314	cc-1	21/11/2006	K_s	10.425 ± 0.018	10.51 ± 0.20	11.8 ± 0.2	PB	HST
HIP26373	cc-1	26/12/2006	K_s	8.795 ± 0.024	28.18 ± 0.20	$13. \pm 0.2$	U	
HIP1481	cc-1	21/10/2006	K_s	10.218 ± 0.025	232.58 ± 0.18	13.4 ± 0.2	PB	HST
HIP3556	cc-1	22/10/2006	K_s	9.160 ± 0.017	206.22 ± 0.15	8.3 ± 0.1	U	
HIP96334	cc-1	09/06/2007	K_s	12.173 ± 0.023	184.16 ± 0.20	12.8 ± 0.2	U	
	cc-2	09/06/2007	K_s	7.104 ± 0.016	260.85 ± 0.20	13.5 ± 0.1	PB	HST
	cc-3	09/06/2007	K_s	4.451 ± 0.018	322.03 ± 0.30	4.6 ± 0.2	PB	HST
HIP92680	cc-1	13/06/2007	K_s	8.284 ± 0.020	335.54 ± 0.20	11.1 ± 0.1	PB	HST
	cc-2	13/06/2007	K_s	4.008 ± 0.008	166.30 ± 0.20	10.7 ± 0.1	PB	HST
	cc-3	13/06/2007	K_s	10.74 ± 0.030	128.42 ± 0.21	11.5 ± 0.1	U	
	cc-4	13/06/2007	K_s	9.013 ± 0.025	159.75 ± 0.22	11.9 ± 0.2	U	
HIP92024	cc-1	04/06/2007	K_s	7.429 ± 0.025	318.53 ± 0.26	14.3 ± 0.2	PB	HST
HIP113579	cc-1	15/06/2007	K_s	5.352 ± 0.012	107.69 ± 0.20	11.8 ± 0.1	PB	HST
HIP105404	cc-1	30/05/2007	K_s	3.253 ± 0.009	48.43 ± 0.22	8.5 ± 0.1	PB	HST
	cc-2	30/05/2007	K_s	5.861 ± 0.017	161.27 ± 0.20	11.7 ± 0.30	U	
FS1174	cc-1	06/05/2005	K_s	6.571 ± 0.020	246.02 ± 0.20	6.2 ± 0.2	U	
FS903	cc-1	19/08/2005	K_s	7.172 ± 0.016	19.96 ± 0.20	8.1 ± 0.1	U	
	cc-2	19/08/2005	K_s	5.232 ± 0.010	357.52 ± 0.20	12.1 ± 0.2	U	
	cc-3	19/08/2005	K_s	5.256 ± 0.012	341.52 ± 0.20	10.5 ± 0.1	U	
	cc-4	19/08/2005	K_s	7.980 ± 0.019	339.09 ± 0.20	10.9 ± 0.1	U	
	cc-5	19/08/2005	K_s	6.970 ± 0.014	282.91 ± 0.20	$11. \pm 0.1$	U	
	cc-6	19/08/2005	K_s	7.421 ± 0.018	244.76 ± 0.20	12.1 ± 0.1	U	
	cc-7	19/08/2005	K_s	12.637 ± 0.024	177.28 ± 0.20	10.5 ± 0.2	U	
	cc-8	19/08/2005	K_s	9.867 ± 0.026	149.58 ± 0.20	10.7 ± 0.1	U	
	cc-9	19/08/2005	K_s	13.576 ± 0.036	146.13 ± 0.20	10.3 ± 0.1	U	
	cc-10	19/08/2005	K_s	11.234 ± 0.024	106.61 ± 0.20	11.3 ± 0.1	U	
	cc-11	19/08/2005	K_s	3.907 ± 0.007	86.47 ± 0.20	10.3 ± 0.1	U	
	cc-12	19/08/2005	K_s	9.802 ± 0.023	22.70 ± 0.20	11.9 ± 0.2	U	

Table 13. Contaminants and companion identified

Name	Candidate	UT Date	Filter	Separation (arcsec)	P.A. ($^{\circ}$)	Δm (mag)	Status	Note
	cc-13	19/08/2005	K _s	10.2140 ± 0.024	20.55 ± 0.20	12.6 ± 0.2	U	
	cc-14	19/08/2005	K _s	15.5660 ± 0.109	40.75 ± 0.47	13.6 ± 0.2	U	
	cc-15	19/08/2005	K _s	15.7480 ± 0.043	52.83 ± 0.21	12.6 ± 0.2	U	
	cc-16	19/08/2005	K _s	10.6060 ± 0.023	74.40 ± 0.20	12.6 ± 0.2	U	
	cc-17	19/08/2005	K _s	7.913 ± 0.015	84.50 ± 0.20	12.4 ± 0.2	U	
	cc-18	19/08/2005	K _s	8.452 ± 0.023	117.150 ± 0.2	13.3 ± 0.2	U	
	cc-19	19/08/2005	K _s	8.233 ± 0.023	138.790 ± 0.21	12.7 ± 0.2	U	
	cc-20	19/08/2005	K _s	15.0430 ± 0.042	134.810 ± 0.23	13. ± 0.2	U	
	cc-21	19/08/2005	K _s	5.707 ± 0.013	161.20 ± 0.20	12.6 ± 0.2	U	
	cc-22	19/08/2005	K _s	6.737 ± 0.014	167.080 ± 0.20	12.4 ± 0.2	U	
	cc-23	19/08/2005	K _s	8.008 ± 0.015	184.020 ± 0.20	12.4 ± 0.2	U	
	cc-24	19/08/2005	K _s	9.701 ± 0.026	214.510 ± 0.20	12.5 ± 0.2	U	
	cc-25	19/08/2005	K _s	11.4670 ± 0.031	234.780 ± 0.20	12.4 ± 0.2	U	
	cc-26	19/08/2005	K _s	5.860 ± 0.034	253.960 ± 0.33	12.5 ± 0.2	U	
	cc-27	19/08/2005	K _s	4.645 ± 0.061	282.620 ± 0.37	12.9 ± 0.2	U	
	cc-28	19/08/2005	K _s	11.7810 ± 0.031	329.050 ± 0.2	13.7 ± 0.2	U	
	cc-29	19/08/2005	K _s	4.99 ± 0.015	311.150 ± 0.23	11.4 ± 0.2	U	
	cc-30	19/08/2005	K _s	4.574 ± 0.030	311.460 ± 0.50	13.1 ± 0.2	U	
FS979	cc-1	18/08/2005	K _s	7.466 ± 0.019	119.00 ± 0.20	0.70 ± 0.1	U	
	cc-2	18/08/2005	K _s	9.708 ± 0.030	49.40 ± 0.24	13.2 ± 0.2	U	
	cc-3	18/08/2005	K _s	8.123 ± 0.023	69.50 ± 0.22	9.6 ± 0.2	U	
	cc-4	18/08/2005	K _s	13.773 ± 0.040	52.26 ± 0.22	10.9 ± 0.2	U	
	cc-5	18/08/2005	K _s	12.744 ± 0.032	69.13 ± 0.21	11.4 ± 0.2	U	
	cc-6	18/08/2005	K _s	8.875 ± 0.022	80.60 ± 0.22	11.8 ± 0.2	U	
	cc-7	18/08/2005	K _s	11.495 ± 0.025	87.28 ± 0.21	9.9 ± 0.2	U	
	cc-8	18/08/2005	K _s	15.265 ± 0.032	96.87 ± 0.21	12.4 ± 0.2	U	
	cc-9	18/08/2005	K _s	13.839 ± 0.036	113.76 ± 0.21	9.4 ± 0.2	U	
	cc-10	18/08/2005	K _s	12.594 ± 0.036	123.64 ± 0.21	12.1 ± 0.2	U	
	cc-11	18/08/2005	K _s	19.220 ± 0.051	118.95 ± 0.20	10.6 ± 0.2	U	
	cc-12	18/08/2005	K _s	19.108 ± 0.053	123.28 ± 0.21	9.4 ± 0.2	U	
	cc-13	18/08/2005	K _s	19.719 ± 0.054	123.76 ± 0.21	9.8 ± 0.2	U	
	cc-14	18/08/2005	K _s	18.911 ± 0.054	137.2 ± 0.23	10.3 ± 0.2	U	
	cc-15	18/08/2005	K _s	16.818 ± 0.048	142.48 ± 0.21	9.3 ± 0.2	U	
	cc-16	18/08/2005	K _s	17.371 ± 0.048	148.61 ± 0.20	10.5 ± 0.2	U	
	cc-17	18/08/2005	K _s	16.05 ± 0.040	157.82 ± 0.20	9.6 ± 0.2	U	
	cc-18	18/08/2005	K _s	9.561 ± 0.028	150.28 ± 0.22	9.2 ± 0.2	U	
	cc-19	18/08/2005	K _s	9.335 ± 0.025	162.81 ± 0.22	11.2 ± 0.2	U	
	cc-20	18/08/2005	K _s	10.5330 ± 0.026	166. ± 0.21	9.6 ± 0.2	U	
	cc-21	18/08/2005	K _s	13.1630 ± 0.031	165.12 ± 0.21	9.2 ± 0.2	U	
	cc-22	18/08/2005	K _s	15.0450 ± 0.033	170.09 ± 0.21	10.5 ± 0.2	U	
	cc-23	18/08/2005	K _s	14.9610 ± 0.032	172.92 ± 0.21	11.4 ± 0.2	U	
	cc-24	18/08/2005	K _s	13.3330 ± 0.028	178.26 ± 0.21	10.9 ± 0.2	U	
	cc-25	18/08/2005	K _s	12.0260 ± 0.026	179.48 ± 0.21	8.4 ± 0.2	U	
	cc-26	18/08/2005	K _s	13.5530 ± 0.029	181.5 ± 0.21	10.6 ± 0.2	U	
	cc-27	18/08/2005	K _s	14.6020 ± 0.030	179.2 ± 0.21	10.4 ± 0.2	U	
	cc-28	18/08/2005	K _s	11.2080 ± 0.027	194.240 ± 0.21	9.9 ± 0.2	U	
	cc-29	18/08/2005	K _s	11.41 ± 0.028	196.670 ± 0.21	11.1 ± 0.2	U	
	cc-30	18/08/2005	K _s	7.599 ± 0.022	202.230 ± 0.22	9.9 ± 0.2	U	
	cc-31	18/08/2005	K _s	7.318 ± 0.023	210.770 ± 0.23	8.6 ± 0.2	U	
	cc-32	18/08/2005	K _s	8.455 ± 0.026	212.350 ± 0.23	10.9 ± 0.2	U	
	cc-33	18/08/2005	K _s	12.2310 ± 0.037	221.730 ± 0.23	9.3 ± 0.2	U	
	cc-34	18/08/2005	K _s	14.2890 ± 0.041	215.540 ± 0.21	9.8 ± 0.2	U	
	cc-35	18/08/2005	K _s	15.3130 ± 0.043	213.530 ± 0.21	10.5 ± 0.2	U	
	cc-36	18/08/2005	K _s	15.72 ± 0.043	209.010 ± 0.20	10.8 ± 0.2	U	
	cc-37	18/08/2005	K _s	6.003 ± 0.021	310.140 ± 0.27	9.6 ± 0.2	U	
	cc-38	18/08/2005	K _s	7.943 ± 0.026	306.510 ± 0.24	8.2 ± 0.2	U	
	cc-39	18/08/2005	K _s	11.25 ± 0.032	329.780 ± 0.21	10.7 ± 0.2	U	
	cc-40	18/08/2005	K _s	10.2740 ± 0.027	338.870 ± 0.21	10.2 ± 0.2	U	
	cc-41	18/08/2005	K _s	9.583 ± 0.024	347.890 ± 0.21	8.9 ± 0.2	U	

Table 14. Contaminants and companion identified

Name	Candidate	UT Date	Filter	Separation (arcsec)	P.A. ($^{\circ}$)	Δm (mag)	Status	Note
FS1017	cc-1	19/08/2005	K_s	12.041 ± 0.032	57.93 ± 0.20	4.8 ± 0.1	U	
	cc-2	19/08/2005	K_s	9.463 ± 0.025	213.830 ± 0.20	5.9 ± 0.1	U	
	cc-3	19/08/2005	K_s	9.689 ± 0.024	243.940 ± 0.20	4.1 ± 0.1	U	
	cc-4	19/08/2005	K_s	13.799 ± 0.038	318.650 ± 0.21	6.3 ± 0.1	U	
	cc-5	19/08/2005	K_s	15.149 ± 0.042	317.320 ± 0.22	6.1 ± 0.1	U	
	cc-6	19/08/2005	K_s	14.507 ± 0.040	119.520 ± 0.21	7.5 ± 0.2	U	
	cc-7	19/08/2005	K_s	13.537 ± 0.038	148.030 ± 0.21	7.6 ± 0.2	U	
	cc-8	19/08/2005	K_s	9.057 ± 0.022	170.110 ± 0.22	7.2 ± 0.2	U	
	cc-9	19/08/2005	K_s	17.1820 ± 0.050	319.390 ± 0.22	7.0 ± 0.2	U	
	cc-10	19/08/2005	K_s	17.046 ± 0.049	319.840 ± 0.22	7.4 ± 0.2	U	
	cc-11	19/08/2005	K_s	7.984 ± 0.020	184.820 ± 0.22	8.2 ± 0.2	U	
FS1035	cc-1	19/08/2005	K_s	5.402 ± 0.020	27.05 ± 0.25			
		28/06/2008	K_s	5.862 ± 0.020	26.98 ± 0.25	7.4 ± 0.2	B	

Deep imaging survey of young, nearby austral stars

VLT/NACO Near-Infrared Lyot-Coronagraphic Observations

G. Chauvin¹, A.-M. Lagrange¹, M. Bonavita^{2,3}, B. Zuckerman⁴, C. Dumas⁵, M. S. Bessell⁶, J.-L. Beuzit¹, M. Bonnefoy¹, S. Desidera², J. Farihi⁷, P. Lowrance⁸, D. Mouillet¹, and I. Song⁹

¹ Laboratoire d'Astrophysique, Observatoire de Grenoble, UJF, CNRS: 414, Rue de la piscine, 38400 Saint-Martin d'Hères, France

² INAF - Osservatorio Astronomico di Padova, Vicolo dell' Osservatorio 5, 35122 Padova, Italy

³ Università di Padova, Dipartimento di Astronomia, Vicolo dell'Osservatorio 2, 35122 Padova, Italy

⁴ Department of Physics & Astronomy and Center for Astrobiology, University of California: Los Angeles, Box 951562, CA 90095, USA

⁵ European Southern Observatory: Casilla 19001, Santiago 19, Chile

⁶ Research School of Astronomy and Astrophysics Institute of Advance Studies, Australian National University: Cotter Road, Weston Creek, Canberra, ACT 2611, Australia

⁷ Department of Physics & Astronomy, University of Leicester, Leicester LE1 7RH, United Kingdom

⁸ Spitzer Science Center, IPAC/Caltech: MS 220-6, Pasadena, CA 91125, USA

⁹ Department of Physics & Astronomy, University of Georgia, Athens, GA 30602-2451, USA

Received September, 2008

ABSTRACT

Context. High contrast and high angular resolution imaging is the optimal technique to search for substellar companions to nearby stars at physical separations larger than typically 10 AU. Two distinct populations of substellar companions, brown dwarfs and planets, can be probed and characterized. Fossil traces of their different formation processes should be revealed by their respective physical and orbital properties and should then allow testing basic aspects of their respective formation and evolution mechanisms.

Aims. Since November 2002, we have conducted the largest deep imaging survey of the young, nearby associations of the southern hemisphere. Our goal is detection and characterization of substellar companions at intermediate (10 – 500 AU) physical separations. We have observed a sample of 88 stars, mostly G to M dwarfs, that we essentially identify as younger than 100 Myr and closer to Earth than 100 pc.

Methods. The VLT/NACO adaptive optics instrument of the ESO Paranal Observatory was used to explore the faint circumstellar environment between typically 0.1 and 10". Diffraction-limited observations in *H* and *K_s*-band combined with Lyot-coronagraphy enabled us to reach contrast performances as small as 10⁻⁶. The existence of planetary mass companions could therefore be probed. We used a standardized observing sequence to precisely measure the position and flux of all detected sources relative to their visual primary star. Repeated observations at several epochs enabled us to discriminate comoving companions from contaminants.

Results. We report the discovery of 17 new close (0.1 – 5.0 ") multiple systems. HIP 108195 AB and C (F1 III-M6), HIP 84642 AB (*a* ~ 14 AU, K0-M5) and TWA22 AB (*a* ~ 1.8 AU; M6-M6) are confirmed comoving systems. TWA22 AB is likely to be a rare astrometric calibrator that can be used to test evolutionary model predictions. Among our complete sample, a total of 65 targets were observed with deep coronagraphic imaging. About 240 faint companion candidates were detected around 36 stars. Follow-up observations with VLT or HST for 83% of these stars enabled us to identify a large fraction of contaminants. The latest results about the substellar companions to GSC 08047-00232, AB Pic and 2M1207, confirmed during this survey and published earlier, are reviewed. Finally, the statistical analysis of our complete set of coronagraphic detection limits enables us to place constraints on the physical and orbital properties of giant planets between typically 20 and 150 AU.

Conclusions.

Key words. Instrumentation: adaptive optics, high angular resolution – Methods: observational, data analysis, statistical – Techniques: photometric, astrometric – Stars: low-mass, brown dwarfs, planetary systems

1. Introduction

The search for substellar objects, isolated, multiple or companion to nearby stars, has been an important driver for observers in the two last decades. Their detection and characterization contribute to developing our understanding of the formation and evolution of stars, brown dwarfs and planets. Since the discovery of the first unambiguous brown dwarf Gl229 B (Nakajima et al. 1995), the development of new instruments and observing techniques has diversified. Large surveys (2MASS, Skrutskie et al. 1997; DENIS, Epchtein et al. 1997; SLOAN, York et al. 2000) are the best method for the study of isolated substellar objects.

Hundreds of brown dwarfs have been discovered in the field motivating the introduction of the new L and T spectral classes (Delfosse et al. 1997; Kirkpatrick et al 1999; Burgasser et al. 1999). Dedicated spectroscopic observations offer the opportunity to study the physical and chemical processes of these very cool atmospheres, such as grain and molecule formation, vertical mixing and cloud coverage. In the field, in young open clusters or in star forming regions, the study of the initial-mass function and of stellar and substellar multiplicity shows an apparent continuous sequence supporting the idea that stellar mechanisms (collapse, fragmentation, ejection, photo-evaporation of accre-

tion envelopes) form objects over a wide range of masses, down to planetary masses predicted by theoretical models (Bonnell et al. 2007; Burgasser et al. 2007; Zuckerman & Song 2009). Despite limited spatial resolution, a dozen substellar companions to nearby stars have been discovered at wide (≥ 100 AU) orbits (Goldman et al. 1999, Kirkpatrick et al. 2000, Wilson et al. 2001).

To access the near (≤ 5 AU) environment of stars, other observing techniques (radial velocity, transit, micro-lensing, pulsar-timing), are so far best suited. The radial velocity (RV) and transit techniques are nowadays the most successful methods for detecting and characterizing the properties of exoplanetary systems. The RV surveys have focused on main sequence solar-type stars, with numerous narrow optical lines and low activity, to ensure high RV precision. Recently, planet-search programs have been extended to lower and higher mass stars (Endl et al. 2006, Lagrange et al. 2009) and younger and more evolved systems (Joergens et al. 2006, Johnson et al. 2007). Since the discovery of 51 Peg b (Mayor & Queloz 1995), more than 300 exo-planets have been identified featuring a broad range of physical (mass) and orbital (P , e) characteristics (Udry & Santos 2007; Butler et al. 2006). This technique also revealed the existence of the so-called brown dwarf desert at small (≤ 5 AU) separations (Grether & Lineweaver 2006). The bimodal aspect of the secondary mass distribution indicates different formation mechanisms for two populations of substellar companions, brown dwarfs and planets. The transit technique coupled with RV enables determination of the radius and density of giant planets and thus a probe of their internal structure. Moreover, spectral elements of a planetary atmosphere can be revealed during primary or secondary eclipse (Swain et al. 2008, Grillmair et al. 2008).

To extend such systematic characterization at larger scales (≥ 10 AU), the deep imaging technique is particularly well suited to probe the existence of planets and brown dwarf companions and complete our view of planetary formation and evolution. To access small angular separations, the space telescope (HST) or the combination of Adaptive Optics (AO) system with very large ground-based telescopes (Palomar, CFHT, Keck, Gemini, Subaru, VLT) have become mandatory. Moreover, deep imaging surveys take advantage of exhaustive work on identification of young (≤ 100 Myr), nearby (≤ 100 pc) stellar associations. Due to their youth and proximity, such stars offer an ideal niche for detection of warm planetary mass companions that are still moderately bright at near-infrared wavelengths. Since the recognition of the TW Hydrae association (TWA; Kastner et al. 1997; Webb et al. 1999), more than 200 young, nearby stars have been identified. Many such stars reside in several coeval moving groups (e.g., TWA, β Pictoris, Tucana-Horologium, η Cha, AB Dor, Columba and Carinae), sharing common kinematics, photometric and spectroscopic properties (see Zuckerman & Song 2004, hereafter ZS04; Torres et al. 2008, T08). A few young brown dwarf companions have been detected from space, HR 7329 B and TWA5 B (Lowrance et al. 2000, 1999), and from the ground, GSC 08047-00232 B (Chauvin et al. 2005a). Companions down to the planetary mass regime were discovered around the star AB Pic (Chauvin et al. 2005c) and the young brown dwarf 2M1207 (Chauvin et al. 2004, 2005b). Various deep imaging surveys of young, nearby stars have recently been completed using different high contrast imaging techniques such as coronagraphy, differential imaging or L -band imaging (see Table 1). A significant number have reported a null-detection result of substellar companions. Kasper et al. (2007), Lafrenière et al. (2007) and Nielsen et al. (2008) have initiated a statistical analysis to

Table 1. Deep imaging surveys of young (< 100 Myr), nearby (< 100 pc) stars dedicated to the search for planetary mass companions and published in the literature. The telescope and the instrument (Tel/Instr.), the imaging mode (CI: coronagraphic imaging; Sat-DI; saturated direct imaging; DI direct imaging; SDI: simultaneous differential imaging; ADI: angular differential imaging) and filters, the field of view (FoV) and the number of stars observed (#) are given. The typical survey sensitivity in terms of mass is also reported with the survey reference.

Tel/Instr.	Mode & Filter	FoV (arcsec)	#	Mass (M_{Jup})	Ref.
3.6m/ADONIS	CI, $H - K$	13×13	29	5	(1)
NTT/Sharp	Sat-DI, K	11×11	23	5	(2)
NTT/Sofi	Sat-DI, H	13×13	10	5	(2)
HST/NICMOS	DI, H	19×19	45	1	(3)
VLT/NaCo	Sat-DI, $H - K$	14×14	28	5	(4)
VLT/NaCo	SDI, H	5×5	45	1	(5)
VLT/NaCo	DI, L'	28×28	22	1	(6)
Gemini/NIRI	ADI, H	22×22	85*	1	(7)

- REFERENCES: (1) Chauvin et al. 2003, (2) Neuhäuser et al. 2003, (3) Lowrance et al. 2005, (4) Masciadri et al. 2005, (5) Biller et al. 2007, (6) Kasper et al. 2007, (7) Lafrenière et al. 2007

- (*): half have age estimates younger than 200 Myr (see Fig. 1, Lafrenière et al. 2007)

constrain the physical and orbital properties (mass, period, eccentricity distributions) of a giant planet population. Despite the model-dependency on the mass predictions, the approach is attractive for exploiting the complete set of detection performances of the survey and characterizing the outer portions of exo-planetary systems.

Deep imaging surveys were performed on other classes of targets: distant young associations (Taurus, Chamaeleon, Lupus, Upper Sco), nearby intermediate-age (0.1 – 1.0 Gyr) stars, very nearby stars and old stars with planets detected by RV. Additional substellar companions were detected with masses at the edge or inside the planetary mass regime around the star, DH Tau (Itoh et al. 2005), GQ Lup (Neuhäuser et al. 2005), CHXR 73 (Luhman et al. 2006), HD230030 (Metchev et al. 2006) and more recently IRXS J160929.1-210524 (Lafrenière et al. 2008) and CT Cha (Schmidt et al. 2008). The uncertain fraction of brown dwarf secondaries led various teams (McCarthy & Zuckerman 2004; Carson et al. 2005, 2006; Metchev et al. 2008) to test the extension of the brown desert to intermediate separations. Another purpose was to probe the existence and the impact of wide massive substellar companions to exoplanetary systems detected by RV (Patience et al. 2002; Luhman & Jayawardhana 2002; Chauvin et al. 2006; Mugrauer et al. 2007; Eggenberger et al. 2007). Only very recently, an important breakthrough has been achieved with the imaging detection of planetary mass companions HR 8799 bcd (Marois et al. 2008b), Fomalhaut b (Kalas et al. 2008) and the candidate β Pic b (Lagrange et al. 2009). Such discoveries offer new attractive perspectives for current on-going surveys until the arrival of the second generation of deep imaging instruments like Gemini Planet Imager (GPI; Macintosh et al. 2006) and VLT/SPHERE (Dohlen et al. 2006).

In this paper we report results of a deep coronagraphic imaging survey of several young, nearby austral stars, aimed at discovering substellar companions. In regards to previous works (see Table 1), it represents one of the largest and deepest surveys obtained so far on this class of targets. This survey, initi-

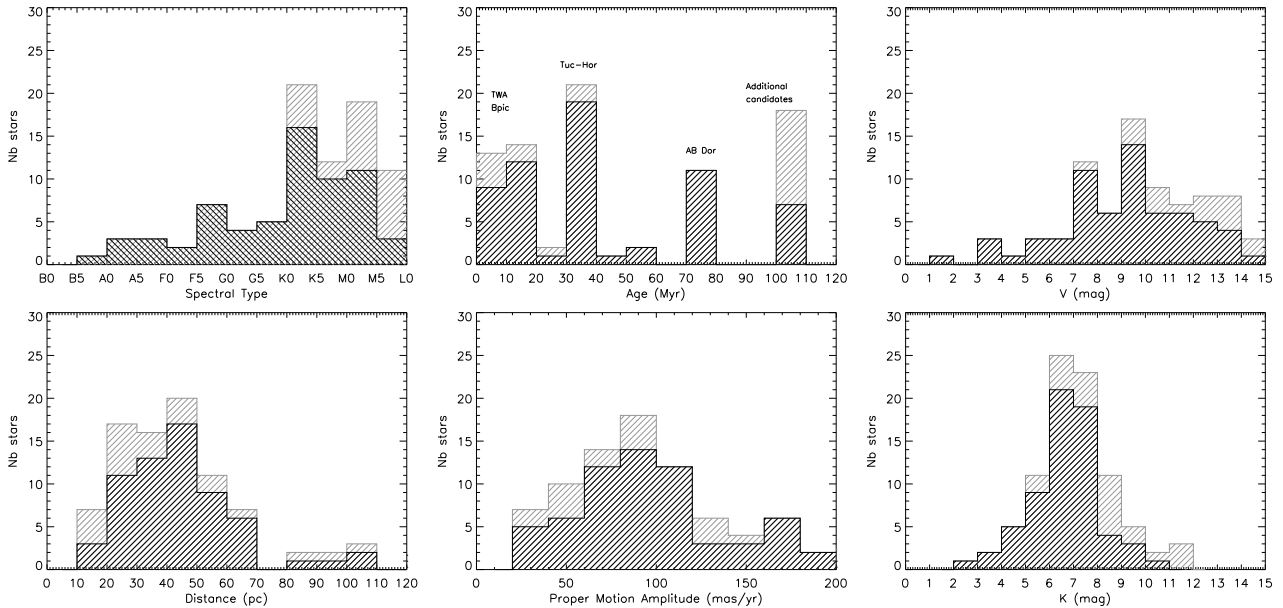


Fig. 1. Histograms summarizing the main properties of the sample of young, nearby stars observed with NACO at VLT. *Top-Left:* Histogram of spectral types for the stars observed in coronagraphic imaging (*crossed lines*) and in direct imaging (*simple lines*). *Top-Middle:* Histogram of ages for members of known young, nearby associations (TWA, β Pic, Tuc-Hor, AB Dor) and additional young candidates. *Top-Right:* Histogram of V-band fluxes. The performances of the AO correction with the NACO visible-WFS decreases between $12 \leq V \leq 16$. *Bottom-Right:* Histogram of K-band fluxes. The coronagraphic mode is not efficient anymore for stars fainter than $K \geq 9 - 10$.

ated in November 2000 with the ADONIS/SHARPII instrument on a 3.6 m telescope (Chauvin et al. 2003), was then extended with the VLT/NACO instrument between November 2002 and October 2007. In Section 2, the sample definition and properties are presented. In Section 3, we describe the characteristics of the VLT/NACO instrument and the different observing set-up and modes that we used. The different observing campaigns, the atmospheric conditions and the observing strategy are detailed in Section 4. The dedicated data reduction and analysis to clean the science images, to calibrate our measurements, to derive the relative position and photometry of the detected sources in the NACO field of view and to estimate the detection performances are reported in Section 5. We then present the main results of our survey in Section 6, including the discovery of new close binary systems and the identification of background contaminants and comoving companions. In Section 7, we finally consider the detection sensitivity of our complete survey to statistically constrain the physical and orbital properties of the population of giant planets with 20 – 150 AU physical separations.

2. Sample Selection

The building up of our target sample relied on a synergy between the exhaustive work of young, nearby stars identification and selection criteria (age, distance, binarity and observability) to optimize the detection of close-in planetary mass companions with NACO at VLT. Youth indicators generally rely on the use of photometry and pre-main sequence isochrones, spectroscopic line (Lithium and H_{α}) analysis and study of X-ray activity and IR excess (see ZS04). Association membership is inferred from coordinates, proper motion, radial velocity and distance estimation. Since the beginning of the present survey, the number of known young, nearby stars more than doubled and newly identified members were regularly included in our target sample. Previously known binaries (see Tables 2 and 3) with $1.0 - 12.0''$

separation were excluded to avoid degrading the NACO AO and/or coronagraphic detection performances. Our initial complete sample was composed of 88 stars; 51 are members of young, nearby comoving groups, 32 are young, nearby stars currently not identified as members of any currently known association and 5 have been reclassified by us as older (>100 Myr) systems.

For stars not in a known moving group (Table 3), based on existing data we employed as many of the techniques for age dating as possible (see, e.g., Section 3 in ZS04). The principal diagnostics were Lithium abundance, Galactic space motion UVW, and fractional X-ray luminosity (Figs. 3, 6 and 4, respectively in ZS04). With the possible exception of a few of the FS stars (see following paragraph), all Table 3 stars with ages 100 Myr or less have UVW in or near the “good UVW box” in Fig. 6 of ZS04. With the exception of the A-type stars (unknown Lithium abundances), all Table 3 stars have Lithium abundances (we have measured) consistent with the ages we list and their spectral type (as per Fig. 3 in ZS04). With the exception of the A-type stars, X-ray fluxes are consistent with Fig. 4 in ZS04 for the indicated ages. Age uncertainties for non-FS stars in Table 3 are typically 50% of the tabulated age (i.e., 30 ± 15 Myr, 100 ± 50 Myr). The ages of the two A-type stars are based on UVW and location on a young star HR diagram.

When their radial velocity is known (based on our echelle spectra) then the FS stars usually have a “good UVW”. In all cases they are strong X-ray emitters and also have H alpha in emission, usually strongly. Lithium is usually not detected in the FS stars, or occasionally weakly. Because the data sets for these stars are sometimes incomplete (e.g., radial velocity not measured) and because fractional X-ray luminosity and UVW are imprecise measures of age, we have assigned an age of 100 Myr to all observed FS stars. Perhaps a few FS stars have ages older than 100 Myr (FS 588 being the most likely of these). But, similarly, some are likely younger than 100 Myr. By assuming an

Table 2. Sample of southern young, nearby stars observed during our VLT/NACO deep imaging survey. In addition to name, coordinates, galactic latitude (b), spectral type, distance and V and K photometry, the observing filter is given. All sources were observed in direct imaging, we have therefore indicated the 65 stars observed in addition in coronagraphy (CI). Finally, the multiplicity status of the primary and the presence of companion candidates (CCs) are also reported. For the multiplicity status we have flagged the following information: binary (B), triple (T) and quadruple (Q); new (N) or known/cataloged (K) multiple system; identified visual (VIS), Hipparcos astrometric (HIP) and spectroscopic (SB) binary system; and a final flag in case of a confirmed physical (Ph) or comoving (Co) system, but nothing if only an optical binary. FS stars are from a paper by Fuhrmeister & Schmitt (2003).

Name	α [J2000]	δ [J2000]	b (deg)	SpT	d (pc)	Age (Myr)	V (mag)	K (mag)	Mode & Filter	Stellar Multiplicity	Note
TWA											
TWA22 AB	10 17 26.9	-53 54 28	2	M5	18	8	13.2	7.69	CI, Ks	B (N/VIS/Ph)	CCs
SSSPMJ1102	11 02 09.83	-34 30 35	23	M8	65	8		11.88	Ks		
TWA3 AB	11 10 28.8	-37 32 04	21	M3	42	8	12.1	6.77	CI, H	B (K/VIS/Co)	
Twa14	11 13 26.3	-45 23 43	14	M0	63	8	13.8	8.50	CI, Ks		CCs
Twa12	11 21 05.6	-38 45 16	21	M2	32	8	13.6	8.05	CI, Ks		CCs
2M1139	11 39 51.1	-31 59 21	28	M8	49	8		11.50	Ks		
HIP57524	11 47 24.6	-49 53 03	11	G5	104	8	9.1	7.51	CI, H		CCs
Twa23	12 07 27.4	-32 47 0	30	M1	37	8	12.7	7.75	CI, H		
2M1207	12 07 33.4	-39 32 54	23	M8	52	8		11.95	Ks	B (N/VIS/Co)	
Twa25	12 15 30.7	-39 48 42	22	M5	44	8	11.4	7.31	CI, Ks		
HR4796 A	12 36 01.0	-39 52 10	23	A0	67	8	5.8	5.77	CI, H	B (K/VIS/Co)	
Twa17	13 20 45.4	-46 11 38	17	K5	133	8	12.6	9.01	CI, H		CCs
β Pictoris											
HIP27321	05 47 17.0	-51 03 59	-31	A5	20	12	3.9	3.53	CI, Ks		
V343Nor B	15 38 56.9	-57 42 18	-2	M4	40.0	12	14.8	9.19	CI, H	T (K/VIS+SB2/Co+Ph)	
HD155555 AB	17 17 25.5	-66 57 03	-16	K1	31.4	12	6.9	4.70	CI, H	T (K/SB2+VIS/Ph+Co)	CCs
TYC-8742-2065 AB	17 48 33.7	-53 06 43	-13	K0	42	12	9.0	6.78	H	B (K/SB2 and VIS/Ph)	
HIP88399 A	18 03 03.4	-51 38 56	-14	F5	46.9	12	7.0	5.91	CI, Ks	B (K/VIS/Co)	CCs
HIP92024	18 45 26.9	-64 52 16	-24	A7V	29.2	12	4.8	4.25	CI, Ks		CCs
CD-641208 AB	18 45 37.0	-64 51 46	-24	K7	29.2	12	9.5	6.10	CI, H	B (N/VIS)	
OES1847	18 50 44.5	-31 47 47	-14	K5	50	12	10.9	7.46	CI, H		CCs
HIP92680	18 53 05.8	-50 10 49	-21	K0V	49.6	12	8.4	6.37	CI, Ks		CCs
HIP95270	19 22 58.9	-54 32 16	-26	F5	50.6	12	7.0	5.91	CI, H		CCs
Tucana-Horologium											
HIP1113	00 13 53.01	-74 41 17	-42	G6V	43.7	30	8.7	6.96	CI, Ks		
HIP1481	00 18 26.1	-63 28 38	-59	F9V	41.0	30	8.0	6.15	CI, Ks		CCs
CD-7824	00 42 20.2	-77 47 40	-40	K5	69	30	10.4	7.53	CI, H		
HIP3556	00 45 28.1	-51 37 33	-58	M1	38.5	30	11.9	7.62	CI, Ks		CCs
HIP6485	01 23 21.2	-57 28 50	-59	G6	49.3	30	8.5	6.85	CI, Ks		CCs
HIP6856	01 28 08.6	-52 38 19	-64	K1	37.1	30	9.1	6.83	CI, Ks		CCs
HD13246 AB	02 07 26.1	-59 40 45	-55	F8V	45.0	30	7.5	6.20	CI, Ks	B (K/SB and VIS/Ph)	
GSC08056-00482	02 36 51.5	-52 03 04	-58	M3	25	30	12.1	7.50	CI, Ks		
HIP21632 B	04 38 45.6	-27 02 02	-40	M3V	54.7	30	7.5	10.41	CI, Ks*		CCs
HIP30034	06 19 12.9	-58 03 15	-30	K2	45.5	30	9.1	6.98	CI, H		CCs
HIP100751 AB	20 25 38.9	-56 44 06	-35	B7	56	30	1.9	2.48	CI, Ks	B (K/SB/Ph)	
HIP105404 ABC	21 20 59.8	-52 28 40	-44	K0V	46.0	30	8.9	6.57	CI, Ks	T (K/SB3/Ph)	CC
HIP107947	21 52 09.7	-62 03 09	-44	F6	45	30	7.2	6.03	CI, Ks		CCs
HIP108195 ABC	21 55 11.4	-61 53 12	-45	F3	47	30	5.9	4.91	CI, Ks	T (K+N/VIS/Ph+Co)	CCs
AB Dor											
HIP5191 A	01 06 26.1	-14 17 47	-76	K1	50	70	9.5	7.34	CI, H	B (K/VIS/Co)	
HIP25283	05 24 30.2	-38 58 11	-33	K7	18	70	9.2	5.92	CI, H	B (K/VIS/Co)	
ABDor BaBb	05 28 44.3	-65 26 46	-33	M3	15	70	13.0	7.34	CI, H	Q (K/VIS/Ph)	
HIP26369	05 36 55.1	-47 57 48	-32	K7	24	70	9.8	6.61	CI, H	B (K/VIS/Co)	
HIP26373	05 36 56.8	-47 57 53	-32	K0	24	70	7.9	5.81	CI, H	B (K/VIS/Co)	
HIP30314	06 22 30.9	-60 13 07	-27	G0V	23.5	70	6.5	5.04	CI, Ks	B (K/VIS?)	CCs
GSC08894-00426	06 25 55.4	-60 03 29	-27	M2	22	70	12.7	7.21	CI, Ks		CCs
HIP31878	06 39 50.0	-61 28 42	-25	K7	21.9	70	9.7	6.50	CI, Ks		
HIP76768 AB	15 40 28.4	-18 41 45	28	K7	43	70	10.2	6.95	CI, Ks	B (K/VIS/Co)	CCs
HIP113579	23 00 19.2	-26 09 13	-65	G1	32	70	7.5	5.94	CI, Ks		CCs
HIP118008	23 56 10.7	-39 03 08	-77	K3	22.1	70	8.2	5.91	CI, H		
η Cha, Near Cha, Columba and Carina											
M0838	08 38 51.1	-79 16 13	-22	M5	97	6	16.5	10.43	Ks		
HIP58285(TCha)	11 57 13.7	-79 21 32	-16	F5	66.4	10	11.4	6.95	CI, Ks		CCs
GSC08047-00232 A	01 52 14.6	-52 19 33	-62	K3	85	30	10.9	8.41	CI, Ks	B (K/VIS/Co)	
TYC-9390-0322 AB	05 53 29.1	-81 56 53	-29	K0	54	30	9.1	6.94	H	B (N/VIS)	

-(*): S13 camera used in that case

Table 3. Sample of southern young, nearby stars observed

Name	α [J2000]	δ [J2000]	b (deg)	SpT	d (pc)	Age (Myr)	V (mag)	K (mag)	Mode & Filter	Stellar Multiplicity	Note
Additional young candidates											
BTR99 AB	01 23 17.0	-79 41 32	-37	K0	103	10	10.1	7.07	CI, H	B (N/VIS)	
CD-53386 AB	02 01 53.7	-52 34 53	-61	K3	120	30	11.0	8.60	H	B (N/VIS)	
FS75	02 04 53.2	-53 46 16	-60	M4	30	100	15.0	9.6	Ks		
FS84	02 22 44.2	-60 22 47	-53	M4	20	100	13.7	8.2	Ks		
GSC08862-00019	02 58 04.6	-62 41 15	-49	K4	138	20	11.7	8.91	CI, Ks		CCs
TYC6461-1120 A	04 00 03.7	-29 02 16	-48	K0	62	40	9.6	7.15	CI, Ks	B (N/VIS/Co)	CCs
HIP28474 AB	06 00 41.3	-44 53 50	-27	G8	53.7	100	9.1	7.32	CI, H	B (N/VIS)	
FS388 ABC	06 43 45.3	-64 24 39	-25	M4	22	100	14.0	8.4	Ks	T (N/VIS)	
FS465 AB	08 17 39.4	-82 43 30	-24	M4	10	100	12.6	6.6	Ks	B (N/VIS)	
HIP41307	08 25 39.6	-03 54 23	18	A0	38	100	3.9	4.08	CI, Ks		
FS485	08 47 22.6	-49 59 57	-4	M2	33	100	12.0	7.71	Ks		
FS488 AB	08 54 02.4	-30 51 36	9	M5	15	100	13.4	8.10	Ks	B (N/VIS)	
HIP51386	10 29 42.2	+01 29 28	47	F5	31.5	50	6.9	5.52	CI, Ks		CCs
FS588	11 20 06.1	-10 29 47	46	M3	20	100	12.1	7.0	Ks		
HIP59315	12 10 06.4	-49 10 50	13	G5	37.8	100	8.2	6.50	CI, H		CCs
CD-497027	12 21 55.6	-49 46 12	13	K0	89	20	10.1	8.01	Ks		
HIP61468	12 35 45.5	-41 01 19	21	A7	34.6	100	5.1	4.57	CI, H		
TYC-8992-0605	12 36 38.9	-63 44 43	0	K3	50	10	9.9	7.37	CI, H		CCs
TYC-09012-1005	13 44 42.6	-63 47 49	-1	K5	95	10	11.0	7.74	CI, H		CCs
TYC-7818-0504 AB	14 30 13.5	-43 50 09	16	K5	100	10	10.4	7.64	H	B (N/VIS)	
HIP74405	15 12 23.4	-75 15 15	-15	K0	50.2	100	9.4	7.38	CI, H		
TYC-7846-1538	15 53 27.3	-42 16 02	9	G1	48	30	7.9	6.34	CI, H		CCs
HIP80448 ABC	16 25 17.5	-49 08 52	0	K1	45.5	100	7.1	5.70	H	T (K/SB+VIS/Ph+Co)	
HIP84642 AB	17 18 14.7	-60 27 27	-13	K0	54.6	40	9.5	7.53	CI, Ks	B (N/VIS)	CCs
FS903	17 37 46.5	-13 14 47	9	K7	45	100	10.2	6.835	CI, Ks		CCs
FS979 AB	18 35 20.8	-31 23 24	-11	M5	18	100	13.1	7.8	Ks	B (N/VIS)	CCs
FS1017	19 19 20.2	-01 33 54	-6	M5	25	100	16.6	9.667	Ks		CCs
FS1035	19 42 12.8	-20 45 48	-20	M5	20	100	14.4	8.756	Ks		CCs
HIP98495	20 00 35.5	-72 54 37	-31	A0	33.3	50	3.9	3.80	CI, H		
HIP102626	20 47 45.0	-36 35 40	-38	K0	44.4	30	9.4	6.79	CI, H	B (K/HIP?)	
FS1136 AB	21 49 06.2	-64 12 55	-43	M5	25	100	15.5	9.5	CI, Ks	B (N/VIS)	
FS1174	22 44 08.0	-54 13 20	-54	M4	30	100	13.4	8.5	Ks		CCs
Reclassified as older systems											
HIP7805	01 40 24.1	-60 59 57	-55	F2	67	≥ 100	7.7	6.63	CI, H		
HIP69562 ABC	14 14 21.3	-15 21 21	42	K5V	26.5	≥ 100	10.5	6.60	Ks	T (N/VIS)	
HIP76107	15 32 36.7	-52 21 21	3	M0	30.6	≥ 100	11.0	7.60	CI, Ks	B (K/HIP?)	CCs
HIP96334	19 35 09.7	-69 58 32	-29	G1V	35.4	≥ 100	7.9	6.30	CI, Ks		CCs
HIP107705 AB	21 49 05.8	-72 06 09	-39	M0	16.1	200	9.8	5.65	Ks	B (N/VIS)	

overall uniform age of 100 Myr for the sample of FS stars, we are probably somewhat overestimating their mean age. The age determination of the ensemble of FS stars is likely to be accurate to within about a factor 2 in general, although the age of some FS stars could well lie outside of this range.

The sample properties are summarized in Tables 2 and 3 and illustrated in Fig. 1. 93% of the selected stars are younger than about 100 Myr and 94% closer than 100 pc. The spectral types cover the sequence from B to M spectral types with 19% BAF stars, 48% GK stars and 33% M dwarfs.

3. Observations

3.1. Telescope and instrument

NACO¹ is the first Adaptive Optics instrument that was mounted at the ESO Paranal Observatory near the end of 2001 (Rousset et al. 2002). NACO provides diffraction limited images in the near infrared (nIR). The observing camera CONICA (Lenzen et al. 2002) is equipped with a 1024 × 1024 pixel Aladdin InSb

array. NACO offers a Shack-Hartmann visible wavefront sensor and a nIR wavefront sensor for red cool (M5 or later spectral type) sources. nIR wavefront sensing was only used on 8% of our sample. Note that in May 2004, the CONICA detector was changed and the latter detector was more efficient thanks to an improved dynamic, a lower readout noise and cleaner arrays. Among NACO's numerous observing modes, only the direct and coronagraphic imaging modes were used. The two occulting masks offered for Lyot-coronagraphy have a diameter of $\varnothing = 0.7''$. and $\varnothing = 1.4''$. According to the atmospheric conditions, we used the broad band filters H and K_s , the narrow band filters, NB1.64, NB1.75 and Br γ ² and a neutral density filter (providing a transmissivity factor of 0.014). In order to correctly sample the NACO PSF (better than Nyquist), the S13 and S27 objectives were used, offering mean plate scales of 13.25 and 27.01 mas per pixel and fields of view of 14'' × 14'' and 28'' × 28'' respectively.

Our deep imaging survey was initiated during guaranteed time observations shared between different scientific programs and scheduled between November 2002 and September 2003.

¹ <http://www.eso.org/instruments/naos/>

² see filters description: <http://www.eso.org/instruments/naco/inst/filters.html>

Table 4. Summary of the different observing campaigns of our survey. For each campaign, we report the ESO programme numbers, the observation type, Guaranteed Time (GTO) or Open Time (OT), if obtained in visitor (Vis) or service (Ser) modes, the starting nights of observation, the number of nights allocated and the time loss. Finally, the number of visits, corresponding to the number of observing sequences executed on new and follow-up targets, is given.

ESO Program	Mode	Start. Night (UT-date)	Night (Nb)	Loss (%)	Visits (Nb)
070.C-0565(A)	GTO-Vis	26-11-2002	1		6
070.D-0271(B)	GTO-Vis	16-03-2003	1.5		8
071.C-0507(A)	GTO-Vis	07-06-2003	0.5	50	2
071.C-0462(A)	GTO-Vis	07-09-2003	0.5	50	2
072.C-0644(A)	OT-Vis	05-03-2004	1	100	0
072.C-0644(B)	OT-Vis	05-03-2004	1	0	9
073.C-0469(A)	OT-Vis	27-04-2004	1	0	16
073.C-0469(B)	OT-Vis	25-09-2004	1	0	12
075.C-0521(A)	OT-Vis	06-05-2005	1	0	15
075.C-0521(B)	OT-Vis	19-08-2005	0.5	0	10
076.C-0554(A)	OT-Vis	08-01-2006	1	0	13
076.C-0554(B)	OT-Vis	26-02-2006	1	30	8
078.C-0494(A)	OT-Ser	2006/2007	0.7	30	7
079.C-0908(A)	OT-Ser	2007	1	0	10
Total	-	-	11.7		127

The survey was extended using open time observations between March 2004 and June 2007. The open time observations were shared between classical visitor mode and remote service mode as offered by ESO at the Paranal Observatory. The observing programs, observing modes, the number of nights allocated, the time loss due to technical or weather reasons and the number of targets observed per run are reported in Table 4.

3.2. Image quality

For ground-based telescopes, atmospheric conditions have always been critical to ensure astronomical observations of good quality. Although AO instruments aim at compensating the distortion induced by atmospheric turbulence, the correction quality (generally measured by the *strehl ratio* and *Full Width Half Maximum (FWHM)* parameters) is still related to the turbulence speed and strength. For bright targets, the NACO AO system can correct for turbulence with a coherent time (τ_0) longer than 2 ms. For faster ($\tau_0 \leq 2$ ms) turbulence, the system is always late and the image quality and the precision of astrometric and photometric measurements are consequently degraded. During our NACO observing runs, the averaged τ_0 was about 5 ms and larger than 2 ms 80% of the time. The average seeing conditions over all runs was equal to 0.8'' (which happens to be the median seeing value measured in Paranal over the last decade³). Fig. 2 shows the (*strehl ratio*) performances of the NACO AO system with the visible wavefront sensor as a function of the correlation time of the atmosphere τ_0 , the seeing and the primary visible magnitude. As expected, the degradation of the performances is seen with a decrease of τ_0 , the coherent length (r_0), inversely proportional to the seeing) and the primary flux. Still, the results clearly demonstrate the good NACO performances and capabilities over a wide range of observing conditions.

³ <http://www.eso.org/gen-fac/pubs/astclim/paranal/seeing/adaptive-optics/statfwhm.html>

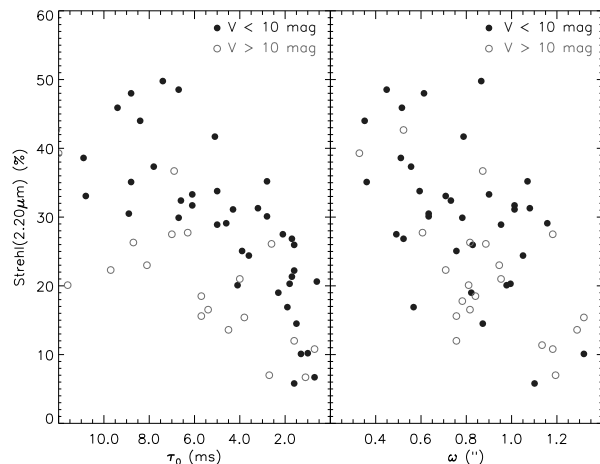


Fig. 2. VLT/NACO adaptive optics system performances. Strehl ratio at 2.20 μm as a function of the correlation time τ_0 and the seeing ω of the atmospheric turbulence for two regimes of V -band magnitude of the primary star (AO reference target). Only the targets observed with the visible WFS are plotted. Close binaries have also been rejected. The results demonstrate the good behavior of NACO over a wide range of stellar magnitudes and under different turbulent conditions. A clear degradation of the performances is seen for decreasing τ_0 , increasing ω and fainter visible ($V \geq 10$) targets. A clear drop is seen for τ_0 faster than 2 ms, the limit of the NACO wavefront sensor sampling frequency.

3.3. Observing strategy

The VLT/NACO survey was conducted as a continuation of our earlier coronagraphic survey with the ADONIS/SHARPII instrument at the ESO 3.6 m telescope at La Silla Observatory (Chauvin et al. 2003). A similar observing strategy was adopted to optimize the detection of faint close substellar companions. Most of our stars are relatively bright ($K_s \leq 10$) in nIR. To improve our detection performances, we have opted for the use of Lyot coronagraphy. High contrast imaging techniques, such as Lyot and phase mask coronagraphy, L -band saturated imaging and simultaneous differential imaging, enable achievement of contrasts of 10^{-5} to 10^{-6} . Their main differences are inherent in the nature of the substellar companions searched and the domain of separations explored. Broad-band nIR Lyot coronagraphy and thermal (L' -band or 4 μm) saturated imaging are among the most sensitive techniques at typical separations between 1.0 to 10.0''. The contrast performances are currently mandatory to access the planetary mass regime when searching for faint close companions.

To measure precisely the positions of the faint sources detected in the coronagraphic field relative to the primary star, a dedicated observing block was executed. This block was composed of three successive observing sequences and lasted in total ~ 45 min (including pointing). After the centering of the star behind the coronagraphic mask, a deep coronagraphic observing sequence on source was started. Several exposures of less than one minute each were accumulated to monitor the star centering and the AO correction stability. An effective exposure time of 300 sec was generally spent on target. During the second sequence, a neutral density or a narrow band filter was inserted and the occulting mask and Lyot stop removed. The goal was to precisely measure the star position behind the coronagraphic mask

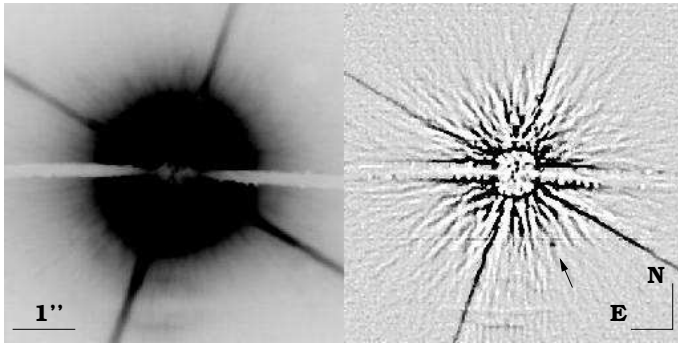


Fig. 3. *Left:* VLT/NACO coronagraphic image of HIP 95270 obtained in H -band with the S13 camera. The small ($\varnothing = 0.7''$) coronagraphic mask was used. *Right:* Coronagraphic image after high-pass filtering. A kernel of $3 \times FWHM$ is used to remove the low spatial frequencies of the coronagraphic PSF wings. A fake $\Delta H = 12$ companion has been inserted at $1.2''$ from the star to test the detection performances. Minimum and maximum thresholds of the filtered image were divided by a factor 15 to show the fake companion and the PSF residuals.

(once corrected for filter shifts). An effective exposure time of 60 sec was spent on source. Counts were adjusted to stay within the 1% linearity range of the detector. The image is also used to estimate the quality of the AO correction. Finally, the last sequence was the coronagraphic sky. This measure was obtained $\sim 45''$ from the star using a jittering pattern of several offset positions to avoid any contaminants in the final median sky. In case of positive detections, whenever possible, the companion candidates (CCs) were re-observed to check whether a faint object shared common proper motion with the primary star. Depending on each object's proper motion (see Fig. 1), the timespan between successive epochs was about 1-2 years. When comoving companions were identified, images were recorded with additional nIR filters to directly compare the spectral energy distribution with that predicted by (sub)stellar evolutionary models.

4. Data reduction and analysis

4.1. Cosmetic and image processing

Classical cosmetic reduction including bad pixels removal, flat-fielding, sky subtraction and shift-and-add, was made with the *Eclipse*⁴ reduction software developed by Devillar (1997) for both direct and coronagraphic imaging observations. Median filtering by a kernel of 3×3 pixels was applied to correct for remaining hot pixels. To remove the central part of the PSF in our reduced coronagraphic images, two methods were applied. The first method considered different angular sectors uncontaminated by the diffraction spikes and by the coronagraphic mask support. For each sector, the PSF azimuthal average is calculated, circularised and subtracted from the coronagraphic image. The alternative method was to apply directly a high-pass filter with a kernel of $3 \times FWHM$ (assuming the theoretical $FWHM$ at each observing set-up). As a result, low spatial frequencies, including the coronagraphic PSF wings, were removed from the reduced image. Finally, each resulting image was inspected by eye for the CCs identification. Fig. 3 is an illustration of the data processing applied to the coronagraphic images of HIP 95270, in the case of the second method.

Table 5. Mean plate scale and true north orientation for each observing run. The astrometric field Θ_1 Ori C field and the astrometric binary IDS21506S5133 (van Dessel & Sinachopoulos 1993) were the calibrators.

ESO Program	UT Date	Obj.	Platescale (mas)	True north (deg)
070.C-0565	21-11-2002	S13	13.24 ± 0.05	-0.05 ± 0.10
	21-11-2002	S27	27.01 ± 0.05	0.08 ± 0.18
070.D-0271	16-03-2003	S13	13.21 ± 0.11	-0.05 ± 0.10
071.C-0507	29-05-2003	S13	13.24 ± 0.05	-0.10 ± 0.10
	03-06-2003	S27	27.01 ± 0.05	0.01 ± 0.19
071.C-0507	07-09-2003	S13	13.24 ± 0.05	0.05 ± 0.10
072.C-0644	05-03-2004	S13	13.24 ± 0.05	0.04 ± 0.10
	05-03-2004	S27	27.01 ± 0.05	-0.18 ± 0.20
073.C-0469	27-04-2004	S27	27.01 ± 0.05	0.08 ± 0.20
073.C-0469	22-09-2004	S13	13.25 ± 0.05	0.20 ± 0.10
	22-09-2004	S27	27.01 ± 0.05	0.0 ± 0.19
075.C-0521	19-08-2005	S13	13.25 ± 0.06	-0.02 ± 0.10
	19-08-2005	S27	27.01 ± 0.06	-0.07 ± 0.11
076.C-0654	08-01-2006	S13	13.25 ± 0.06	0.18 ± 0.10
	08-01-2006	S27	27.02 ± 0.06	0.12 ± 0.13
076.C-0654	28-02-2006	S13	13.25 ± 0.06	0.19 ± 0.10
	28-02-2006	S27	27.02 ± 0.05	0.13 ± 0.14
078.C-0494	24-10-2006	S13	13.26 ± 0.07	-0.19 ± 0.23
	23-12-2006	S13	13.26 ± 0.08	-0.23 ± 0.15
	22-10-2006	S27	27.01 ± 0.03	-0.30 ± 0.16
	25-12-2006	S27	27.01 ± 0.04	-0.20 ± 0.18
079.C-0908	18-07-2007	S27	27.01 ± 0.05	-0.06 ± 0.15

4.2. Astrometric calibration

The astrometric calibration of high angular resolution images as provided by NACO is not a simple task. As NACO is not a multi-conjugated AO system, the diffraction limited images have a small FoV limited by the anisoplanatism angle. Therefore, classical high-precision astrometric techniques over crowded fields of thousands of stars cannot be transposed. In addition, ESO does not currently provide any detector distortion map. For this reason, astrometric calibrators were observed within a week for each observing run (in visitor and service mode) to determine a mean platescale and the true north orientation. Our primary astrometric calibrator was the Θ_1 Ori C field observed with HST by McCaughrean & Stauffer (1994). The same set of stars (TCC058, 057, 054, 034 and 026) were observed with the same observing set-up (K_s with S27 and H with S13) to avoid introduction of systematic errors. When not observable, we used as secondary calibrator the astrometric binary IDS21506S5133 (van Dessel & Sinachopoulos 1993), yearly recalibrated with the Θ_1 Ori C field. The mean orientation of true north and the mean platescale of the S13 and S27 cameras are reported in Table 5.

4.3. Companion candidate characterization

For direct imaging, the relative photometry and astrometry of visual binaries were obtained using the classical deconvolution algorithm of Véran & Rigaut (1998). This algorithm is particularly adapted for stellar field analysis. Several PSF references were used to measure the influence of the AO correction. They were selected to optimize a set of observing criteria relative to the target observation (observing time, airmass, spectral type and V or K -band flux according to the wavefront sensor).

In coronagraphy, the relative astrometry of the CCs was obtained using a 2D-gaussian PSF fitting. The deconvolution algorithm of Véran & Rigaut (1998) and the maximization of

⁴ <http://www.eso.org/projects/aot/eclipse/>

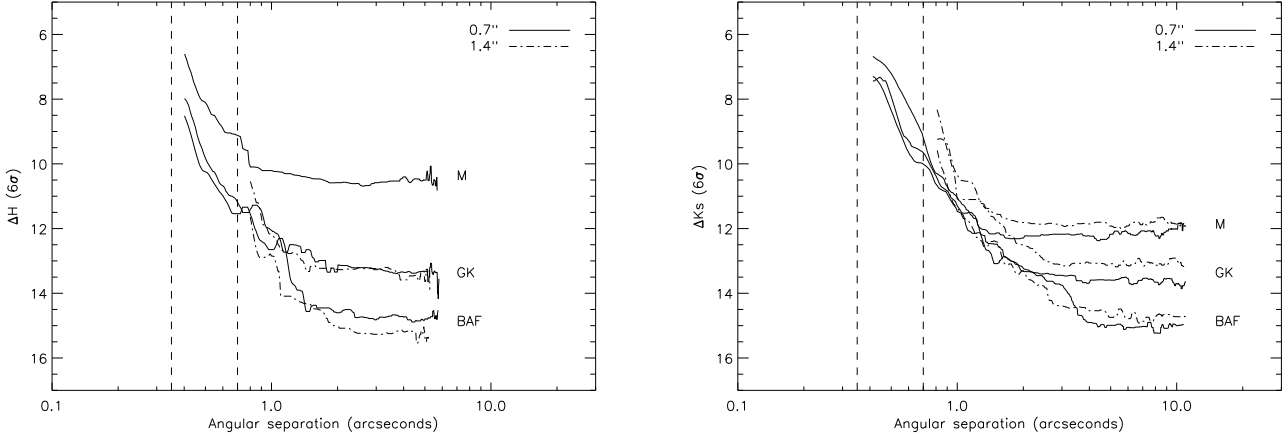


Fig. 4. *Left:* VLT/NACO coronagraphic detection limits in H-band (combined with the S13 camera). The median detection limits are given for different target spectral types (BAF, GK and M stars) and for the 0.7'' (solid line) and 1.4'' (dash dotted line) coronagraphic masks. *Right:* VLT/NACO coronagraphic detection limits in K_s -band (combined with the S27 camera). The median detection limits are also given for different target spectral types and coronagraphic masks.

the cross-correlation function were applied using the primary star (directly imaged) as PSF reference. The shifts (≤ 1 pixel) induced between direct and coronagraphic images taken with different filters, including neutral density, have been accounted for. For the relative photometry, classical aperture ($R_{ap} = 2 \times FWHM$) photometry with residual sky-subtraction and classical deconvolution were used. For faint sources detected at less than $\sim 10 \sigma$, the background subtraction become more critical and is responsible for larger uncertainties in the deconvolution analysis. Our analysis was then limited to a 2D-gaussian fitting coupled to aperture photometry to derive the relative astrometry and photometry.

For observations obtained at several epochs, the proper motion and parallactic motion of the primary star were taken into account to investigate the nature of detected faint CCs. The relative positions recorded at different epochs can be compared to the expected evolution of the position measured at the first epoch under the assumption that the CC is either a stationary background object or a comoving companion (see below). For the range of semi-major axes explored, any orbital motion can be considered of lower order compared with the primary proper and parallactic motions.

4.4. Detection limits

The coronagraphic detection limits were obtained using combined direct and coronagraphic images. On the final coronagraphic image, the pixel-to-pixel noise was estimated within a box of 5×5 pixels sliding from the star to the limit of the NACO field of view. Angular directions free of any spike or coronagraphic support contamination were selected. Additionally, the noise estimation was calculated within rings of increasing radii, a method which is more pessimistic at close angular separation due to the presence of coronagraphic PSF non-axisymmetric residuals. Final detection limits at 6σ were obtained after division by the primary star maximum flux and multiplication by a factor taking into account the ratio between the direct imaging and coronagraphic integration times and the difference of filter transmissions and bandwidths. Spectral type correction due to the use of different filters has been simulated and is smaller than 0.04 mag. The variation of the image quality (*strehl ratio*) over

the observation remains within 10% and should not impact our contrast estimation from more than 0.1 mag. The median detection limits, using the sliding box method, are reported in Fig. 4. They are given for observations obtained in H- and K_s -bands, with the $\phi = 0.7''$ and $\phi = 1.4''$ coronagraphic masks and for different target spectral types (BAF, GK and M stars) and will be used for the following statistical analysis of the survey.

At large separations ($\geq 1.0 - 2.0''$) from the star when limited by detector read-out noise or background noise, the contrast variation with the primary spectral type is actually related to the primary nIR brightness. This is shown in Fig. 5 in the case of K_s -band detection limits at $5.0''$ as a function of the primary K_s apparent magnitude. The contrast varies linearly due to the flux normalization. At shorter separations, the situation is more complex as AO deep images are actually limited by the speckle noise. Our detection limits remain constant over a wide range of primary K_s apparent magnitudes.

All published deep imaging surveys dedicated to planet search (Masciadri et al. 2005; Kasper et al. 2007; Lafrenière et al. 2007; Biller et al. 2007), including this one, derived detection threshold assuming that the residual noise in the final processed image follows a Gaussian intensity distribution. A typical detection threshold at 5 or 6σ is then usually assumed over the complete angular range. Whereas the approximation of a Gaussian distribution for the residual noise is valid within the detector read-out noise or background noise regime, careful analysis by Marois et al. (2008a) shows that this is not adequate at small separations when speckle noise limited (typically $\leq 1.0 - 2.0''$ in our survey; see Fig. 4). In this regime, AO deep images are actually not limited by random, short-lived atmospheric speckles, but by instrumental quasi-static speckles. A non-gaussian distribution of the residual noise must be taken into account to specify a detection threshold at a given confidence level. Therefore, our current 6σ detection threshold at small separations is probably too optimistic. However, the systematic error induced in our sensitivity limits is probably of lower significance than uncertainties in planet age and use of uncalibrated planet evolutionary models as described below.

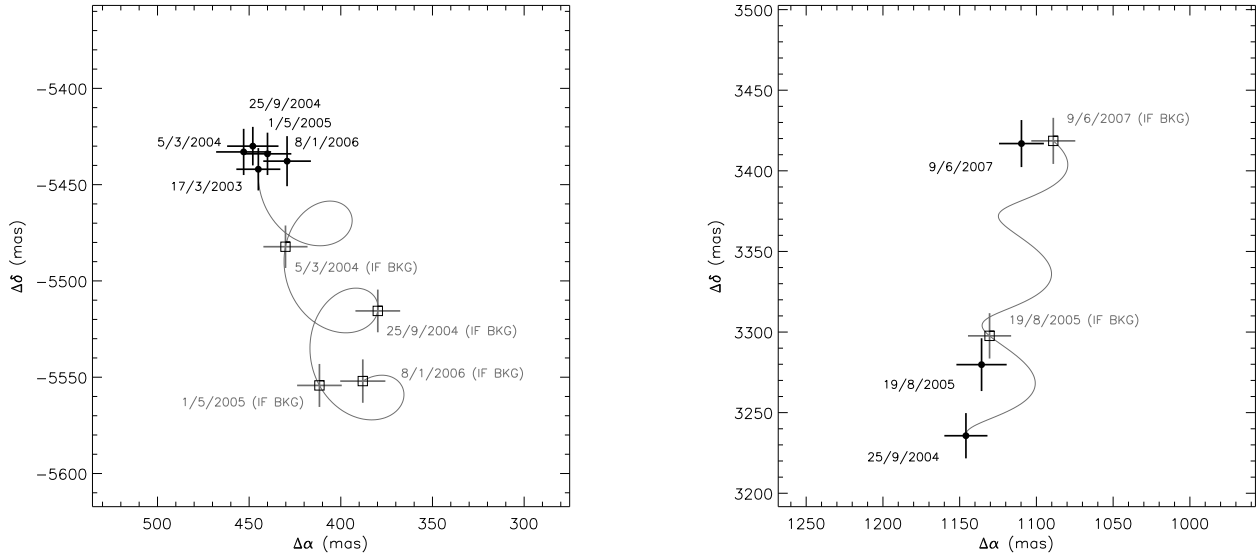


Fig. 6. VLT/NACO Measurements (*full circles* with uncertainties) of the offset positions of the comoving companion AB Pic b to A (*left*) and of the CC relative to 0ES1847 (*right*). For each diagram, the expected variation of offset positions, if the candidate is a background object, is shown (*solid line*). The variation is estimated based on the parallactic and proper motions of the primary star, as well as the initial offset position of the CC from A. The *empty boxes* give the corresponding expected offset positions of a background object for the different epochs of observations (with uncertainties). In the case of AB Pic b, the relative positions do not change with time confirming that AB Pic b is comoving. On the contrary, the relative position of the CC to 0ES1847 varies in time as predicted for a background stationary contaminant. For our sample, astrometric follow-up over 1-2 years enabled a rapid identification.

5. Results

The main purpose of our survey was the detection of close brown dwarf and planetary mass companions using the deep imaging technique on an optimized sample of nearby stars. Compared to other works, our strategy has been successful with the confirmation of the brown dwarf companion to GSC 08047-00232 (Chauvin et al. 2003; 2005a) and the discoveries of one planetary mass companion, around the young brown dwarf 2MASSW J1207334-393254 (hereafter 2M1207; Chauvin et al. 2004; 2005c) and one companion at the planet/brown dwarf boundary to the young star AB Pic (Chauvin et al. 2005b).

In this section, we detail the three main results of this survey:

1. the identification of a large fraction of contaminants in the close angular environment of our sample of young, nearby stars. This identification step is necessary for the statistical analysis of our complete set of detection limits (see below). Contaminants identification serves in addition to the preparation of future deep imaging search of exoplanets that will re-observe most of these stars.
2. the discovery of several new close stellar multiple systems, despite our binary rejection process. Three systems are actually confirmed to be comoving. One is a possible low-mass calibrator for the predictions of evolutionary models.
3. Finally, we review the status of the three substellar companions, confirmed with NACO, in regards of the latest results in the literature and from our survey.

5.1. Contaminant identification

Among the complete sample composed of 88 stars, a total of 65 were observed with coronagraphic imaging. The remaining 23 targets were observed in direct or saturated imaging because the system was resolved as a $1.0 - 12''$ visual binary inappropriate for deep coronagraphic imaging, because the atmospheric conditions were unstable or because the system was simply too faint to warrant efficient use of the coronagraphic mode.

Among the 65 stars observed with both direct imaging and coronagraphy, nothing was found around 29 (45%) stars and at least one CC was detected around the 36 (55%) others. A total of ~ 236 CCs were detected. To identify their nature, 14 (39%) systems were observed at two epochs (at least) with VLT and 16 (44%) have combined VLT and HST observations at more than a one year interval (Song et al. 2009, in prep). Finally, 6 (17%) were observed at only one epoch and require further follow-up observations. The position and photometry of each detected CC relative to its primary star, at each epoch, are given in Tables 7-13. For multi-epoch observations, to statistically test the probability that the CCs are background objects or comoving companions, a χ^2 probability test of $2 \times N_{epochs}$ degrees of freedom (corresponding to the measurements: separations in the $\Delta\alpha$ and $\Delta\delta$ directions for the number N_{epochs} of epochs) was applied. This test takes into account the uncertainties in the relative positions measured at each epoch and the uncertainty in the primary proper motion and parallax (or distance). Fig. 6 gives an illustration of a $(\Delta\alpha, \Delta\delta)$ diagram that was used to identify a stationary background contaminant near 0ES1847. A status of each CC has been assigned as confirmed companion (C; $P_{\chi^2} < 0.1\%$), background contaminant (B; $P_{\chi^2} > 99\%$), probably background (PB;

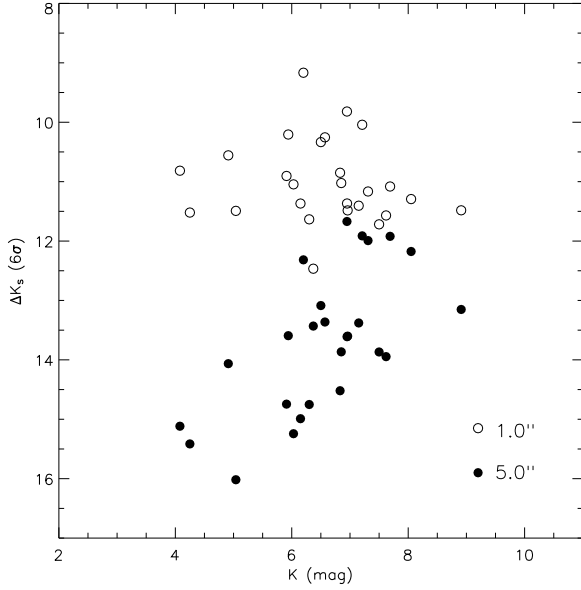


Fig. 5. VLT/NACO coronagraphic detection limits in K_s -band as a function of the primary star brightness for two angular separations (1.0'' and 5.0''). Two regimes can be seen; one at large separations (shown here at 5.0'') when the detection is limited by detector read-out noise or background noise. The contrast varies then linearly with the primary K_s apparent magnitude due to the flux normalization; a second regime at shorter separations (shown here at 1.0'') when the detection is speckle noise limited. Instrumental quasi-static speckles are expected to dominate random, short-lived atmospheric speckles and the contrast remains relatively constant over a wide range of primary K_s apparent magnitudes.

$P_{\chi^2} > 99\%$, but combining data from two different instruments) and undefined (U). Over the complete coronagraphic sample, 1% of the CCs detected have been confirmed as comoving companions, 43% have been identified as probable background contaminants and about 56% need further follow-up observations. The remaining CCs come mostly from the presence of background crowded fields in the field of view of the 6 stars observed at one epoch.

Among the 23 stars and brown dwarfs observed only in direct or saturated imaging, several have been resolved as tight multiple systems (see below). 4 stars (FS1174, FS979, FS1017 and FS1035) have at least one substellar CC (see Tables 12, 13 and 14). FS1035 was observed at two successive epochs and the faint object detected at $\sim 5.6''$ has been identified as a contaminant.

5.2. Close stellar multiple systems

5.2.1. New visual binaries

Our survey was not aimed at detecting new stellar binaries. Known bright equal-mass binaries of 1.0 – 12.0'' separation were rejected from our sample as they degrade the coronagraphic detection performances by limiting dynamical range. A few tight binaries were kept when both components could be placed behind the coronagraphic masks. Despite our binary rejection process, 17 new close visual multiple systems were re-

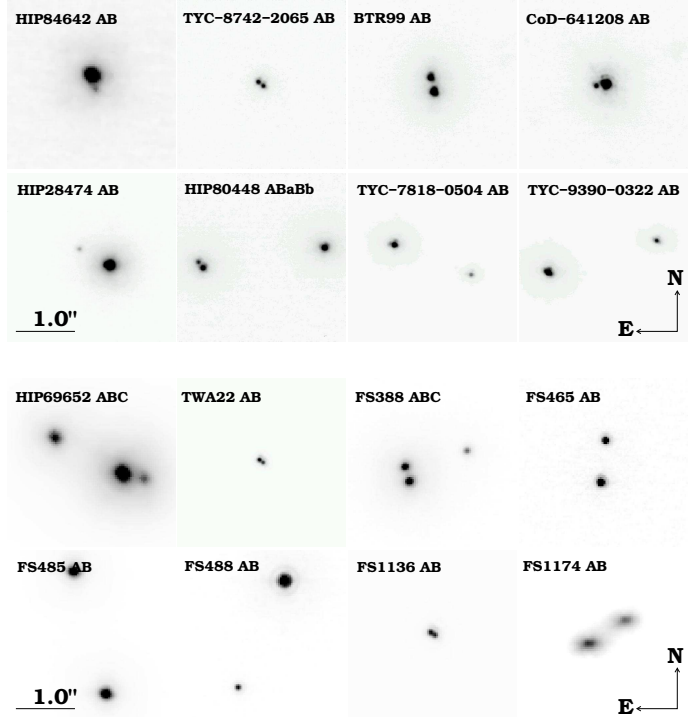


Fig. 7. New visual binaries resolved with NACO at VLT. HIP 108195 AB, HIP 84642 AB and TWA22 AB were in addition confirmed as comoving multiple systems. TWA22 AB was monitored for 4 years to constrain the binary orbit and determine its total dynamical mass (see Bonnefoy et al. 2009, accepted)

solved (see Fig. 7 and 8). They include 13 tight resolved binaries and 4 triple systems. Their relative flux and position are reported in Table 6. Their separations range between 0.1 – 5.0'' and their H and K_s contrasts between 0.0 – 4.8 mag. Among them, HIP 108195 ABC, HIP 84642 AB and TWA22 AB were observed at different epochs and are confirmed as comoving systems.

5.2.2. The comoving multiple systems HIP 108195 ABC and HIP 84642 AB

Close to the Hipparcos double star HIP 108195 AB (F3, 46.5 pc), member of Tuc-Hor, we resolved a faint source at $4.96''$ ($\Delta_{proj} = 230$ AU; i.e. $a \sim 290$ AU). In addition to a confirmation that HIP 108195 AB is a comoving pair, we found that the fainter source is a third component of this comoving multiple system (Fig. 8). Combined distance, age and apparent photometry are compatible with an M5-M7 dwarf according to PMS model predictions (Siess et al. 2000) and places the companion at the stellar/brown dwarf boundary.

HIP 84642 (K0, 58.9 pc) is not reported as a double star in the Hipparcos Visual Double Stars catalog (Dommanget et al. 2000), possibly due to the small angular separation and the flux ratio with the visual companion. Based on combined VLT/NACO images from our programme and from the SACY survey (Huélamo et al. 2009, in prep), we confirm that the companion shares common proper motion with HIP 84642. This object is likely to be an M4-M6 young dwarf comparing its photometry to predictions of PMS models. Based on the statistical relation between projected separation and semi-major

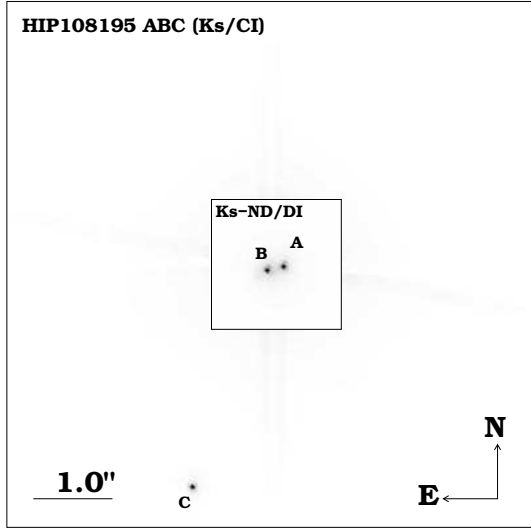


Fig. 8. Composite VLT/NACO K_s -band image of the triple comoving system HIP108195 ABC. The inner part shows the direct image (DI) of HIP108195 AB (attenuated by a factor ~ 100) using the K_s -band with a neutral density filter to avoid saturation. Both components of the astrometric binary cataloged by Hipparcos are resolved. The outer part shows the deeper coronagraphic image obtained in K_s -band with the C component about 100 times fainter than A or B.

Table 6. Relative positions and K_s and H -band contrast of the new binaries resolved by NACO at VLT. Contrast uncertainty is about 0.1 mag.

Name	UT Date	Δ (mas)	P.A. (deg)	ΔK_s (mag)
HIP108195 AB	19-08-2005	339 ± 5	102.7 ± 0.2	0.0
AC	19-08-2005	4964 ± 9	158.4 ± 0.2	4.8
HIP84642 AB	05-06-2007	220 ± 14	191.3 ± 0.8	2.5
TYC-8742-2065 AB	27-04-2004	114 ± 2	232.5 ± 0.4	0.2
BTR99 AB	25-09-2004	264 ± 3	12.8 ± 0.3	0.5
CoD-641208 AB	25-09-2004	178 ± 3	95.3 ± 0.4	2.3
HIP80448 BaBb	27-04-2004	134 ± 2	37.5 ± 0.7	1.1
HIP69652 AB	26-02-2006	319 ± 6	256.8 ± 0.5	1.3
AC	26-02-2006	1123 ± 6	61.8 ± 0.4	0.8
TWA22 AB	05-03-2004	100 ± 5	80.2 ± 0.2	0.4
FS388 AB	08-01-2006	224 ± 5	16.4 ± 0.6	0.3
AC	08-01-2006	963 ± 6	297.7 ± 0.2	1.6
FS465 AB	08-01-2006	619 ± 6	353.4 ± 0.3	0.7
FS488 AB	08-01-2006	1710 ± 7	156.6 ± 0.1	2.8
FS485 AB	26-02-2006	1862 ± 7	14.7 ± 0.1	0.2
FS1136 AB	19-08-2005	74 ± 5	122.0 ± 0.8	0.2
FS1174 AB	19-08-2005	626 ± 6	302.7 ± 0.5	0.4

Name	UT Date	Δ (mas)	P.A. (o)	ΔH (mag)
HIP28474 AB	27-04-2004	613 ± 3	61.7 ± 0.2	3.8
TYC-7818-0504 AB	17-03-2003	1463 ± 6	111.3 ± 0.2	1.7
TYC-9390-0322 AB	17-03-2003	2005 ± 7	286.3 ± 0.1	1.6

axis of Couteau (1960), HIP 84642 AB is likely to be a tight ($\Delta_{proj} = 14$ AU; $a \sim 18$ AU; K0-M5) binary with a period of several tens of years.

5.2.3. The young, tight astrometric binary TWA22 AB

The tight (~ 100 mas; $a \sim 1.8$ AU) binary TWA22 AB was observed at several epochs. We aimed at monitoring the system orbit to determine the total dynamical mass of this system using an accurate distance determination (17.53 ± 0.21 pc, Teixeira et al. 2009, submitted). The physical properties (luminosity, effective temperature and surface gravity) of each component were obtained based on near-infrared photometric and spectroscopic observations. By comparing these parameters with evolutionary model predictions, we consider the age and the association membership of the binary. A possible under-estimation of the mass predicted by evolutionary model for young stars close to the sub-stellar boundary is presented in two dedicated papers (Bonnetfoy et al. 2009, accepted; Teixeira et al. 2009, accepted).

5.3. Substellar companions

We review below the latest results about the three substellar companions GSC 08047-00232 B, AB Pic b and 2M1207 b since their initial companionship confirmation. Recent age, distance, astrometric and spectroscopic measurements enable us to refine their predicted physical properties and their origin in regards to other confirmed substellar companions in young, nearby associations.

5.3.1. GSC 08047-00232 B

Based on the ADONIS/SHARPII observations of two dozen probable association members of Tuc-Hor, Chauvin et al. (2003) identified a $20 \pm 5 M_{Jup}$ candidate to GSC 08047-00232 (CoD-52381). This candidate was independently detected by Neuhäuser et al. (2003) with the SHARP instrument at the ESO *New Technology Telescope* (NTT). Neuhäuser & Guenther (2004) acquired H - and K -band spectra and derived a spectral type $M8 \pm 2$, corroborated by Chauvin et al. (2005a). Finally, in the course of our VLT/NACO observations, we confirmed that GSC 08047-00232 B was comoving with A (Chauvin et al. 2005a). Mass, effective temperature and luminosity were determined by comparing its JHK photometry with evolutionary model predictions and the Tuc-Hor age and photometric distance for the system. The results are reported in Table 7 and compared to the complete list of confirmed substellar companions discovered among the young, nearby associations. Membership in Tuc-Hor and the assigned age of GSC 08047-00232 AB have been debated for a time. Further studies of loose young associations sharing common kinematical and physical properties recently led Torres et al. (2008) to identify GSC 08047-00232 AB as a high-probability (80%) member of the Columba association of age 30 Myr, confirming the young age and the brown dwarf status of GSC 08047-00232 B.

5.3.2. AB Pic b

During our survey, a $13 \pm 2 M_{Jup}$ companion was discovered near the young star AB Pic (Chauvin et al. 2005b). Initially identified by Song et al. (2003) as a member of Tuc-Hor, the membership of AB Pic has been recently discussed by Torres et al. (2008) who attached this star to the young (~ 30 Myr) Columba association. Additional astrometric measurements of the relative position of AB Pic b to A firmly confirm the companionship reported by Chauvin et al. (2005b; see Fig. 6, *left panel*). Based on age, distance and nIR photometry, Chauvin et al. (2005b) derived the physical properties of AB Pic b based on evolutionary

models (see Table 7). As per the three young substellar companions to TWA5A, HR7329 and GSC 08047-00232, AB Pic b is located at a projected physical separation larger than 80 AU. Formation by core accretion of planetesimals seems unlikely because of inappropriate timescales to form planetesimals at such large distances. Gravitational instabilities within a protoplanetary disk (Papaloizou & Terquem 2001; Rafikov 2005; Boley 2009) or Jeans-mass fragmentation proposed for brown dwarf and stellar formation appear to be more probable pathways to explain the origin of the Table 7 secondaries.

5.3.3. 2M1207 b

Among the young candidates of our sample, a small number of very low mass stars and brown dwarfs were selected to take advantage of the unique capability offered by NACO at VLT to sense the wavefront in the IR. Most were observed in direct and saturated imaging. This strategy proved to be successful with the discovery of a planetary mass companion in orbit around the young brown dwarf 2M1207 (Chauvin et al. 2004; 2005c). HST/NICMOS observations independently confirmed this result (Song et al. 2006). A low signal-to-noise spectrum in H-band enabled Chauvin et al. (2004) to suggest a mid to late-L dwarf spectral type, supported by its very red nIR colors. Additional low signal-to-noise spectroscopic observations compared with synthetic atmosphere spectra led Mohanty et al. (2007) to suggest an effective spectroscopic temperature of 1600 ± 100 K and a higher mass of $8 \pm 2 M_{\text{Jup}}$. To explain the companion under-luminosity, Mohanty et al. (2007) have suggested the existence of a circum-secondary edge-on disk responsible for a gray extinction of ~ 2.5 mag between 0.9 and $3.8 \mu\text{m}$. However, synthetic atmosphere models clearly encounter difficulties in describing faithfully the late-L to mid-T dwarfs transition (~ 1400 K for field L/T dwarfs), corresponding to the process of cloud clearing. Similar difficulties have been encountered by Marois et al. (2008b) to reproduce all photometric data of the three planetary mass companions to HR 8799 that fall also at the edge or inside the transition of cloudy to cloud-free atmospheres. In the case of 2M1207 b, future spectroscopic or polarimetric observations should help to distinguish between the two scenarios (obscured or non-obscured by a circumstellar disk). Recent precise parallax determinations (Gizis et al. 2007; Ducourant et al. 2008) allowed a reevaluation of the distance and the physical properties of the companion (see Table 7).

6. Statistical analysis

6.1. Context

Over the past years, a significant number of deep imaging surveys have been reported in the literature, dedicated to the search for exoplanets around young, nearby stars (Chauvin et al. 2003; Neuhäuser et al. 2003; Lowrance et al. 2005; Masciadri et al. 2005; Biller et al. 2007; Kasper et al. 2007; Lafrenière et al. 2007). Various instruments and telescopes were used with different imaging techniques (coronagraphy, angular or spectral differential imaging, L' -band imaging) and observing strategies. None of those published surveys have reported the detection of planetary mass companions that could have formed by a core-accretion model (as expected for a large fraction of planet candidates reported by RV measurements). Several potential planetary mass companions were discovered, but generally at relatively large physical separations or with a small mass-ratio with their primaries, suggesting a formation mechanisms sim-

ilar to (sub)stellar binaries and stars. Only very recently, planet candidates perhaps formed by core-accretion have been imaged around the stars Fomalhaut (Kalas et al. 2008), HR 8799 (Marois et al. 2008b) and β Pictoris (Lagrange et al. 2009), initiating the study of giant exo-planets at the (mass, distance) scale of our solar system.

Confronted with a null-detection of planets formed by core-accretion, several groups (Kasper et al. 2007; Lafrenière et al. 2007; Nielsen et al. 2008) have developed statistical analysis tools to exploit the complete deep imaging performances of their surveys. A first approach is to test the consistency of various sets of (mass, eccentricity, semi-major axes) parametric distributions of a planet population in the specific case of a null detection. A reasonable assumption is to extrapolate and normalize planet mass, period and eccentricity distributions using statistical results of RV studies at short periods. Given the detection performances of a survey, the rate of detected simulated planets (over the complete sample) enables derivation of the probability of non-detection of a given planet population associated with a normalized distribution set. Then comparison with a survey null-detection sample tests directly the statistical significance of each distribution and provides a simple approach for constraining the outer portions of exoplanetary systems.

A second more general approach aims at actually constraining the exoplanet fraction f within the physical separation and mass probed by the survey, in the case of null or positive detections. Contrary to what was assumed before, f becomes an output of the simulation, that actually depends on the assumed (mass, period, eccentricity) distributions of the giant planet population. This statistical analysis aims at determining f within a confidence interval as a function of mass and semi-major axis, given a set of individual detection probabilities p_j directly linked to the detection limits of each star observed during the survey and the considered giant planet distributions. One can refer to the work of Lafrenière et al. (2007) and Carson et al. (2006), for a general description of the statistical formalism applied for this analysis.

For our survey, we will consider the specific case of a null detection of planet formation by core-accretion within a Poisson statistical formalism that leads to a simple analytical solution for the exoplanet fraction upper limit (f_{max}). In the following, we will consider both approaches to exploit the full survey detection potential.

6.2. Simulation description

The simulation process is similar to the one adopted by Kasper et al. (2007), Lafrenière et al. (2007) and Nielsen et al. (2008). Due to the important spectral type dispersion of our sample, we have included in addition a planet mass dependency on primary mass. The different steps of the simulation process are described below:

1. Our simulation star sample is composed of 65 stars observed in coronagraphic imaging mode (see Table 2 and 3). Binaries that could impact the presence of a planet within a range of semi-major axis of $a = [5 - 150]$ AU were removed. Apparent magnitude, distance, age and mass are the prime simulation parameters.
2. The detection limits were converted to predicted masses using COND03 and DUSTY evolutionary models of Chabrier et al. (2000) and Baraffe et al. (2003). COND03 models are adapted to predict properties of cool (≤ 1700 K) substellar objects, whereas DUSTY model predictions were considered

Table 7. Properties of the confirmed comoving substellar companions discovered in the young, nearby associations: TW Hydrae (Twa), β Pictoris (β Pic), Columba (Col) and Carina (Car). Tentative spectral type have been determined from nIR spectroscopic observations, whereas masses and effective temperatures are predicted by evolutionary models based on the nIR photometry, the age and the distance of the system. (*), for 2M1207 b, Mohanty et al. (2007) suggests a higher mass of $8 \pm 2 M_{\text{Jup}}$ and the existence of a circum-secondary edge-on disk to explain their measured effective spectroscopic temperature of 1600 ± 100 K.

Name	Grp	Age (Myr)	d (pc)	SpT _A	SpT _B	M_B (M_{Jup})	T_{eff}^B (K)	$q_{B/A}$	Δ_{proj} (AU)
TWA5	TWA	8	(45-50)	M1.5	M8.5	25 ± 5	2500 ± 150	0.055	93 ± 10
HR7329	β Pic	12	$48.2^{+1.8}_{-1.6}$	A0V	M8	25 ± 5	2550 ± 150	0.010	199 ± 10
GSC-08047-00232	Tuc-Hor/Col	30	(85-95)	K3V	$M9^{+1}_{-3}$	20 ± 5	2100 ± 200	0.025	295 ± 30
AB Pic	Tuc-Hor/Car	30	$46.0^{+1.6}_{-1.5}$	K2V	$L1^{+2}_{-1}$	13 ± 2	1700 ± 200	0.015	250 ± 10
2M1207	TWA	8	$52.4^{+1.7}_{-1.1}$	M8	late-L	$4 \pm 1^*$	$1150 \pm 150^*$	0.16^*	40 ± 2

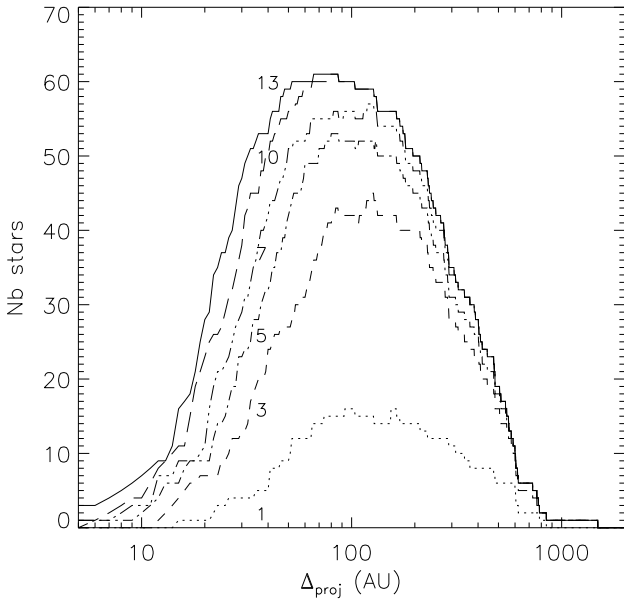


Fig. 9. Histogram of projected physical separations explored, for various planetary masses (1, 3, 5, 7, 10 and 13) M_{Jup} , in the close vicinity of the 65 young, nearby stars observed with NACO at VLT in coronagraphy. Contrast performances have been converted into masses based on the nIR photometry, age and distance of the primary stars.

for hotter temperatures. Based on our (6σ) individual detection limits and target (distance, age, H or K_s -band magnitude) properties, we derived the space of predicted masses and projected physical separation explored around each star of the sample (see histogram in Fig. 9).

- For the giant planet population, we have considered input distributions based on parametric laws for mass and period extrapolated from RV studies. The eccentricity distribution was chosen to follow the empirical planet distributions of RV planets. For mass and period, we consider power laws $dN/dM_p \text{ sini} \propto (M_p \text{ sini})^\alpha$ and $dN/dP \propto P^\beta$ respectively. In addition, the influence of a planetary mass distribution scaled as a function of the stellar mass ($M_p \propto M_*^\gamma$) was tested.
- Monte Carlo simulations were run to take into account the the exoplanet distributions and orbital phase. For each run, 10,000 values of $M_p \text{ sini}$ and P are randomly generated, following the adopted exoplanet distributions, together with all

the other orbital elements, which are supposed to be uniformly distributed. The real characteristics of each target star (mass, distance) are taken into account to evaluate the semi-major axis and projected physical separation of the planets.

- The final step is a comparison with the survey null-detection results and detection performances: either for a derivation of a non-detection probability and thus constraining the statistical significance of various sets of input distributions or for a derivation of the planet fraction upper limit (f_{max}) for a given set of exoplanet distributions. Dead zones of our coronagraphic images due to the presence of the mask support or the diffraction spikes have been considered in our detection performances and simulations.

6.3. Statistical results

6.3.1. Extrapolating radial velocity distributions

As a starting point, we used the mass and period distributions derived by Cumming et al. (2008) with $\alpha = -1.31$ and $\beta = -0.74$. We considered a giant planet frequency of 8.5% in the range 0.3 – 15 M_{Jup} for periods less than 1986 days (≤ 3 AU for a 1 M_\odot host star). The resulting value is consistent with RV studies of Marcy et al. (2005). Running several sets of simulations, we explored independently the influence of period, planet mass and primary mass distributions on the non-detection probability determined as a function of the period cut-off. The period cut-off was chosen to correspond to a semi-major axis cut-off between 20 and 150 AU. The results are reported in Fig. 10, to study the impact of the planet mass power law index α with $\beta = -0.74$ and $\gamma = 0.0$ (Top), of β the period power law index with $\alpha = -1.31$ and $\gamma = 0.0$ (Middle), and the evolution implied by a planet mass dependency with the primary mass when γ varies and $\alpha = -1.31$ and $\beta = -0.74$ (Bottom). As reference, Cumming et al. (2008) extrapolated distributions are reported in *thick solid* lines in all panels of Fig. 10. As a result, the non-detection probability of our survey as a function of the period cut-off is more sensitive to the variation of β , the period power law index. A reasonable set of values can significantly be excluded for large semi-major axis cut-off. In comparison, the influence of α and γ remains limited under the current assumptions.

6.3.2. Exoplanet fraction upper limit

The probability of planet detection for a survey of N stars is described by a binomial distribution, given a success probability $f p_j$ with f the fraction of stars with planets and p_j the individual detection probabilities of detecting a planet if present around the

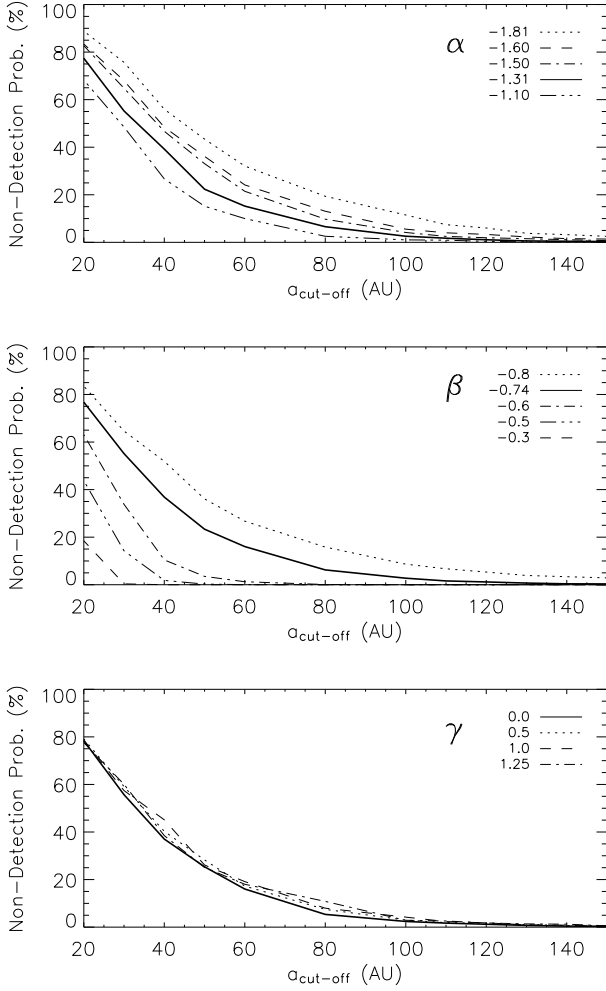


Fig. 10. Non-detection probability for our survey, based on various sets of period and mass distributions as a function of the semi-major axis cut-off of the period distribution. Mass and period distributions are extrapolated and normalized from RV studies. *Top:* Variation of the non-detection probability with α and fixing $\beta = -0.74$ and $\gamma = 0.0$. *Middle:* Variation of the non-detection probability with β and fixing $\alpha = -1.31$ and $\gamma = 0.0$. *Bottom:* Variation with γ a planet mass scaling with the primary mass and fixing $\alpha = -1.31$ and $\beta = -0.74$.

star j . In our case, we can consider a null detection result and replace each individual p_j by $\langle p_j \rangle$ the mean survey detection probability of detecting a planet if present. Finally, assuming that the number of expected detected planets is small compared to the number of stars observed ($f \langle p_j \rangle \ll 1$), the binomial distribution can be approximated by a Poisson distribution to derive a simple analytical solution for the exoplanet fraction upper limit f_{\max} for a given level of credibility CL.

$$f_{\max} = \frac{-\ln(1 - \text{CL})}{N \langle p_j \rangle} \quad (1)$$

We consider the period and mass power law indexes from Cumming et al. (2008) $\alpha = -1.31$, $\beta = -0.74$ and $\gamma = 1.25$ for the period and mass distribution of giant planet. For the set of detection limits of our survey, we can then determine $\langle p_j \rangle$, the survey mean probability of detecting a planet if present around each star of our sample. Then, given a confidence level $\text{CL} = 0.95$,

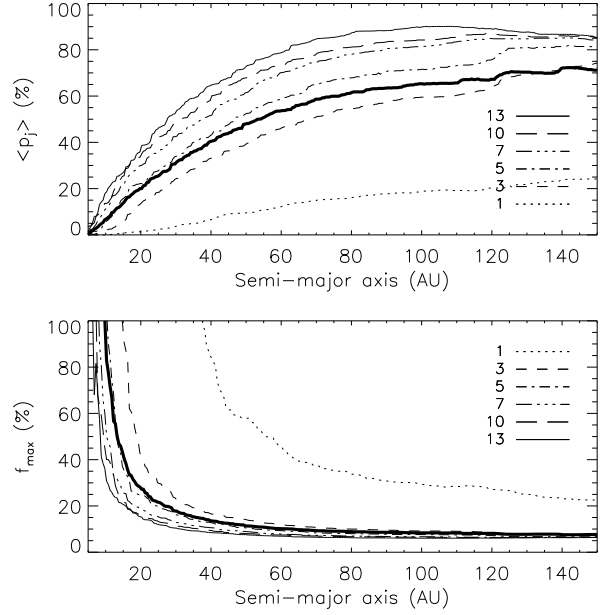


Fig. 11. *Top:* Survey mean detection probability derived as a function of semi-major axis assuming parametric mass and period distributions derived by Cumming et al. (2008), i.e with $\alpha = -1.31$, $\beta = -0.74$ and $\gamma = 1.25$. The results are reported for individual masses: 1, 3, 5, 7, 10 and 13 M_{Jup} . The integrated probability for the planetary mass regime is shown with the *thick solid line*. *Bottom:* Planet fraction upper limit derived as a function of semi-major axis, given the same mass and period distributions.

we obtain f_{\max} as a function of planet mass and semi-major axis. The survey mean detection probability and f_{\max} are reported in Fig. 11. It is important to note that both results depend on the assumed (mass, period, eccentricity) distributions of the giant planet population. Similar to other deep imaging surveys, our study begins to constrain the fraction of stars with giant planets to less than 10% for semi-major axes larger than typically 40 AU for this specific set of period, mass and eccentricity distributions. We also see that we barely constrain the fraction of 1 M_{Jup} planets potentially detectable for 24% of our targets (67% for the 3 M_{Jup} planets). Increasing the sample size will enable refinement of the statistical constraints on the upper limits of the fraction of stars with giant planets as a function of their mass and semi-major axis. However, a number of intrinsic limitations (detection threshold, age determination and model calibration) remain that will have to be overcome to draw more robust conclusions. Future work gathering detection performances from multiple surveys should help refine our knowledge of the occurrence of giant planets at wide orbits (> 10 AU) and thus complement RV survey results.

6.4. Limitations

Added to the detection threshold determination (detailed previously), the age determination of the young, nearby stars and the use of uncalibrated evolutionary models are the three main limitations that directly impact the estimation of the explored planetary masses from observed luminosities. Added to the current assumption made on the extrapolation of close-in exoplanet distributions at wide orbits, they limit the current relevancy of all

statistical analysis of deep imaging surveys aimed at constraining the population of giant planets.

6.4.1. Age determination

Ages of young stars near the Sun are deduced based on photometric, spectroscopic and kinematics studies; various diagnostics are commonly used, depending on the spectral type and age of a given star. Details may be found in ZS04 and T08. In general, the most reliable ages are obtained for stars that can be placed reliably into a moving group or association.

Our sample is composed of 88 stars, including 51 members of known young, nearby associations (TWA, β Pic, Tuc-Hor and AB Dor). Ages for the TWA and β Pic associations have been reasonably well constrained by various and independent (stellar properties characterization and dynamical trace-back) studies to: 8_{-3}^{+4} Myr (TWA; de la Reza et al. 2006; Barrado y Navasúes 2006; Scholz et al. 2007) and 12_{-4}^{+8} Myr (β Pic, Zuckerman et al. 2001b, Ortega et al. 2004) respectively. Isochrones, lithium depletion and X-ray luminosities indicate an age for Tuc-Hor of 30 Myr (Zuckerman et al. 2001a). The age of the AB Dor association is in some dispute (see Zuckerman et al. 2004, Luhman et al. 2005, Luhman & Potter 2006, Lopez-Santiago et al. 2006, Janson et al. 2007, Ortega et al. 2007, Close et al. 2007, Boccaletti et al. 2008, Torres et al. 2008). In our simulations, we have assumed an age of 70 Myr for AB Dor stars.

In our statistical analysis of 65 stars observed in coronagraphic imaging mode, 45 are confirmed members of known associations while 17 are young candidates, currently not identified as members of any kinematic group which makes an age estimate particularly difficult. An excellent example of a young star not known to be a member of the above listed moving groups is HR 8799, identified by Marois et al (2008b) as orbited by 3 giant planets but with an age uncertainly between 30 and 160 Myr. In our analysis, age is directly used to convert the detection limits to mass using evolutionary models. Therefore, age determination remains a main limitation in this work and others to constrain reliably the properties of a putative population of giant planets around young, nearby stars.

6.4.2. Evolutionary models

Evolutionary model predictions are commonly used to infer substellar masses from observed luminosities, as we did to convert our survey detection performances into planetary mass limits. For stars and brown dwarfs formed by gravitational collapse and fragmentation, models consider the idealized description of non-accreting systems contracting at large initial radii. Remaining circumstellar material, accretion and uncertainties related to choice of initial conditions imply that comparison between observations and models are quite uncertain at young ≤ 100 Myr ages (Baraffe et al. 2002). This could be even worse for young giant planets; the implementation of the core-accretion mechanism as initial conditions for evolutionary calculation could substantially change the model predictions (Marley et al. 2007). Then massive giant planets could be significantly fainter than equal-mass objects formed in isolation via gravitational collapse. However, a critical issue is treatment of the accretion shock through which most of the giant planet mass is processed and which remains highly uncertain. In previous analyses of survey detection performances, only predictions from Chabrier et al. (2000) and Baraffe et al. (2003) models were used. Use of Burrows et al. (2003), assuming the same initial

conditions, does not change significantly the results (Nielsen et al. 2008).

7. Conclusions

We have conducted a deep adaptive optics imaging survey with NACO at the VLT of 88 nearby stars of the southern hemisphere. Our selection criteria favored youth (≤ 100 Myr) and proximity to Earth (≤ 100 pc) to optimize the detection of close planetary mass companions. Known visual binaries were excluded to avoid degrading the NACO AO and/or coronagraphic detection performances. Among our sample, 51 stars are members of young, nearby comoving groups. 32 are young, nearby stars currently not identified as members of any currently known association and 5 have been reclassified as older (≥ 100 Myr) systems. The spectral types cover the sequence from B to M spectral types with 19% BAF stars, 48% GK stars and 33% M dwarfs. The separation investigated typically ranges between $0.1''$ to $10''$, i.e. between typically 10 to 500 AU. A sample of 65 stars was observed in deep coronagraphic imaging to enhance our contrast performances to 10^{-6} and to be sensitive to planetary mass companions down to $1 M_{\text{Jup}}$ (at 24% of our sample) and $3 M_{\text{Jup}}$ (at 67%). We used a standard observing sequence to precisely measure the position and the flux of all detected sources relative to their visual primary star. Repeated observations at several epochs enabled us to discriminate comoving companions from background objects. The main results are that:

- we discovered of 17 new close ($0.1 - 5.0''$) multiple systems. HIP 108195 AB and C (F1III-M6), HIP 84642 AB ($a \sim 14$ AU, K0-M5) and TWA22 AB ($a \sim 1.8$ AU; M6-M6) are confirmed as comoving systems. TWA22 AB, with 80% of its orbit already resolved, is likely to be a rare astrometric calibrator for testing evolutionary model predictions.
- about 236 faint CCs were detected around 36 stars observed in coronagraphy. Follow-up observations with VLT or HST for 30 stars enabled us to identify their status. 1% of the CCs detected have been confirmed as comoving companions, 43% have been identified as probable background contaminants and about 56% need further follow-up observations. The remaining CCs come mostly from the presence of crowded fields in the background of the 6 stars observed at one epoch.
- we confirmed previously discovered substellar companions around GSC 08047-00232, AB Pic and 2M1207 and placed them in the perspective of confirmed substellar companions among young, nearby associations.
- finally, the statistical analysis of our complete set of detection limits enables us to constrain at large semi-major axes, 20 to a few 100 AU, various mass, period and eccentricity distributions of giant planets extrapolated and normalized from RV surveys. It enables us to derive limits on the occurrence of giant planets for a given set of physical and orbital distributions. The survey starts constraining significantly the population of giant planet for masses $\geq 3 M_{\text{Jup}}$.

In the first few years following the discovery of the companion to 2M1207 (Chauvin et al. 2004), all planetary mass companions were discovered at relatively wide separations or with small mass ratio with their primaries. However, the recent discoveries of planetary mass objects around the star Fomalhaut (Kalas et al. 2008), HR 8799 (Marois et al. 2008b) and β Pictoris (Lagrange et al. 2009), now open a new era for the deep imaging study of giant planets that probably formed like those of our solar system.

In the perspective of on-going and future deep imaging instruments either from the ground (Gemini/NICI, Subaru/HiCIAO, SPHERE, GPI, EPICS) or from space (JWST, TPF/Darwin), this work represents a pioneer successful study, providing, with other surveys, precise information (stellar and substellar multiplicity, non-detections and background contaminants) to better characterize the overall environment of young, nearby stars, that will be prime targets for futur exoplanets search.

Acknowledgements. We thank the ESO Paranal staff for performing the service mode observations. We also acknowledge partial financial support from the PNPS and Agence National de la Recherche, in France, from INAF through PRIN 2006 “From disk to planetary systems: understanding the origin and demographics of solar and extrasolar planetary systems” and from NASA in the USA. We also would like to thanks France Allard and Isabelle Baraffe for their inputs on evolutionary models and synthetic spectral libraries. Finally, our anonymous referee for her/his detailed and very constructive report.

References

- Baraffe I., Chabrier G., Allard F. & Hauschildt P.H. 2002, *A&A* 382, 563
 Baraffe, I., Chabrier, G., Barman, T. S., Allard, F., & Hauschildt, P. H. 2003, *A&A*, 402, 701
 Barrado Y Navascués D. 2006, *A&A*, 459, 511
 Biller B.A., Close L.M., Masciadri E. et al. 2007, *ApJS*, 173, 143
 Boccaletti A., Chauvin G., Baudoz P. & Beuzit J.-L. 2008, *A&A*, 482, 939
 Boley A.C. 2009, *ApJ*, 695, L53
 Bonnell I. A., Larson R. B. & Zinnecker H. 2007, *Protostars and Planets V*, 951, 149-164
 Burgasser A. J., Kirkpatrick J. D., Brown M. E. et al. 1999, *ApJ*, 522, 65
 Burgasser A. J., Reid I.N., Siegler N. et al. 2007, *Protostars and Planets V*, 951, 427-441
 Burrows A., Sudarsky D. & Lunine J.I. 2003, *ApJ*, 596, 587
 Butler R. P., Wright J.T., Marcy G.W. et al. 2006, *ApJ*, 646, 505
 Carson J. C., Eikenberry S. S., Brandl B. R., Wilson, J. C. & Hayward T. L. 2005, *AJ*, 130, 1212
 Carson J. C., Eikenberry S. S., Smith J. J. & Cordes, J. M. 2006, *AJ*, 132, 1146
 Chabrier, G., Baraffe, I., Allard, F., & Hauschildt, P. H. 2000, *ApJ*, 542, 464
 Chauvin G., Thomson M., Dumas C. et al. 2003, *A&A*, 404, 157
 Chauvin G., Lagrange A.-M., Dumas C. et al. 2004, *A&A*, 425, L25
 Chauvin G., Lagrange A.-M., Lacombe F. et al. 2005a, *A&A*, 430, 1027
 Chauvin G., Lagrange A.-M., Dumas C. et al., 2005b, *A&A*, 438, L25
 Chauvin G., Lagrange A.-M., Zuckerman B. et al. 2005c, *A&A*, 438, L29
 Chauvin G., Lagrange A.-M., Udry S. et al. 2006, *A&A*, 456, 1165
 Close, Laird M.; Thatte, Niranjan; Nielsen, Eric L. et al. 2007, *ApJ*, 665, 736
 Couteau, P. 1960, *J. Obs.*, 43, 13
 Cumming A., Butler R. P., Marcy G. W. et al. 2008, *PASP*, 120, 531
 de la Reza R., Jilinski E. & Ortega V.G. 2006, *AJ*, 131, 2609
 Delfosse X., Tinney C. G., Forveille, T. et al. 1997, *A&A*, 327, 25
 Devillar N. 1997, *The messenger*, 87
 Dohlen K., Beuzit J.-L., Feldt M. et al. 2006, *SPIE*, 6269, 24
 Dommanget, J. & Nys, O. 2000, *A&A*, 363, 991
 Ducourant C., Teixeira R., Chauvin G. et al. 2008, *A&A*, 477, L1
 Eggenberger A., Udry S., Chauvin G. et al. 2007, *A&A*, 474, 273
 Endl M., Cochran W.D., Krster M. et al. 2006, *ApJ*, 649, 436
 Epchtein N., de Batz B., Capoani L., Chevallier L. et al. 1997, *Msgr*, 87, 27
 Fuhrmeister & Schmitt 2003, *A&A* 403, 247
 Gizis, J., Jao, W., Subsavage, J.P., Henry, T.J., 2007, *ApJ*, 669, L45-L48
 Goldman B., Delfosse X., Forveille T. et al. 1999, *A&A*, 351, L5
 Grether & Lineweaver 2006, *ApJ*, 640, 1051
 Grillmair C.J., Burrows A., Charbonneau D. et al. 2008, *Nature*, 456, 767
 Itoh Y., Hayashi M., Tamura M. et al. 2005, *ApJ*, 620 984
 Janson M., Brandner W., Lenzen R. et al. 2007, *A&A*, 462, 615
 Joergens V. 2006, *A&A*, 446, 1165
 Johnson J.A., Fischer D.A., Marcy G.W. et al. 2007, *ApJ*, 665, 785
 Kalas P., Graham J. R., Chiang E. et al. 2008, *Science*, 322, 1345
 Kastner, J.H., Zuckerman, B., Weintraub, D.A. & Forveille T. 1997, *Science* 277, 67
 Kasper M., Apai D., Janson M. & Brandner W. 2007, *A&A*, 472, 321
 Kirkpatrick J. D., Reid I. N., Liebert J. et al. 1999, *ApJ* 519, 802
 Kirkpatrick J. D., Reid I. N., Liebert J. et al. 2000, *ApJ* 120, 447
 Lafrenière, David; Doyon, René; Marois, Christian et al. 2007, *ApJ*, 670, 1367
 Lafrenière D., Jayawardhana R., van Kerkwijk M.H. et al. 2008, *ApJ*, 689, 153
 Lagrange A.-M., Gratadour D., Chauvin G. et al. 2009, *A&A*, 493, L21
 Lagrange A.-M., Desort M., Galland F., Udry S. & Mayor M. 2009, *A&A*, 495, 335
 Lenzen, R., Hofmann, R., Bizenberger, P. & Tusche, A., 1998, *SPIE*, Vol. 3354
 López-Santiago J., Montes D., Crespo-Chacón I., & Fernández-Figueroa M.J. 2006, *ApJ*, 643, 1160
 Lowrance, P. J., McCarthy, C., Becklin, E. E. et al. 1999, *ApJ*, 512, L69
 Lowrance, P. J., Schneider, G., Kirkpatrick, J. et al. 2000, *ApJ*, 541, L390
 Lowrance P.J., Becklin E.E., Schneider G. et al. 2005, *AJ*, 130, 1845
 Luhman, K. & Jayawardhana, R. 2002, *ApJ*, 566, 1132
 Luhman K.L., Stauffer J.R. & Mamajek E.E. 2005, 628, L69
 Luhman K.L. & Potter D. 2006, *ApJ*, 638, 887
 Luhman K.L., Wilson J.C., Brandner W. et al. 2006, *ApJ*, 649, 894
 Marcy G., Butler R. P., Fischer D. et al. 2005, *PTHP*, 158, 24
 Marley M.S., Fortney J.J., Hubickyj O., Bodenheimer P. & Lissauer J.J. 2007, *ApJ*, 655, 541
 Marois C., Lafrenière D., Macintosh B. & Doyon R. 2008a, *ApJ*, 673, 647
 Marois C., Macintosh B., Barman, T. et al. 2008b, *Science* 322, 1348
 Masciadri, E., Mundt, R., Henning, Th. & Alvarez, C. 2005, *ApJ*, 625, 1004
 Mayor, M. & Queloz, D. 1995, *Nature* 378, 355
 McCarthy, C. & Zuckerman, B. 2004, *AJ*, 127, 2871
 McCaughrean M.J. & Stauffer J.R. 1994, *AJ*, 108, 1382
 Macintosh B., Troy M. Doyon R. et al. 2006, *SPIE*, 6272, 20
 Masciadri E., Mundt R., Henning Th., Alvarez C. & Barrado y Navascués D. 2005, *ApJ*, 625, 1004
 Metchev S. & Hillenbrand L. 2006, *ApJ*, 651, 1166
 Metchev S. & Hillenbrand L. 2008, *ApJ*, 676, 1281
 Mohanty S., Jayawardhana R., Huéramo N. & Mamajek E. 2007, *ApJ*, 657, 1064
 Mugrauer M., Seifahrt A. & Neuhäuser R. 2007, *MNRAS*, 378, 1328
 Nakajima T., Oppenheimer B.R., Kulkarni S.R. et al. 1995, *Nature* 378, 463
 Neuhäuser, R., Guenther, E.W., Alves, J. et al. 2003, *AN*, 324, 535
 Neuhäuser, R. & Guenther, E.W. 2004, *A&A*, 420, 647
 Neuhäuser R., Guenther E.W., Wuchterl G. et al. 2005, *A&A*, 435, 13
 Nielsen E.L., Close L.M., Biller B.A., Masciadri E. & Lenzen R. 2008, *ApJ*, 674, 466
 Ortega V. G., de la Reza R., Jilinski E. & Bazzanella B. 2004, *ApJ*, 609, 243
 Ortega, V. G.; Jilinski, E.; de La Reza, R.; Bazzanella, B. 2007, *MNRAS*, 377, 441
 Papaloizou, J. C. B., Terquem, C. 2001, *MNRAS*, 325, 221
 Patience J., White R.J., Ghez, A. M. et al. 2002, *ApJ*, 581, 654
 Rafikov R.R. 2005, *ApJ*, 621, L69
 Rousset G., Lacombe F., Puget P. et al., 2002, *SPIE*, Vol. 4007
 Schmidt T.O.B., Neuhäuser R., Seifahrt A. et al. 2008, arXiv0809.2812S
 Scholz A., Coffey J., Brandeker A. & Jayawardhana R. 2007, *ApJ*, 662, 1254
 Siess L., Dufour, E. & Forestini M. 2000, *A&A*, 358, 593
 Skrutskie M. F., Schneider S. E., Stiening R., Strom S. E. et al. 1997, *ASSL*, 210, 25
 Song I., Zuckerman B. & Bessel M.S. 2003, *ApJ*, 599, 342
 Song I., Schneider G., Zuckerman B. et al. 2006, *ApJ*, 26, 282
 Swain M.R., Vasisht G. & Tinetti G. 2008, *Nature*, 452, 329
 Torres C.A.O., Quast G.R., Melo C.H.F. & Sterzik M.F. 2008, *Handbook of Star Forming Regions, Volume II: The Southern Sky*, ASP Monograph Publications, Vol. 5, p.757
 Udry S. & Santos N. C. 2007, *ARA&A*, 45, 397
 van Dessel E. & Sinachopoulos D. 1993, *A&AS*, 100, 517
 Véran, J.P. & Rigaut, F. 1998, *SPIE*, 3353, 426
 Webb R. A., Zuckerman B., Platais I. et al. 1999, *ApJ* 512, L63
 Wilson J.C., Kirkpatrick J.D., Gizis J.E. et al. 2001, *AJ*, 122, 1989
 York D. G., Adelman J., Anderson J. E. Jr et al. 2000, *AJ*, 120, 1579
 Zuckerman B., Song I. & Webb R.A. 2001a, *ApJ*, 559, 388
 Zuckerman B., Song I., Bessell M.S. & Webb R.A. 2001b, *ApJ*, 562, 87
 Zuckerman B., Song I. & Bessell M.S. 2004, *ApJ*, 613, L65
 Zuckerman, B. & Song, I. 2004, *ARAA*, 42, 685
 Zuckerman & Song 2009, *A&A*, 493, 1149

Table 8. Characterization and identification (for multi-epochs observations) of all faint sources detected during the VLT/NACO survey. Target name, observing date and set-up are given, as well as the different sources identified with their relative position, relative flux and their status identification based on follow-up observations. Sources referred as undefined (U) are objects detected at only one epoch, (B) objects identified as stationary background contaminants and (C) confirmed comoving companion. When VLT observations are combined to other instrumentation (HST, USNO, 2MASS), a flag or a reference is reported in the last column.

Name	Candidate	UT Date	Filter	Separation (arcsec)	P.A. ($^{\circ}$)	Δm (mag)	Status	Note
GSC08047-00232	cc-1	23/11/2002	K_s	3.274 ± 0.012	358.85 ± 0.23	6.3 ± 0.1	C	
		07/09/2003	K_s	3.266 ± 0.011	358.89 ± 0.23			
		05/03/2004	K_s	3.260 ± 0.012	358.82 ± 0.22			
HIP30034 (AB Pic)	cc-1	17/03/2003	H	5.460 ± 0.014	175.33 ± 0.18	7.6 ± 0.1	C	
		05/03/2004	H	5.450 ± 0.016	175.13 ± 0.21			
		26/09/2004	H	5.453 ± 0.014	175.10 ± 0.20			
		01/05/2005	H	5.452 ± 0.015	175.37 ± 0.20			
		08/01/2006	H	5.455 ± 0.014	175.49 ± 0.21			
HIP6856	cc-1	26/11/2002	K_s	4.585 ± 0.014	105.70 ± 0.30	10.6 ± 0.2	B	
		08/06/2003	K_s	4.547 ± 0.014	105.80 ± 0.30			
	cc-2	07/09/2003	K_s	4.503 ± 0.013	105.40 ± 0.30	12.8 ± 0.2	B	
		26/11/2002	K_s	2.830 ± 0.013	85.40 ± 0.30			
		08/06/2002	K_s	2.791 ± 0.015	85.30 ± 0.30			
TWA19 A	cc-1	07/06/2003	H	3.574 ± 0.019	303.66 ± 0.35	10.3 ± 0.2	B	
		08/01/2006	H	3.507 ± 0.012	305.78 ± 0.20			
HIP95270	cc-1	25/09/2004	H	4.826 ± 0.019	250.45 ± 0.23	11.9 ± 0.2	B	
		19/08/2005	H	4.825 ± 0.027	251.29 ± 0.19			
	cc-2	25/09/2004	H	5.806 ± 0.023	274.00 ± 0.13			
		19/08/2005	H	5.839 ± 0.035	274.52 ± 0.11			
HIP59315	cc-1	27/04/2004	H	5.412 ± 0.020	97.71 ± 0.22	9.3 ± 0.3	B	
		06/05/2005	H	5.526 ± 0.021	96.89 ± 0.21			
HIP84586	cc-1	27/04/2004	H	7.960 ± 0.026	120.23 ± 0.19	11.3 ± 0.2	B	
		27/04/2004	K_s	7.860 ± 25	119.55 ± 0.23			
GSC-08894-00426	cc-1	05/03/2004	H	9.904 ± 0.028	246.13 ± 0.21	15.1 ± 0.2	B	
		26/02/2006	K_s	9.917 ± 0.024	245.36 ± 0.15			
HIP108195 AB	cc-1	26/02/2006	K_s	4.966 ± 0.010	158.22 ± 0.14	5.4 ± 0.2	C	stellar
		18/06/2007	K_s	4.962 ± 0.012	158.22 ± 0.20			
	cc-2	26/02/2006	K_s	13.041 ± 0.025	190.71 ± 0.14			
		18/06/2007	K_s	12.920 ± 0.026	191.44 ± 0.20			
TYC-09012-1005-1	cc-1	27/04/2004	H	3.709 ± 0.015	21.20 ± 0.24	6.1 ± 0.1	B	
		08/05/2007	K_s	3.790 ± 0.014	22.68 ± 0.22			
	cc-2	27/04/2004	H	6.725 ± 0.025	50.64 ± 0.28			
		08/05/2007	K_s	6.826 ± 0.025	50.87 ± 0.27			
	cc-3	27/04/2004	H	3.010 ± 0.013	141.40 ± 0.31			
		08/05/2007	K_s	3.029 ± 0.011	139.80 ± 0.27			
	cc-4	27/04/2004	H	4.771 ± 0.019	188.03 ± 0.22			
		08/05/2007	K_s	4.695 ± 0.018	186.84 ± 0.20			
	cc-5	27/04/2004	H	3.686 ± 0.015	245.09 ± 0.25			
		08/05/2007	K_s	3.565 ± 0.013	245.14 ± 0.23			
	cc-6	27/04/2004	H	2.814 ± 0.012	302.49 ± 0.29			
		08/05/2007	K_s	2.753 ± 0.010	304.57 ± 0.25			
	cc-7	27/04/2004	H	5.591 ± 0.021	307.61 ± 0.28			
		08/05/2007	K_s	5.528 ± 0.020	308.73 ± 0.27			
	cc-8	27/04/2004	H	4.800 ± 0.019	324.79 ± 0.27			
08/05/2007		K_s	4.765 ± 0.017	326.40 ± 0.25				
cc-9	27/04/2004	H	5.264 ± 0.021	339.50 ± 0.23				
	08/05/2007	K_s	5.262 ± 0.020	340.93 ± 0.22				
cc-10	27/04/2004	H	2.691 ± 0.012	121.77 ± 0.29				
	08/05/2007	K_s	2.751 ± 0.010	119.75 ± 0.24				
cc-11	27/04/2004	H	4.324 ± 0.017	146.38 ± 0.27				
	08/05/2007	K_s	4.332 ± 0.016	144.88 ± 0.25				
cc-12	27/04/2004	H	5.996 ± 0.024	180.21 ± 0.21				
	08/05/2007	K_s	5.930 ± 0.023	179.20 ± 0.2				
cc-13	08/05/2007	K_s	1.566 ± 0.009	28.17 ± 0.36	U			
cc-14	08/05/2007	K_s	3.809 ± 0.015	59.80 ± 0.27	U			
cc-15	08/05/2007	K_s	5.608 ± 0.021	52.01 ± 0.28	U			

Table 9. Table 7 - cont

Name	Candidate	UT Date	Filter	Separation (arcsec)	P.A. ($^{\circ}$)	Δm (mag)	Status	Note
	cc-16	08/05/2007	K _s	5.083 ± 0.020	81.32 ± 0.22	11.3 ± 0.2	U	
	cc-17	08/05/2007	K _s	7.208 ± 0.027	53.12 ± 0.27	10.5 ± 0.2	U	
	cc-1	08/05/2007	K _s	8.158 ± 0.030	51.12 ± 0.27	11.1 ± 0.2	U	
	cc-19	08/05/2007	K _s	7.650 ± 0.029	61.15 ± 0.24	10.5 ± 0.2	U	
	cc-20	08/05/2007	K _s	6.792 ± 0.026	80.03 ± 0.21	11.1 ± 0.2	U	
	cc-21	08/05/2007	K _s	7.705 ± 0.030	75.99 ± 0.21	9.2 ± 0.2	U	
	cc-22	08/05/2007	K _s	6.870 ± 0.027	103.87 ± 0.22	11.4 ± 0.2	U	
	cc-23	08/05/2007	K _s	7.838 ± 0.030	110.93 ± 0.22	10.9 ± 0.2	U	
	cc-24	08/05/2007	K _s	7.538 ± 0.028	132.55 ± 0.29	11.3 ± 0.2	U	
	cc-25	08/05/2007	K _s	4.932 ± 0.019	134.47 ± 0.31	11.5 ± 0.2	U	
	cc-26	08/05/2007	K _s	6.124 ± 0.023	144.73 ± 0.27	11.3 ± 0.2	U	
	cc-27	08/05/2007	K _s	8.245 ± 0.031	153.07 ± 0.24	10.2 ± 0.2	U	
	cc-28	08/05/2007	K _s	2.783 ± 0.012	130.62 ± 0.33	10.8 ± 0.2	U	
	cc-29	08/05/2007	K _s	3.180 ± 0.013	151.96 ± 0.27	10.4 ± 0.2	U	
	cc-30	08/05/2007	K _s	6.175 ± 0.024	162.80 ± 0.22	10.3 ± 0.2	U	
	cc-31	08/05/2007	K _s	1.475 ± 0.009	174.39 ± 0.33	10.1 ± 0.2	U	
	cc-32	08/05/2007	K _s	4.265 ± 0.017	211.89 ± 0.27	10.3 ± 0.2	U	
	cc-33	08/05/2007	K _s	3.552 ± 0.015	218.25 ± 0.30	10.8 ± 0.2	U	
	cc-34	08/05/2007	K _s	2.453 ± 0.011	218.09 ± 0.33	10.1 ± 0.2	U	
	cc-35	08/05/2007	K _s	5.548 ± 0.021	234.93 ± 0.27	10.5 ± 0.2	U	
	cc-36	08/05/2007	K _s	4.715 ± 0.019	248.43 ± 0.24	11.1 ± 0.2	U	
	cc-37	08/05/2007	K _s	4.672 ± 0.019	253.54 ± 0.23	9.9 ± 0.2	U	
	cc-38	08/05/2007	K _s	2.808 ± 0.012	258.37 ± 0.25	10.8 ± 0.2	U	
	cc-39	08/05/2007	K _s	1.933 ± 0.010	296.55 ± 0.32	10.7 ± 0.2	U	
	cc-40	08/05/2007	K _s	2.948 ± 0.013	299.78 ± 0.28	10.5 ± 0.2	U	
	cc-41	08/05/2007	K _s	2.387 ± 0.011	307.50 ± 0.33	11. ± 0.2	U	
	cc-42	08/05/2007	K _s	3.077 ± 0.013	273.18 ± 0.24	11.8 ± 0.2	U	
GSC00862-0019-1	cc-1	22/11/2002	K _s	7.780 ± 0.020	3.58 ± 0.22	3.5 ± 0.2	B	USNO
TWA22 AB	cc-1	27/04/2004	H	5.096 ± 0.018	340.78 ± 0.25			
		26/02/2006	K _s	5.070 ± 0.017	343.91 ± 0.21	9.7 ± 0.2	B	
	cc-2	27/04/2004	H	4.786 ± 0.016	5.90 ± 0.26			
		26/02/2006	K _s	4.867 ± 0.016	8.85 ± 0.21	7.5 ± 0.2	B	
	cc-3	27/04/2004	H	7.103 ± 0.020	14.89 ± 0.23			
		26/02/2006	K _s	7.217 ± 0.020	16.82 ± 0.18	6.1 ± 0.2	B	
	cc-4	27/04/2004	H	11.298 ± 0.029	20.84 ± 0.21			
		26/02/2006	K _s	11.428 ± 0.027	22.04 ± 0.16	10.2 ± 0.2	B	
	cc-5	27/04/2004	H	9.984 ± 0.030	31.87 ± 0.22			
		26/02/2006	K _s	10.151 ± 0.025	32.97 ± 0.18	10.8 ± 0.2	B	
	cc-6	27/04/2004	H	12.557 ± 0.037	36.83 ± 0.22			
		26/02/2006	K _s	12.798 ± 0.031	38.28 ± 0.18	10.9 ± 0.2	B	
	cc-7	27/04/2004	H	11.191 ± 0.032	121.56 ± 0.21			
		26/02/2006	K _s	11.348 ± 0.027	120.74 ± 0.17	9.7 ± 0.2	B	
	cc-8	27/04/2004	H	8.755 ± 0.028	130.40 ± 0.24			
		26/02/2006	K _s	8.889 ± 0.023	129.15 ± 0.20	9.6 ± 0.2	B	
	cc-9	27/04/2004	H	4.395 ± 0.017	160.47 ± 0.27			
		26/02/2006	K _s	4.409 ± 0.016	157.12 ± 0.24	11.5 ± 0.2	B	
	cc-10	27/04/2004	H	7.045 ± 0.020	163.39 ± 0.23			
		26/02/2006	K _s	7.036 ± 0.019	161.34 ± 0.18	10.7 ± 0.2	B	
	cc-11	27/04/2004	H	12.575 ± 0.037	142.06 ± 0.22			
		26/02/2006	K _s	12.650 ± 0.030	141.10 ± 0.18	10.6 ± 0.2	B	
	cc-12	27/04/2004	H	12.965 ± 0.039	138.25 ± 0.23			
		26/02/2006	K _s	13.061 ± 0.031	137.36 ± 0.19	11.0 ± 0.2	B	
	cc-13	27/04/2004	H	14.471 ± 0.039	152.71 ± 0.21			
		26/02/2006	K _s	14.485 ± 0.033	151.74 ± 0.16	11.2 ± 0.2	B	
	cc-14	27/04/2004	H	13.474 ± 0.028	179.70 ± 0.21			
		26/02/2006	K _s	13.383 ± 0.028	178.69 ± 0.15	8.6 ± 0.2	B	
	cc-15	27/04/2004	H	10.628 ± 0.027	195.67 ± 0.21			
		26/02/2006	K _s	10.487 ± 0.024	194.57 ± 0.16	11.0 ± 0.2	B	

Table 10. Contaminants and companion identified

Name	Candidate	UT Date	Filter	Separation (arcsec)	P.A. ($^{\circ}$)	Δm (mag)	Status	Note
	cc-16	27/04/2004	H	6.266 ± 0.019	193.90 ± 0.24			
		26/02/2006	K_s	6.133 ± 0.018	191.73 ± 0.19	10.4 ± 0.2	B	
	cc-17	27/04/2004	H	3.466 ± 0.017	227.25 ± 0.37	10.8 ± 0.2	PB	HST
	cc-18	27/04/2004	H	13.912 ± 0.037	205.66 ± 0.21			
		26/02/2006	K_s	13.701 ± 0.031	204.91 ± 0.16	10.2 ± 0.2	B	
	cc-19	27/04/2004	H	14.827 ± 0.040	207.38 ± 0.20			
		26/02/2006	K_s	14.611 ± 0.033	206.70 ± 0.16	9.7 ± 0.2	B	
	cc-20	27/04/2004	H	9.794 ± 0.028	241.51 ± 0.22			
		26/02/2006	K_s	9.516 ± 0.024	241.37 ± 0.17	7.0 ± 0.2	B	
	cc-21	27/04/2004	H	14.004 ± 0.040	235.61 ± 0.21	8.9 ± 0.2	U	
	cc-22	27/04/2004	H	13.297 ± 0.037	239.78 ± 0.21	10.6 ± 0.2	U	
	cc-23	27/04/2004	H	13.353 ± 0.033	251.30 ± 0.21	10.1 ± 0.2	U	
	cc-24	27/04/2004	H	6.902 ± 0.019	264.46 ± 0.23	10.5 ± 0.2	U	
	cc-25	27/04/2004	H	10.633 ± 0.032	310.28 ± 0.23			
		26/02/2006	K_s	10.454 ± 0.026	311.58 ± 0.19	11.1 ± 0.2	B	
	cc-26	27/04/2004	H	10.342 ± 0.032	318.06 ± 0.24			
		26/02/2006	K_s	10.204 ± 0.026	319.54 ± 0.19	9.5 ± 0.2	B	
	cc-27	27/04/2004	H	16.843 ± 0.049	317.34 ± 0.23	9.7 ± 0.2	U	
	cc-28	26/02/2006	K_s	4.552 ± 0.016	207.87 ± 0.24	11.3 ± 0.2	PB	HST
0ES1847	cc-1	25/09/2004	H	3.433 ± 0.014	19.50 ± 0.18			
		09/06/2007	H	3.593 ± 0.014	17.99 ± 0.17	11.1 ± 0.2	B	
	cc-2	25/09/2004	H	1.946 ± 0.010	74.66 ± 0.24			
		09/06/2007	H	1.946 ± 0.009	69.29 ± 0.25	11.3 ± 0.2	B	
	cc-3	25/09/2004	H	5.033 ± 0.018	68.11 ± 0.17			
		09/06/2007	H	5.053 ± 0.018	66.21 ± 0.18	10.7 ± 0.2	B	
	cc-4	25/09/2004	H	5.196 ± 0.020	80.45 ± 0.13			
		09/06/2007	H	5.688 ± 0.022	81.30 ± 0.13	13.5 ± 0.2	B	
	cc-5	25/09/2004	H	3.913 ± 0.015	155.61 ± 0.19			
		09/06/2007	H	3.724 ± 0.014	155.30 ± 0.19	11.5 ± 0.2	B	
	cc-6	25/09/2004	H	3.756 ± 0.016	173.50 ± 0.15			
		09/06/2007	H	3.559 ± 0.015	174.35 ± 0.15	11.0 ± 0.2	B	
	cc-7	25/09/2004	H	7.100 ± 0.027	175.19 ± 0.12			
		09/06/2007	H	6.907 ± 0.027	175.71 ± 0.12	11.0 ± 0.2	B	
	cc-8	25/09/2004	H	4.684 ± 0.019	185.48 ± 0.13			
		09/06/2007	H	4.379 ± 0.018	186.28 ± 0.14	12.6 ± 0.2	B	
	cc-9	25/09/2004	H	5.777 ± 0.021	198.20 ± 0.15			
		09/06/2007	H	5.628 ± 0.021	199.45 ± 0.16	12.6 ± 0.2	B	
TYC-7846-1538-1	cc-1	27/04/2004	H	4.658 ± 0.017	59.39 ± 0.21		B	
		06/05/2005	K_s	4.755 ± 0.019	59.35 ± 0.26	10.8 ± 0.3	B	
	cc-2	27/04/2004	H	7.703 ± 0.025	54.64 ± 0.21	12.6 ± 0.3	U	
	cc-3	27/04/2004	H	9.121 ± 0.029	127.94 ± 0.22		U	
	cc-4	27/04/2004	H	5.287 ± 0.020	196.43 ± 0.15		B	
		06/05/2005	K_s	5.185 ± 0.021	195.89 ± 0.22	9.9 ± 0.3	B	
	cc-5	06/05/2005	K_s	5.874 ± 0.023	247.71 ± 0.24	12.6 ± 0.3	U	
TCha	cc-1	05/03/2004	K_s	3.762 ± 0.068	227.75 ± 1.37	11.4 ± 0.1	U	
	cc-2	05/03/2004	K_s	9.326 ± 0.026	327.22 ± 0.21	11.8 ± 0.2	U	
	cc-3	05/03/2004	K_s	12.045 ± 0.026	14.47 ± 0.20	11.7 ± 0.3	U	
TWA17	cc-1	17/03/2003	H	2.637 ± 0.011	109.39 ± 0.21	10.4 ± 0.2	U	
	cc-2	17/03/2003	H	1.833 ± 0.009	335.39 ± 0.28	9.3 ± 0.2	U	
	cc-3	17/03/2003	H	3.977 ± 0.016	181.71 ± 0.14	7.7 ± 0.2	U	
	cc-4	17/03/2003	H	6.026 ± 0.019	317.01 ± 0.25	9.9 ± 0.2	U	
TWA25	cc-1	16/03/2003	K_s	8.922 ± 0.025	341.62 ± 0.22	11.2 ± 0.3	PB	HST
TWA12	cc-1	17/03/2003	K_s	5.695 ± 0.020	296.32 ± 0.26	10.9 ± 0.3	PB	HST
	cc-2	17/03/2003	K_s	6.344 ± 0.021	245.90 ± 0.24	8.4 ± 0.3	PB	MZ04, HST
	cc-3	17/03/2003	K_s	6.769 ± 0.019	5.38 ± 0.23	11.5 ± 0.3	PB	HST
TYC-8992-0605-1	cc-1	17/03/2003	H	4.567 ± 0.018	356.39 ± 0.13			
		27/04/2004	H	4.581 ± 0.019	356.98 ± 0.22	10.4 ± 0.2	B	
	cc-2	17/03/2003	H	2.462 ± 0.010	63.53 ± 0.24			
		27/04/2004	H	2.530 ± 0.011	63.52 ± 0.28	8.9 ± 0.2	B	
	cc-3	17/03/2003	H	6.509 ± 0.020	50.64 ± 0.23			
		27/04/2004	H	6.574 ± 0.025	50.54 ± 0.28	9.1 ± 0.2	B	

Table 11. Contaminants and companion identified

Name	Candidate	UT Date	Filter	Separation (arcsec)	P.A. ($^{\circ}$)	Δm (mag)	Status	Note
	cc-4	17/03/2003	H	4.691 ± 0.017	66.56 ± 0.18			
		27/04/2004	H	4.763 ± 0.019	66.30 ± 0.24	10.3 ± 0.2	B	
	cc-5	17/03/2003	H	6.891 ± 0.025	70.95 ± 0.15			
		27/04/2004	H	6.971 ± 0.027	70.51 ± 0.22	11.2 ± 0.2	B	
	cc-6	17/03/2003	H	3.166 ± 0.014	97.83 ± 0.16			
		27/04/2004	H	3.229 ± 0.014	96.97 ± 0.23	9.3 ± 0.2	B	
	cc-7	17/03/2003	H	2.554 ± 0.011	111.75 ± 0.22			
		27/04/2004	H	2.606 ± 0.012	110.53 ± 0.27	8.5 ± 0.2	B	
	cc-8	17/03/2003	H	6.360 ± 0.023	112.51 ± 0.16			
		27/04/2004	H	6.411 ± 0.025	111.87 ± 0.23	10.1 ± 0.2	B	
	cc-9	17/03/2003	H	2.322 ± 0.010	145.80 ± 0.28			
		27/04/2004	H	2.351 ± 0.011	144.03 ± 0.32	10.5 ± 0.2	B	
	cc-10	17/03/2003	H	5.411 ± 0.017	134.01 ± 0.25			
		27/04/2004	H	5.456 ± 0.021	133.00 ± 0.30	10.7 ± 0.2	B	
	cc-11	17/03/2003	H	6.066 ± 0.019	134.44 ± 0.25			
		27/04/2004	H	6.105 ± 0.023	133.49 ± 0.30	11.1 ± 0.2	B	
	cc-12	17/03/2003	H	6.642 ± 0.026	179.24 ± 0.12			
		27/04/2004	H	6.626 ± 0.026	178.39 ± 0.21	8.5 ± 0.2	B	
	cc-13	17/03/2003	H	2.534 ± 0.010	226.43 ± 0.31			
		27/04/2004	H	2.474 ± 0.011	225.66 ± 0.36	10.7 ± 0.2	B	
	cc-14	17/03/2003	H	7.632 ± 0.025	210.15 ± 0.19			
		27/04/2004	H	7.583 ± 0.029	209.49 ± 0.24	9.0 ± 0.2	B	
	cc-15	17/03/2003	H	7.159 ± 0.022	228.54 ± 0.23			
		27/04/2004	H	7.085 ± 0.027	227.98 ± 0.29	11.1 ± 0.2	B	
V343Nor B	cc-1	05/03/2004	H	2.303 ± 0.009	42.41 ± 0.32	6.7 ± 0.2	PB	HST
	cc-2	05/03/2004	H	5.656 ± 0.020	63.36 ± 0.18	8.7 ± 0.2	PB	HST
	cc-3	05/03/2004	H	6.121 ± 0.023	78.82 ± 0.13	7.2 ± 0.2	PB	HST
	cc-4	05/03/2004	H	3.313 ± 0.014	103.55 ± 0.17	7.5 ± 0.2	PB	HST
	cc-5	05/03/2004	H	5.232 ± 0.017	135.05 ± 0.26	4.7 ± 0.2	U	
	cc-6	05/03/2004	H	7.940 ± 0.024	136.49 ± 0.24	4.5 ± 0.2	U	
	cc-7	05/03/2004	H	7.551 ± 0.027	161.27 ± 0.15	7.7 ± 0.2	U	
	cc-8	05/03/2004	H	5.234 ± 0.019	157.88 ± 0.17	8.1 ± 0.2	U	
	cc-9	05/03/2004	H	6.503 ± 0.025	169.91 ± 0.13	7.2 ± 0.2	U	
	cc-10	05/03/2004	H	4.444 ± 0.018	185.95 ± 0.14	7.4 ± 0.2	PB	HST
	cc-11	05/03/2004	H	5.215 ± 0.020	188.31 ± 0.13	5.2 ± 0.2	U	
	cc-12	05/03/2004	H	1.421 ± 0.008	205.46 ± 0.34	7.3 ± 0.2	PB	HST
	cc-13	05/03/2004	H	2.724 ± 0.010	221.71 ± 0.29	7.4 ± 0.2	PB	HST
	cc-14	05/03/2004	H	6.000 ± 0.019	225.61 ± 0.25	5.8 ± 0.2	U	
	cc-15	05/03/2004	H	7.233 ± 0.022	226.59 ± 0.24	7.4 ± 0.2	U	
	cc-16	05/03/2004	H	2.438 ± 0.011	248.22 ± 0.22	9.1 ± 0.2	PB	HST
	cc-17	05/03/2004	H	5.924 ± 0.021	295.92 ± 0.18	5.1 ± 0.2	PB	HST
	cc-18	05/03/2004	H	6.807 ± 0.021	313.78 ± 0.25	7.7 ± 0.2	PB	HST
TYC-6461-1120-1 AB	cc-1	08/01/2006	K_s	7.212 ± 0.013	33.68 ± 0.13	11.7 ± 0.2	PB	HST
	cc-2	08/01/2006	K_s	11.665 ± 0.022	137.29 ± 0.13	10.9 ± 0.2	U	
HIP76768 AB	cc-1	18/08/2005	K_s	8.903 ± 0.023	103.47 ± 0.22	10.7 ± 0.3	U	
	cc-2	18/08/2005	K_s	11.571 ± 0.035	224.06 ± 0.24	10.9 ± 0.3	U	
HIP6485	cc-1	08/01/2006	K_s	10.790 ± 0.029	322.12 ± 0.19	18.7 ± 0.2	PB	HST
TWA14	cc-1	08/01/2006	K_s	16.798 ± 0.038	45.40 ± 0.18	7.6 ± 0.3	U	
	cc-2	08/01/2006	K_s	14.653 ± 0.033	143.98 ± 0.17	8.2 ± 0.3	U	
	cc-3	08/01/2006	K_s	10.233 ± 0.026	223.30 ± 0.20	9.0 ± 0.3	U	
	cc-4	08/01/2006	K_s	2.451 ± 0.015	240.97 ± 0.39	12.0 ± 0.3	PB	HST
HIP84642 AB	cc-1	05/06/2007	K_s	14.663 ± 0.043	51.36 ± 0.22	10.9 ± 0.2	U	
	cc-2	05/06/2007	K_s	7.316 ± 0.022	67.68 ± 0.23	10.0 ± 0.2	U	
	cc-3	05/06/2007	K_s	5.871 ± 0.018	103.39 ± 0.24	10.8 ± 0.2	U	
	cc-4	05/06/2007	K_s	11.579 ± 0.030	70.64 ± 0.21	12.8 ± 0.2	U	
	cc-5	05/06/2007	K_s	12.915 ± 0.033	201.71 ± 0.21	8.2 ± 0.2	B	Hu08
	cc-6	05/06/2007	K_s	10.810 ± 0.027	194.72 ± 0.21	12.1 ± 0.2	U	
	cc-7	05/06/2007	K_s	12.023 ± 0.033	206.74 ± 0.21	12.8 ± 0.2	U	
	cc-8	05/06/2007	K_s	3.926 ± 0.017	315.16 ± 0.36	11.8 ± 0.2	U	
HIP107947	cc-1	19/08/2005	K_s	11.094 ± 0.025	33.18 ± 0.15	14.5 ± 0.2	U	
HIP51386	cc-1	26/02/2006	K_s	5.242 ± 0.0100	187.08 ± 0.14	10.9 ± 0.1	PB	HST
	cc-2	26/02/2006	K_s	12.191 ± 0.023	176.01 ± 0.15	12.8 ± 0.2	U	

Table 12. Contaminants and companion identified

Name	Candidate	UT Date	Filter	Separation (arcsec)	P.A. ($^{\circ}$)	Δm (mag)	Status	Note
HIP88399	cc-1	24/09/2004	K_s	11.242 ± 0.028	17.93 ± 0.21	13.3 ± 0.2	PB	HST
	cc-2	24/09/2004	K_s	13.045 ± 0.038	36.55 ± 0.22	$15. \pm 0.2$	U	
	cc-3	24/09/2004	K_s	11.155 ± 0.034	46.37 ± 0.24	14.6 ± 0.2	U	
	cc-4	24/09/2004	K_s	14.598 ± 0.043	138.5 ± 0.23	$12. \pm 0.2$	U	
	cc-5	24/09/2004	K_s	14.774 ± 0.043	138.87 ± 0.22	11.6 ± 0.2	U	
	cc-6	24/09/2004	K_s	9.735 ± 0.023	178.36 ± 0.22	13.9 ± 0.2	U	
	cc-7	24/09/2004	K_s	7.354 ± 0.021	198.90 ± 0.23	13.3 ± 0.2	U	
	cc-8	24/09/2004	K_s	10.144 ± 0.031	322.37 ± 0.23	14.5 ± 0.2	PB	HST
HIP76107	cc-1	06/05/2005	K_s	4.635 ± 0.017	56.81 ± 0.25	5.3 ± 0.1	U	
	cc-2	06/05/2005	K_s	2.191 ± 0.010	31.99 ± 0.32	9.4 ± 0.2	U	
	cc-3	06/05/2005	K_s	2.549 ± 0.011	57.18 ± 0.30	8.1 ± 0.2	U	
	cc-4	06/05/2005	K_s	2.671 ± 0.012	57.54 ± 0.30	9.3 ± 0.2	U	
	cc-5	06/05/2005	K_s	5.338 ± 0.021	112.95 ± 0.23	9.4 ± 0.2	U	
	cc-6	06/05/2005	K_s	6.038 ± 0.023	114.83 ± 0.24	9.0 ± 0.2	U	
	cc-7	06/05/2005	K_s	6.077 ± 0.023	131.39 ± 0.29	10.5 ± 0.2	U	
	cc-8	06/05/2005	K_s	4.219 ± 0.017	140.92 ± 0.29	10.2 ± 0.2	U	
	cc-9	06/05/2005	K_s	2.729 ± 0.012	153.00 ± 0.28	9.2 ± 0.2	U	
	cc-10	06/05/2005	K_s	2.908 ± 0.013	167.35 ± 0.25	8.2 ± 0.2	U	
	cc-11	06/05/2005	K_s	3.200 ± 0.014	167.50 ± 0.24	9.2 ± 0.2	U	
	cc-12	06/05/2005	K_s	6.578 ± 0.025	158.18 ± 0.23	10.1 ± 0.2	U	
	cc-13	06/05/2005	K_s	6.729 ± 0.026	170.23 ± 0.21	8.5 ± 0.2	U	
	cc-14	06/05/2005	K_s	6.387 ± 0.025	193.80 ± 0.22	10.3 ± 0.2	U	
	cc-15	06/05/2005	K_s	8.177 ± 0.031	216.20 ± 0.26	8.9 ± 0.2	U	
	cc-16	06/05/2005	K_s	7.925 ± 0.030	215.24 ± 0.26	10.3 ± 0.2	U	
	cc-17	06/05/2005	K_s	6.519 ± 0.025	289.28 ± 0.22	9.2 ± 0.2	U	
	cc-18	06/05/2005	K_s	1.759 ± 0.009	287.32 ± 0.31	9.8 ± 0.2	U	
	cc-19	06/05/2005	K_s	4.703 ± 0.022	294.11 ± 0.29	10.7 ± 0.2	U	
	cc-20	06/05/2005	K_s	1.726 ± 0.015	294.01 ± 0.53	10.2 ± 0.2	U	
	cc-21	06/05/2005	K_s	5.171 ± 0.023	130.22 ± 0.33	10.6 ± 0.2	U	
	cc-22	06/05/2005	K_s	4.701 ± 0.022	176.12 ± 0.26	10.6 ± 0.2	U	
	cc-23	06/05/2005	K_s	6.606 ± 0.028	208.78 ± 0.27	10.4 ± 0.2	U	
HIP21632 B	cc-1	22/10/2006	K_s	7.415 ± 0.037	239.87 ± 0.31	4.8 ± 0.2	PB	HST
HIP30314	cc-1	21/11/2006	K_s	10.425 ± 0.018	10.51 ± 0.20	11.8 ± 0.2	PB	HST
HIP26373	cc-1	26/12/2006	K_s	8.795 ± 0.024	28.18 ± 0.20	$13. \pm 0.2$	U	
HIP1481	cc-1	21/10/2006	K_s	10.218 ± 0.025	232.58 ± 0.18	13.4 ± 0.2	PB	HST
HIP3556	cc-1	22/10/2006	K_s	9.160 ± 0.017	206.22 ± 0.15	8.3 ± 0.1	U	
HIP96334	cc-1	09/06/2007	K_s	12.173 ± 0.023	184.16 ± 0.20	12.8 ± 0.2	U	
	cc-2	09/06/2007	K_s	7.104 ± 0.016	260.85 ± 0.20	13.5 ± 0.1	PB	HST
	cc-3	09/06/2007	K_s	4.451 ± 0.018	322.03 ± 0.30	4.6 ± 0.2	PB	HST
HIP92680	cc-1	13/06/2007	K_s	8.284 ± 0.020	335.54 ± 0.20	11.1 ± 0.1	PB	HST
	cc-2	13/06/2007	K_s	4.008 ± 0.008	166.30 ± 0.20	10.7 ± 0.1	PB	HST
	cc-3	13/06/2007	K_s	10.74 ± 0.030	128.42 ± 0.21	11.5 ± 0.1	U	
	cc-4	13/06/2007	K_s	9.013 ± 0.025	159.75 ± 0.22	11.9 ± 0.2	U	
HIP92024	cc-1	04/06/2007	K_s	7.429 ± 0.025	318.53 ± 0.26	14.3 ± 0.2	PB	HST
HIP113579	cc-1	15/06/2007	K_s	5.352 ± 0.012	107.69 ± 0.20	11.8 ± 0.1	PB	HST
HIP105404	cc-1	30/05/2007	K_s	3.253 ± 0.009	48.43 ± 0.22	8.5 ± 0.1	PB	HST
	cc-2	30/05/2007	K_s	5.861 ± 0.017	161.27 ± 0.20	11.7 ± 0.30	U	
FS1174	cc-1	06/05/2005	K_s	6.571 ± 0.020	246.02 ± 0.20	6.2 ± 0.2	U	
FS903	cc-1	19/08/2005	K_s	7.172 ± 0.016	19.96 ± 0.20	8.1 ± 0.1	U	
	cc-2	19/08/2005	K_s	5.232 ± 0.010	357.52 ± 0.20	12.1 ± 0.2	U	
	cc-3	19/08/2005	K_s	5.256 ± 0.012	341.52 ± 0.20	10.5 ± 0.1	U	
	cc-4	19/08/2005	K_s	7.980 ± 0.019	339.09 ± 0.20	10.9 ± 0.1	U	
	cc-5	19/08/2005	K_s	6.970 ± 0.014	282.91 ± 0.20	$11. \pm 0.1$	U	
	cc-6	19/08/2005	K_s	7.421 ± 0.018	244.76 ± 0.20	12.1 ± 0.1	U	
	cc-7	19/08/2005	K_s	12.637 ± 0.024	177.28 ± 0.20	10.5 ± 0.2	U	
	cc-8	19/08/2005	K_s	9.867 ± 0.026	149.58 ± 0.20	10.7 ± 0.1	U	
	cc-9	19/08/2005	K_s	13.576 ± 0.036	146.13 ± 0.20	10.3 ± 0.1	U	
	cc-10	19/08/2005	K_s	11.234 ± 0.024	106.61 ± 0.20	11.3 ± 0.1	U	
	cc-11	19/08/2005	K_s	3.907 ± 0.007	86.47 ± 0.20	10.3 ± 0.1	U	
	cc-12	19/08/2005	K_s	9.802 ± 0.023	22.70 ± 0.20	11.9 ± 0.2	U	

Table 13. Contaminants and companion identified

Name	Candidate	UT Date	Filter	Separation (arcsec)	P.A. ($^{\circ}$)	Δm (mag)	Status	Note
	cc-13	19/08/2005	K _s	10.2140 ± 0.024	20.55 ± 0.20	12.6 ± 0.2	U	
	cc-14	19/08/2005	K _s	15.5660 ± 0.109	40.75 ± 0.47	13.6 ± 0.2	U	
	cc-15	19/08/2005	K _s	15.7480 ± 0.043	52.83 ± 0.21	12.6 ± 0.2	U	
	cc-16	19/08/2005	K _s	10.6060 ± 0.023	74.40 ± 0.20	12.6 ± 0.2	U	
	cc-17	19/08/2005	K _s	7.913 ± 0.015	84.50 ± 0.20	12.4 ± 0.2	U	
	cc-18	19/08/2005	K _s	8.452 ± 0.023	117.150 ± 0.2	13.3 ± 0.2	U	
	cc-19	19/08/2005	K _s	8.233 ± 0.023	138.790 ± 0.21	12.7 ± 0.2	U	
	cc-20	19/08/2005	K _s	15.0430 ± 0.042	134.810 ± 0.23	13. ± 0.2	U	
	cc-21	19/08/2005	K _s	5.707 ± 0.013	161.20 ± 0.20	12.6 ± 0.2	U	
	cc-22	19/08/2005	K _s	6.737 ± 0.014	167.080 ± 0.20	12.4 ± 0.2	U	
	cc-23	19/08/2005	K _s	8.008 ± 0.015	184.020 ± 0.20	12.4 ± 0.2	U	
	cc-24	19/08/2005	K _s	9.701 ± 0.026	214.510 ± 0.20	12.5 ± 0.2	U	
	cc-25	19/08/2005	K _s	11.4670 ± 0.031	234.780 ± 0.20	12.4 ± 0.2	U	
	cc-26	19/08/2005	K _s	5.860 ± 0.034	253.960 ± 0.33	12.5 ± 0.2	U	
	cc-27	19/08/2005	K _s	4.645 ± 0.061	282.620 ± 0.37	12.9 ± 0.2	U	
	cc-28	19/08/2005	K _s	11.7810 ± 0.031	329.050 ± 0.2	13.7 ± 0.2	U	
	cc-29	19/08/2005	K _s	4.99 ± 0.015	311.150 ± 0.23	11.4 ± 0.2	U	
	cc-30	19/08/2005	K _s	4.574 ± 0.030	311.460 ± 0.50	13.1 ± 0.2	U	
FS979	cc-1	18/08/2005	K _s	7.466 ± 0.019	119.00 ± 0.20	0.70 ± 0.1	U	
	cc-2	18/08/2005	K _s	9.708 ± 0.030	49.40 ± 0.24	13.2 ± 0.2	U	
	cc-3	18/08/2005	K _s	8.123 ± 0.023	69.50 ± 0.22	9.6 ± 0.2	U	
	cc-4	18/08/2005	K _s	13.773 ± 0.040	52.26 ± 0.22	10.9 ± 0.2	U	
	cc-5	18/08/2005	K _s	12.744 ± 0.032	69.13 ± 0.21	11.4 ± 0.2	U	
	cc-6	18/08/2005	K _s	8.875 ± 0.022	80.60 ± 0.22	11.8 ± 0.2	U	
	cc-7	18/08/2005	K _s	11.495 ± 0.025	87.28 ± 0.21	9.9 ± 0.2	U	
	cc-8	18/08/2005	K _s	15.265 ± 0.032	96.87 ± 0.21	12.4 ± 0.2	U	
	cc-9	18/08/2005	K _s	13.839 ± 0.036	113.76 ± 0.21	9.4 ± 0.2	U	
	cc-10	18/08/2005	K _s	12.594 ± 0.036	123.64 ± 0.21	12.1 ± 0.2	U	
	cc-11	18/08/2005	K _s	19.220 ± 0.051	118.95 ± 0.20	10.6 ± 0.2	U	
	cc-12	18/08/2005	K _s	19.108 ± 0.053	123.28 ± 0.21	9.4 ± 0.2	U	
	cc-13	18/08/2005	K _s	19.719 ± 0.054	123.76 ± 0.21	9.8 ± 0.2	U	
	cc-14	18/08/2005	K _s	18.911 ± 0.054	137.2 ± 0.23	10.3 ± 0.2	U	
	cc-15	18/08/2005	K _s	16.818 ± 0.048	142.48 ± 0.21	9.3 ± 0.2	U	
	cc-16	18/08/2005	K _s	17.371 ± 0.048	148.61 ± 0.20	10.5 ± 0.2	U	
	cc-17	18/08/2005	K _s	16.05 ± 0.040	157.82 ± 0.20	9.6 ± 0.2	U	
	cc-18	18/08/2005	K _s	9.561 ± 0.028	150.28 ± 0.22	9.2 ± 0.2	U	
	cc-19	18/08/2005	K _s	9.335 ± 0.025	162.81 ± 0.22	11.2 ± 0.2	U	
	cc-20	18/08/2005	K _s	10.5330 ± 0.026	166. ± 0.21	9.6 ± 0.2	U	
	cc-21	18/08/2005	K _s	13.1630 ± 0.031	165.12 ± 0.21	9.2 ± 0.2	U	
	cc-22	18/08/2005	K _s	15.0450 ± 0.033	170.09 ± 0.21	10.5 ± 0.2	U	
	cc-23	18/08/2005	K _s	14.9610 ± 0.032	172.92 ± 0.21	11.4 ± 0.2	U	
	cc-24	18/08/2005	K _s	13.3330 ± 0.028	178.26 ± 0.21	10.9 ± 0.2	U	
	cc-25	18/08/2005	K _s	12.0260 ± 0.026	179.48 ± 0.21	8.4 ± 0.2	U	
	cc-26	18/08/2005	K _s	13.5530 ± 0.029	181.5 ± 0.21	10.6 ± 0.2	U	
	cc-27	18/08/2005	K _s	14.6020 ± 0.030	179.2 ± 0.21	10.4 ± 0.2	U	
	cc-28	18/08/2005	K _s	11.2080 ± 0.027	194.240 ± 0.21	9.9 ± 0.2	U	
	cc-29	18/08/2005	K _s	11.41 ± 0.028	196.670 ± 0.21	11.1 ± 0.2	U	
	cc-30	18/08/2005	K _s	7.599 ± 0.022	202.230 ± 0.22	9.9 ± 0.2	U	
	cc-31	18/08/2005	K _s	7.318 ± 0.023	210.770 ± 0.23	8.6 ± 0.2	U	
	cc-32	18/08/2005	K _s	8.455 ± 0.026	212.350 ± 0.23	10.9 ± 0.2	U	
	cc-33	18/08/2005	K _s	12.2310 ± 0.037	221.730 ± 0.23	9.3 ± 0.2	U	
	cc-34	18/08/2005	K _s	14.2890 ± 0.041	215.540 ± 0.21	9.8 ± 0.2	U	
	cc-35	18/08/2005	K _s	15.3130 ± 0.043	213.530 ± 0.21	10.5 ± 0.2	U	
	cc-36	18/08/2005	K _s	15.72 ± 0.043	209.010 ± 0.20	10.8 ± 0.2	U	
	cc-37	18/08/2005	K _s	6.003 ± 0.021	310.140 ± 0.27	9.6 ± 0.2	U	
	cc-38	18/08/2005	K _s	7.943 ± 0.026	306.510 ± 0.24	8.2 ± 0.2	U	
	cc-39	18/08/2005	K _s	11.25 ± 0.032	329.780 ± 0.21	10.7 ± 0.2	U	
	cc-40	18/08/2005	K _s	10.2740 ± 0.027	338.870 ± 0.21	10.2 ± 0.2	U	
	cc-41	18/08/2005	K _s	9.583 ± 0.024	347.890 ± 0.21	8.9 ± 0.2	U	

Table 14. Contaminants and companion identified

Name	Candidate	UT Date	Filter	Separation (arcsec)	P.A. ($^{\circ}$)	Δm (mag)	Status	Note
FS1017	cc-1	19/08/2005	K_s	12.041 ± 0.032	57.93 ± 0.20	4.8 ± 0.1	U	
	cc-2	19/08/2005	K_s	9.463 ± 0.025	213.830 ± 0.20	5.9 ± 0.1	U	
	cc-3	19/08/2005	K_s	9.689 ± 0.024	243.940 ± 0.20	4.1 ± 0.1	U	
	cc-4	19/08/2005	K_s	13.799 ± 0.038	318.650 ± 0.21	6.3 ± 0.1	U	
	cc-5	19/08/2005	K_s	15.149 ± 0.042	317.320 ± 0.22	6.1 ± 0.1	U	
	cc-6	19/08/2005	K_s	14.507 ± 0.040	119.520 ± 0.21	7.5 ± 0.2	U	
	cc-7	19/08/2005	K_s	13.537 ± 0.038	148.030 ± 0.21	7.6 ± 0.2	U	
	cc-8	19/08/2005	K_s	9.057 ± 0.022	170.110 ± 0.22	7.2 ± 0.2	U	
	cc-9	19/08/2005	K_s	17.1820 ± 0.050	319.390 ± 0.22	7.0 ± 0.2	U	
	cc-10	19/08/2005	K_s	17.046 ± 0.049	319.840 ± 0.22	7.4 ± 0.2	U	
	cc-11	19/08/2005	K_s	7.984 ± 0.020	184.820 ± 0.22	8.2 ± 0.2	U	
FS1035	cc-1	19/08/2005	K_s	5.402 ± 0.020	27.05 ± 0.25			
		28/06/2008	K_s	5.862 ± 0.020	26.98 ± 0.25	7.4 ± 0.2	B	